TECHNISCHE UNIVERSITÄT DRESDEN

Gross-Neveu quantum criticalities in moiré Dirac materials

Master-Arbeit
zur Erlangung des Hochschulgrades
Master of Science
im Master-Studiengang Physik

vorgelegt von

Hao Yuan
geboren am 04.02.2001 in Zhejiang

Institut für Theoretische Physik
Fakultät Physik
Bereich Mathematik und Naturwissenschaften
Technische Universität Dresden
2026

Eingereicht am 3. April 2026

1. Gutachter: Prof. Dr. Matthias Vojta
2. Gutachter: Prof. Dr. Carsten Timm

Summary

In this thesis, we investigate the Gross-Neveu-Ising, Gross-Neveu-XY, and Gross-Neveu- Heisenberg universality classes in $(2+1)$ dimensions, corresponding respectively to one-, two-, and three-component order parameters, and compare their critical behavior within three complementary renormalization-group descriptions: the purely fermionic formulation, the partially bosonized formulation, and the dynamically bosonized formulation. These models describe interaction-driven quantum phase transitions of Dirac fermions. All RG calculations are performed directly in $D = 3$, corresponding to the physically relevant $(2+1)$-dimensional setting of two-dimensional condensed-matter systems.

We first determine the symmetry-allowed four-fermion interaction channels and derive the corresponding one-loop RG flows in the purely fermionic description. The analysis shows that the Gross-Neveu-Ising model remains structurally simple, since the scalar interaction sector is closed at the present level of truncation. By contrast, the Gross-Neveu-XY and Gross-Neveu-Heisenberg models require an enlarged theory space, as additional symmetry-allowed interaction channels are generated under the RG flow. The resulting fixed-point structure differs qualitatively between the three cases. In the Ising case, the critical fixed point remains stable in the physically relevant regime. In the XY case, two real fixed points collide and exchange their critical character. In the Heisenberg case, the collision drives the fixed points into the complex plane.

We then reformulate the three models in a partially bosonized language, where the order-parameter fluctuations are represented explicitly in terms of bosonic fields, Yukawa couplings, and bosonic self-interactions. This makes the fermion-boson criticality more transparent, but also reveals the limitation of a fixed bosonized truncation once four-fermion interactions are regenerated along the flow. To incorporate this feedback, we finally employ dynamical bosonization, in which the regenerated fermionic interactions are continuously reabsorbed into the bosonic sector. For the Gross-Neveu-Ising model, this procedure does not modify the flow at the present level of truncation. For the Gross-Neveu-XY and Gross-Neveu-Heisenberg models, however, it restores the box-generated contributions and reproduces the fixed-point collision patterns found in the purely fermionic formulation.

The comparison of critical exponents shows that the Ising universality class is comparatively well controlled already in restricted truncations, whereas in the XY and Heisenberg cases the feedback of regenerated interaction channels is quantitatively important. In particular, dynamical bosonization shifts the analytical estimates systematically toward available quantum Monte Carlo results. These findings show that the differences between the three universality classes are not merely quantitative, but are rooted in the symmetry-dependent structure of the RG flow and of the underlying theory space.

Zusammenfassung

In dieser Arbeit werden die Gross-Neveu-Ising-, Gross-Neveu-XY- und Gross-Neveu-Heisenberg Universalitätsklassen in $(2+1)$ Dimensionen untersucht, die jeweils ein-, zwei- beziehungsweise dreikomponentigen Ordnungsparametern entsprechen, und ihr kritisches Verhalten innerhalb von drei komplementären Beschreibungen der Renormierungsgruppe verglichen: der rein fermionischen Formulierung, der partiell bosonisierten Formulierung und der dynamisch bosonisierten Formulierung. Diese Modelle beschreiben wechselwirkungsgetriebene Quantenphasenübergänge von Dirac-Fermionen. Sämtliche RG-Rechnungen werden direkt in $D = 3$ durchgeführt, entsprechend dem physikalisch relevanten $(2 + 1)$-dimensionalen Fall zweidimensionaler Systeme der kondensierten Materie.

Zunächst werden in der rein fermionischen Beschreibung die durch die Symmetrien erlaubten Vier-Fermion-Wechselwirkungskanäle bestimmt und die zugehörigen RG-Flussgleichungen auf Ein-Schleifen-Niveau hergeleitet. Die Analyse zeigt, dass das Gross-Neveu-Ising-Modell strukturell vergleichsweise einfach bleibt, da der skalare Wechselwirkungssektor im Rahmen der vorliegenden Trunkierung abgeschlossen ist. Im Gegensatz dazu erfordern das Gross-Neveu-XY- und das Gross-Neveu-Heisenberg-Modell einen erweiterten Theorieraum, da zusätzliche symmetrieerlaubte Wechselwirkungskanäle unter dem RG-Fluss erzeugt werden. Die daraus resultierende Fixpunktstruktur unterscheidet sich qualitativ in den drei Fällen. Im Ising-Fall bleibt der kritische Fixpunkt im physikalisch relevanten Bereich stabil. Im XY-Fall kollidieren zwei reelle Fixpunkte und tauschen ihren kritischen Charakter aus. Im Heisenberg-Fall treibt die Kollision die Fixpunkte in die komplexe Ebene.

Anschließend werden die drei Modelle in eine partiell bosonisierte Beschreibung überführt, in der die Fluktuationen des Ordnungsparameters explizit durch bosonische Felder, Yukawa-Kopplungen und bosonische Selbstwechselwirkungen dargestellt werden. Dies macht die Fermion-Boson-Kritikalität anschaulicher, zeigt aber zugleich die Einschränkung einer festen bosonisierten Trunkierung, sobald entlang des Flusses Vier-Fermion-Wechselwirkungen regeneriert werden. Um diese Rückkopplung zu berücksichtigen, wird schließlich die dynamische Bosonisierung eingesetzt, bei der die regenerierten fermionischen Wechselwirkungen fortlaufend in den bosonischen Sektor reabsorbiert werden. Für das Gross-Neveu-Ising-Modell verändert dieses Verfahren den Fluss auf dem vorliegenden Trunkierungsniveau nicht. Für das Gross-Neveu-XY- und das Gross-Neveu-Heisenberg-Modell stellt es hingegen die durch Box-Diagramme erzeugten Beiträge wieder her und reproduziert die Fixpunkt-Kollisionsmuster, die bereits in der rein fermionischen Formulierung gefunden wurden.

Der Vergleich der kritischen Exponenten zeigt, dass die Ising-Universalitätsklasse bereits in eingeschränkten Trunkierungen vergleichsweise gut kontrolliert ist, während in den XY- und Heisenberg-Fällen die Rückkopplung regenerierter Wechselwirkungskanäle quantitativ wichtig ist. Insbesondere verschiebt die dynamische Bosonisierung die analytischen Abschätzungen systematisch in Richtung der verfügbaren Quanten-Monte-Carlo-Ergebnisse. Diese Resultate

zeigen, dass die Unterschiede zwischen den drei Universalitätsklassen nicht nur quantitativer Natur sind, sondern in der symmetrieabhängigen Struktur des RG-Flusses und des zugrunde liegenden Theorieraums wurzeln.

Contents

1 Introduction

Interaction-driven quantum phase transitions in Dirac systems constitute an important central problems in modern condensed-matter physics. In a broad class of two-dimensional materials and lattice models, low-energy quasiparticles are described by massless Dirac fermions, including graphene-related systems, topological Dirac materials, and more recently moiré platforms [1–5]. A characteristic feature of such systems is the vanishing density of states at the Dirac point, which renders the semimetallic phase stable against sufficiently weak short-range interactions and implies that symmetry breaking generally requires a finite interaction threshold [2, 4]. Once this threshold is exceeded, however, the Dirac semimetal may become unstable toward a symmetry-broken insulating or superconducting state [4, 6–9]. Because the critical order-parameter fluctuations remain strongly coupled to gapless fermionic degrees of freedom, the resulting quantum phase transitions generally lie beyond a purely bosonic Landau-Ginzburg-Wilson description and are instead governed by fermionic quantum field theories of Gross-Neveu or Gross-Neveu-Yukawa type [4, 10–12]. These universality classes therefore provide the natural field-theoretical framework for relating microscopic models of correlated Dirac matter to universal observables such as scaling dimensions, anomalous dimensions, and correlation-length exponents [4, 11, 13, 14].

The physical relevance of Gross-Neveu criticality is by now well established. The one-component Gross-Neveu-Ising (GNI) universality class describes transitions associated with a discrete mass-generating order parameter, with representative realizations including charge-density-wave ordering of interacting spinless Dirac fermions on the honeycomb lattice and related Ising-type instabilities in Dirac materials [15, 16]. The two-component Gross-Neveu-XY (GNXY) universality class arises for transitions with a continuous $O(2)$ order parameter. Representative examples include the semimetal-to-Kekulé-insulator transition on the honeycomb lattice [7, 8, 17], Dirac systems with superconducting ordering tendencies [9], and, more recently, twist-tuned moiré Dirac materials, where the transition into a Kramers intervalley-coherent insulator has been argued to fall into the $(2+1)$-dimensional Gross-Neveu-XY class [5, 18, 19]. The three-component Gross-Neveu-Heisenberg (GNH) universality class is the natural description of Dirac systems with $SU(2)$-vector order parameters, most prominently the semimetal-to-antiferromagnet transition in the half-filled Hubbard model on the honeycomb lattice and related lattice realizations of Néel ordering in Dirac semimetals [4, 6, 15, 20–22]. Taken together, the GNI, GNXY, and GNH models represent the simplest and most important sym-

metry classes of fermion-bilinear mass generation in interacting Dirac systems.

Correspondingly, these universality classes have been studied with a broad range of analytical and numerical methods. On the analytical side, representative approaches include the expansion around the lower critical dimension $D = 2$ [5, 23, 24], the Gross-Neveu-Yukawa expansion around the upper critical dimension $D = 4$ [11, 13, 25], large-N_f techniques [26, 27], conformal-bootstrap-inspired approaches [14], and functional renormalization group methods [21, 28, 29]. In particular, the $(2 + \epsilon)$- and $(4 - \epsilon)$-expansion frameworks are by now technically well developed and have provided a large body of estimates for critical exponents [5, 11, 13, 23, 25]. However, for the physically most relevant case of $(2 + 1)$-dimensional Dirac systems, these approaches ultimately rely on an extrapolation to $\epsilon = 1$, whose quantitative reliability is not guaranteed *a priori*, especially when the several interaction channels compete near the quantum critical point [5, 13, 23, 25]. On the numerical side, sign-problem-free quantum Monte Carlo simulations have provided increasingly precise estimates for several lattice realizations of GNI-, GNXY-, and GNH-type transitions [6–9, 15, 20, 22]. For this reason, in the present work we formulate all RG calculations directly in $D = 3$ space-time dimensions, rather than relying on an ϵ-expansion extrapolation. While such fixed-dimension RG approach is, a priori, equally uncontrolled in $D = 3$, it allows us to devise approximation schemes that become asymptotically exact in the vicinity of both the upper critical dimension $D = 4$ and the lower critical dimension $D = 2$, thereby providing a controlled interpolation between the results of the $2 + \epsilon$ and $4 - \epsilon$ expansions. For classical phase transitions, the fixed-dimension RG is, in fact, widely regarded as providing some of the most accurate estimates of critical exponents among the various renormalization-group approaches [30]. For the GNI universality class, the overall agreement between different analytical approaches and unbiased numerical simulations is by now relatively satisfactory [13, 15, 16, 29]. By contrast, for GNXY and GNH, noticeable quantitative discrepancies between QMC estimates and existing analytical calculations persist, especially for the anomalous dimensions and, depending on the realization, also for the correlation-length exponent [5, 9, 13, 22, 25–27]. This suggests that, at least for the multi-component cases, the structure of the theory space may play a more decisive role than in the Ising case.

A key difference is that the renormalization-group structure of these models is not equally simple. In the purely fermionic formulation, all four-fermion operators compatible with the microscopic symmetries are in principle generated under the RG, so that an unbiased analysis requires a Fierz-complete theory space containing all symmetry-allowed relevant and marginal interaction channels [5, 23, 31]. For the Gross-Neveu-Ising model, however, the standard interaction is closed under the RG at one loop, which may explain why this case is comparatively well controlled [10, 11]. For the Gross-Neveu-Heisenberg model, by contrast, the interaction is not RG closed, and additional symmetry-allowed channels must be included already at the level of the fermionic action [23, 31]. Recent work has shown that the same issue is crucial

for the Gross-Neveu-XY model as well: near $D = 2$, a faithful treatment requires the determination of the full symmetry-allowed four-fermion theory space rather than the study of a single isolated coupling [5]. From this perspective, the remaining tension between analytical estimates and QMC results for GNXY and GNH may be viewed not merely as a quantitative problem of higher-loop accuracy, but also as a structural problem of whether the chosen RG formulation captures the full operator content generated by the flow.

This observation motivates the present thesis. The main goal is to study the Gross-Neveu-Ising, Gross-Neveu-XY, and Gross-Neveu-Heisenberg universality classes in $(2+1)$ dimensions within a common framework, with particular emphasis on the role of symmetry-allowed interaction channels and on the comparison between different RG formulations. We begin in Sec. 2 from the purely fermionic description and determine the interaction space allowed by the symmetries of the GNXY and GNH models, using the GNI case as the simplest reference where the interaction sector is closed. On this basis, we analyze in Sec. 3 the corresponding fermionic RG flows and fixed-point structure. In Sec. 4, the same models are reformulated in a partially bosonized language, which makes the order-parameter fluctuations explicit and provides direct access to Yukawa couplings and bosonic self-interactions. In Sec. 5, we further incorporate the feedback of regenerated four-fermion interactions through dynamical bosonization and compare the resulting fixed-point structure and critical exponents with those obtained in the purely fermionic and naively partially bosonized schemes. A central aim of this comparison is to clarify to what extent the treatment of regenerated interaction channels affects the analytical description of GNXY and GNH criticality and whether it helps explain the remaining discrepancies with available numerical results. Finally, in Sec. 6 we summarize our findings and discuss possible extensions.

2 Gross-Neveu models

Interacting Dirac fermions in two spatial dimensions provide a natural setting for a broad class of interaction-driven quantum phase transitions. Starting from a gapless semimetallic state, sufficiently strong short-range interactions can induce spontaneous fermion mass generation and drive the system into ordered phases with distinct symmetry-breaking patterns. Although the microscopic realizations may differ substantially depending, for example, on lattice geometry, spin or valley structure, and the detailed form of the interaction, long-wavelength critical behavior is often governed by a small number of relativistic quantum field theories. Among these, Gross-Neveu(GN) theories play a central role, as they furnish a unified effective description of Dirac fermions coupled to fermion-bilinear order parameters and thereby capture the universal properties of a wide range of interaction-driven quantum critical points.

In this section, we adopt a purely fermionic formulation of the GN models. In Euclidean spacetime of dimension $D = d + 1$ (with primary interest in $d = 2$), we write the total action as

$$S = \int \mathrm{d}^D x \Big(\bar{\psi}^\alpha \gamma_\mu \partial_\mu \psi^\alpha + \mathcal{L}_{\mathrm{int}} \Big), \tag{2.1}$$

where $x \equiv (\tau, \mathbf{x})$ denotes the Euclidean spacetime coordinate, with τ the imaginary-time variable and $\mathbf{x}$ the spatial coordinate, and $\mu = 0, 1, \ldots, D-1$. The field ψ^α is the Dirac spinor of flavor $\alpha = 1, \ldots, N_f$, and the Dirac adjoint is defined as $\bar{\psi} \equiv \psi^\dagger \gamma_0$. The gamma matrices satisfy the Euclidean Clifford algebra

$$\{\gamma_\mu, \gamma_\nu\} = 2\delta_{\mu\nu} \mathbb{1}. \tag{2.2}$$

In the absence of interactions, Eq. (2.1) describes massless Dirac fermions with emergent relativistic symmetry at low energies. The interaction term $\mathcal{L}_{\mathrm{int}}$ contains local four-fermion operators and encodes the tendency of the system toward spontaneous formation of fermion-bilinear condensates. At criticality, these condensates act as order parameters for quantum phase transitions out of the gapless Dirac semimetal.

The precise form of $\mathcal{L}_{\mathrm{int}}$ is constrained by the global symmetries of the problem and by the fermion-bilinear mass channels allowed by these symmetries. Different bilinear channels correspond to different order-parameter structures and different symmetry-breaking patterns, and therefore to different GN universality classes. In this sense, GN theories provide a systematic field-theoretic classification of interaction-driven Dirac criticality. In the present work, we

focus on three of the most basic and most frequently encountered cases: a single-component real scalar order parameter, a two-component order parameter, and a three-component vector order parameter. These correspond, respectively, to the Gross-Neveu-Ising, Gross-Neveu-XY, and Gross-Neveu-Heisenberg models. Together, they form a minimal yet representative set for analyzing how the symmetry of the order parameter influences the renormalization-group flow, the fixed-point structure, and the resulting universal critical behavior.

(1) Gross-Neveu-Ising model. The Gross-Neveu-Ising (GNI) model describes Dirac fermions coupled to a single real scalar order parameter, or equivalently to a single fermion mass channel. Its ordered phase is associated with the spontaneous breaking of a discrete $\mathbb{Z}_2$ symmetry and thus describes interaction-driven quantum phase transitions into one of two symmetry-related gapped states. In lattice realizations, this universality class is most commonly associated with charge-density-wave or sublattice-polarized insulating phases in Dirac systems, for instance on the honeycomb lattice, where the ordered state breaks an Ising-like sublattice symmetry [4]. Because of its particularly simple structure, the GNI model provides the most elementary example in our analysis and will therefore be discussed first.

(2) Gross-Neveu-XY model. The Gross-Neveu-XY (GNXY) model is associated with a two-component real order parameter, or equivalently a complex scalar field. Its ordered phase is characterized by the spontaneous breaking of a continuous $U(1) \simeq O(2)$ symmetry and thus describes interaction-driven quantum phase transitions in which two symmetry-related mass components combine into a planar order parameter with a phase degree of freedom. In condensed-matter realizations, this universality class is relevant, for example, to superconducting criticality in graphene [32], to the Kekulé valence-bond solid transition, where the microscopic order parameter is complex but subject to a discrete $\mathbb{Z}_3$ anisotropy [33–35], and to the semimetal-to-insulator transition associated with intervalley-coherent ordering in twisted bilayer graphene [18]. Owing to the presence of two coupled order-parameter components and the possibility of emergent continuous symmetry, the GNXY model exhibits a richer critical structure than the Ising case.

(3) Gross-Neveu-Heisenberg model. The Gross-Neveu-Heisenberg (GNH) model is associated with a three-component vector order parameter and describes Dirac fermions coupled to a mass channel with continuous $SU(2) \simeq O(3)$ [1] symmetry. Its ordered phase is characterized by the spontaneous breaking of spin-rotation symmetry, such that the system selects a direction in a three-dimensional internal space. In condensed-matter realizations, the most prominent

[1] Strictly speaking, one has $SU(2)/\mathbb{Z}_2 \cong SO(3)$, so the identification with $O(3)$ is understood at the level of the connected rotation symmetry acting on the order parameter. The Dirac fermions transform in the fundamental representation of $SU(2)$, while the real three-component order parameter transforms in the vector representation of $SO(3)$.

example is the interaction-driven transition from a Dirac semimetal to an antiferromagnetic insulating state on the honeycomb lattice, where the three order-parameter components form the Néel vector [4, 6, 20]. Related realizations have also been discussed in Bernal-stacked honeycomb bilayers [36], and more recently in moiré Dirac systems. In particular, a continuous semimetal-to-antiferromagnetic-insulator transition in ABBA-stacked twisted double bilayer transition-metal dichalcogenides has been identified as another realization of $(2+1)$-dimensional Gross-Neveu-Heisenberg criticality [37].
In the following, we specify the corresponding purely fermionic interaction terms $\mathcal{L}_{\text{int}}$ for each model and analyze their renormalization-group flows in detail.

2.1 Gross-Neveu-Ising model

As a starting point, we consider the simplest member of the Gross-Neveu family, namely the Gross-Neveu-Ising model. In a purely fermionic formulation, it is defined by a local four-fermion interaction in a single real scalar mass channel,

$$\mathcal{L}_{\text{Ising}} = \bar{\psi}^{\alpha}\gamma_{\mu}\partial_{\mu}\psi^{\alpha} + \frac{g}{2N_f}\left(\bar{\psi}^{\alpha}\psi^{\alpha}\right)^2. \tag{2.3}$$

This model is the simplest example of an interaction-driven Dirac critical theory and is often referred to as the *chiral Ising* Gross-Neveu model. In the reducible four-component formulation adopted here, it describes a single scalar ordering tendency and thus provides the most elementary setting for spontaneous mass generation in a Dirac system.
We choose a reducible four-dimensional representation of the Euclidean Clifford algebra [32], in which the gamma matrices satisfy

$$\{\gamma_{\mu}, \gamma_{\nu}\} = 2\delta_{\mu\nu}\mathbb{1}_4, \tag{2.4}$$

with

$$\gamma_0 = \mathbb{1}_2 \otimes \sigma_z, \qquad \gamma_1 = \sigma_z \otimes \sigma_y, \qquad \gamma_2 = \mathbb{1}_2 \otimes \sigma_x, \tag{2.5}$$

and two further Hermitian matrices

$$\gamma_3 = \sigma_x \otimes \sigma_y, \qquad \gamma_5 = \sigma_y \otimes \sigma_y, \tag{2.6}$$

which anticommute with all γ_{μ} and satisfy

$$\gamma_3^2 = \gamma_5^2 = \mathbb{1}_4. \tag{2.7}$$

This reducible representation is particularly useful in $2+1$ dimensions, since it allows one to define additional matrices beyond the minimal Clifford algebra and thereby makes the chiral

structure of the model manifest.
The scalar fermion bilinear

$$\sigma \equiv \bar{\psi}^{\alpha}\psi^{\alpha} \tag{2.8}$$

changes sign under the discrete chiral transformation

$$\psi^{\alpha} \to \gamma_5\psi^{\alpha}, \qquad \bar{\psi}^{\alpha} \to -\bar{\psi}^{\alpha}\gamma_5. \tag{2.9}$$

Accordingly, the interaction term in Eq. (2.3) is invariant, whereas the scalar bilinear itself is odd under the $\mathbb{Z}_2$ symmetry. A nonvanishing expectation value $\langle\sigma\rangle \neq 0$ therefore signals spontaneous breaking of the discrete chiral symmetry and corresponds to dynamical mass generation for the Dirac fermions. In microscopic realizations, this universality class is commonly associated with transitions into discrete-symmetry-breaking insulating states, such as charge-density-wave or sublattice-polarized phases.
From the renormalization-group point of view, the GNI model already exhibits the basic structural feature of Gross-Neveu theories. In the simplest pointlike truncation, the flow is controlled by a single dimensionless coupling and exhibits, besides the Gaussian fixed point, a non-Gaussian interacting fixed point that governs the continuous quantum phase transition between the gapless Dirac semimetal and the symmetry-broken massive phase. For bare coupling above the critical value, the scalar channel becomes critical and the flow is driven toward spontaneous chiral symmetry breaking.
The same ordering channel may also be reformulated by means of a Hubbard-Stratonovich transformation, which introduces a real scalar bosonic field σ and maps the four-fermion interaction onto a Yukawa theory. This partially bosonized representation is often advantageous for describing the ordered regime and the associated collective fluctuations. This is deferred to Sec. 4. In the present section we remain within the purely fermionic formulation and use it as the starting point for the subsequent RG analysis.

2.2 Gross-Neveu-XY model

2.2.1 Microscopic action

We next turn to the Gross-Neveu-XY model, which describes a four-fermion interaction in a two-component mass channel. In a purely fermionic formulation, the model is defined in D Euclidean space-time dimensions by the microscopic action $S = \int \mathrm{d}^D x\, \mathcal{L}$ with

$$\mathcal{L} = \bar{\psi}^{\alpha}\gamma_{\mu}\partial_{\mu}\psi^{\alpha} + \frac{g}{2N_f}\left[\left(\bar{\psi}^{\alpha}\gamma_3\psi^{\alpha}\right)^2 + \left(\bar{\psi}^{\alpha}\gamma_5\psi^{\alpha}\right)^2\right]. \tag{2.10}$$

Here, $\mu = 0, \ldots, D-1$ denotes the space-time index, $\alpha = 1, \ldots, N_f$ the flavor index, and $\bar{\psi} = \psi^{\dagger}\gamma_0$ the Dirac conjugate spinor. In the following, our main interest is the physically

relevant case $D = 2+1$. In the reducible four-component representation introduced above, the matrices γ_3 and γ_5 define two independent mass bilinears, which together form the microscopic interaction channel characteristic of the GNXY model.

In contrast to the Gross-Neveu-Ising model, which involves only a single real scalar mass channel, the GNXY model is associated with a two-component order parameter. The corresponding fermion bilinears can be grouped into the real doublet

$$\boldsymbol{\phi} \equiv \mathrm{i}\big(\bar{\psi}^{\alpha}\gamma_3\psi^{\alpha},\, \bar{\psi}^{\alpha}\gamma_5\psi^{\alpha}\big)^{T}, \tag{2.11}$$

which transforms as an $O(2)$ vector in the internal order-parameter space. Accordingly, the ordered phase described by this model is characterized by spontaneous breaking of a continuous $U(1) \simeq O(2)$ symmetry. From the low-energy point of view, the GNXY model therefore provides the natural purely fermionic description of Dirac quantum critical points in which two symmetry-related mass components compete on equal footing and combine into a planar order parameter with a phase degree of freedom.

This universality class is of direct relevance to several physically important realizations of interacting Dirac fermions. For $N_f = 2$, the above theory has been identified with the continuous transition from a Dirac semimetal to a Kekulé valence-bond-solid state on the honeycomb lattice [7, 8]. Although the microscopic Kekulé order parameter is subject to a discrete $\mathbb{Z}_3$ anisotropy, it has been argued that this anisotropy becomes irrelevant at criticality, such that the transition exhibits an emergent $U(1)$ symmetry and falls into the Gross-Neveu-XY universality class [7, 8, 38]. For $N_f = 4$, the same field-theoretic structure has been proposed to describe the twist-tuned transition toward Kramers intervalley-coherent order in moiré bilayer graphene [18, 19]. In this sense, the GNXY model provides a unified field-theoretic framework for discussing quantum critical behavior in rather different microscopic systems that nevertheless share the same two-component Dirac mass structure at low energies. In Sec. 3, we will further examine within our RG analysis whether such an emergent $U(1)$ symmetry indeed arises at criticality.

Another important distinction from the Ising case is that the interaction term in Eq. (2.10) is generically not closed under renormalization-group transformations. While the microscopic action starts from the two-component mass channel alone, additional local four-fermion operators compatible with the same symmetries are in general generated along the RG flow near the lower critical dimension. This feature makes the GNXY problem structurally richer than the GNI model and implies that a proper RG analysis cannot, in general, be restricted to the single coupling g appearing in the microscopic Lagrangian. Instead, one must embed Eq. (2.10) into a larger theory space containing all symmetry-allowed local four-fermion interaction terms, and only within this enlarged theory space can one formulate a Fierz-complete and RG-consistent description of the Gross-Neveu-XY criticality.

The resulting fixed-point structure is correspondingly more intricate. In particular, a recent

analysis based on the $2+\epsilon$ expansion [5] showed that close to the lower critical dimension the Gross-Neveu-XY fixed point is stable only above a critical flavor number N_f^c, whereas for smaller flavor number a different quantum critical fixed point may govern a generic transition with broken $U(1)$ symmetry. This observation further underlines that, for the GNXY case, the symmetry characterization of the model and the construction of the full fermionic theory space are essential prerequisites for a controlled RG treatment.

Therefore, as a prerequisite for the subsequent RG analysis, we first specify the symmetry constraints defining the model and, on this basis, systematically identify all local four-fermion interaction operators allowed by these symmetries. We then incorporate these operators into a Gross-Neveu-XY theory space that is self-consistently closed in the RG sense, providing a unified starting point for deriving the RG flow equations and analyzing the fixed-point structure.

2.2.2 Symmetries

To find all symmetry-allowed interactions, we first list the symmetries preserved by the Gross-Neveu-XY model.

a. Relativistic symmetry. In three Euclidean space-time dimensions, the space-time coordinate $x = (x_\mu)$ transforms as $x^\mu \mapsto (x')^\mu = (\Lambda^{-1})^\mu{}_\nu x^\nu$, with Λ being the generator of the three-dimensional rotation. The Dirac spinors transform as

$$\psi(x) \mapsto \mathrm{e}^{-\frac{\mathrm{i}}{4}\omega_{\mu\nu}\gamma_{\mu\nu}}\psi(x'), \quad \bar{\psi}(x) \mapsto \bar{\psi}(x')\mathrm{e}^{\frac{\mathrm{i}}{4}\omega_{\mu\nu}\gamma_{\mu\nu}} \tag{2.12}$$

where $\gamma_{\mu\nu} = \frac{\mathrm{i}}{2}[\gamma_\mu, \gamma_\nu]$ and $\omega_{\mu\nu}$ is an antisymmetric tensor defining the rotation axis and angle in $(2+1)$-dimensional space-time.

b. Flavor symmetry.

$$\psi^\alpha \mapsto U^{\alpha\beta}\psi^\beta, \quad \bar{\psi}^\alpha \mapsto \bar{\psi}^\beta (U^\dagger)^{\beta\alpha} \tag{2.13}$$

with the unitary matrix $U \in \mathrm{SU}(N_f)$.

c. U(1) charge conservation.

$$\psi^\alpha \mapsto \mathrm{e}^{\mathrm{i}\varphi}\psi^\alpha \tag{2.14}$$

with possibly flavor-dependent angle $\varphi \equiv \varphi_\alpha$.

d. U(1) continuous chiral symmetry. The Gross-Neveu-XY model is invariant under the continuous chiral $U(1)$ symmetry:

$$\psi^\alpha \mapsto \mathrm{e}^{\mathrm{i}\theta\gamma_{35}}\psi^\alpha, \quad \psi^\alpha \mapsto \bar{\psi}^\alpha \mathrm{e}^{-\mathrm{i}\theta\gamma_{35}} \tag{2.15}$$

where $\theta \equiv \theta_\alpha$ may depend on the flavor index, and $\gamma_{35} = \mathrm{i}\gamma_3\gamma_5$. Under this transformation, the real two-tuple $\vec{\varphi} = \mathrm{i}(\bar{\psi}^\alpha\gamma_3\psi^\alpha, \bar{\psi}^\alpha\gamma_5\psi^\alpha)^T$ transforms as an $O(2)$ vector.

e. $\mathbb{Z}_2$ *chiral symmetry.*

$$\psi^\alpha \mapsto \gamma_5 \psi^\alpha, \quad \bar{\psi}^\alpha \mapsto -\bar{\psi}^\alpha \gamma_5 \tag{2.16}$$

In the following, this discrete symmetry is denoted by $\mathbb{Z}_2^5 = \{\mathbb{1}, \gamma_5\}$. Combining the $\mathbb{Z}_2^5$ transformation with $e^{i\frac{\pi}{2}\gamma_{35}} \in U(1)$ chiral symmetry, leads us to another discrete chiral symmetry $\mathbb{Z}_2^3$:

$$\psi^\alpha \mapsto \gamma_3 \psi^\alpha, \quad \bar{\psi}^\alpha \mapsto -\bar{\psi}^\alpha \gamma_3 \tag{2.17}$$

f. Parity inversion symmetry. Parity transformation is defined by inverting one spatial coordinate, $x = (x_0, x_1, x_2) \mapsto P_1(x) = x' = (x_0, -x_1, x_2)$,

$$\psi^\alpha(x) \mapsto i\gamma_1\gamma_5 \psi^\alpha(x'), \quad \bar{\psi}^\alpha(x) \mapsto \bar{\psi}^\alpha(x') i\gamma_1\gamma_5 \tag{2.18}$$

Combining P_1, $\mathbb{Z}_2^5$ and the relativistic symmetry with $\omega_{\mu\nu} = \pi(\delta_{\mu 1}\delta_{\nu 2} - \delta_{\mu 2}\delta_{\nu 1})$, another parity transformation that inverses x_2 can be obtained:

$$\psi^\alpha \mapsto \gamma_2 \psi^\alpha, \quad \bar{\psi}^\alpha \mapsto \bar{\psi}^\alpha \gamma_2 \tag{2.19}$$

g. Time-reversal symmetry. Under Euclidean time-reversal symmetry, we have

$$\psi^\alpha(x) \mapsto \mathcal{T} \psi^\alpha(x) \tag{2.20}$$

with the time-reversal operator $\mathcal{T} = i\gamma_1\gamma_5\mathcal{K}$, where $\mathcal{K}$ denotes complex conjugation.

Symmetry-allowed operators

For fermion bilinear terms, relativistic, charge conservation, and flavor symmetries necessitate ensures the form $\bar{\psi}^\alpha \mathcal{O} \psi^\alpha$ with a 4×4 matrix $\mathcal{O}$. A basis in the 16-dimensional space of 4×4 operators is given by the gamma matrices and their products:

$$\mathcal{O} \in \{\mathbb{1}_4, \gamma_\mu, \gamma_3, \gamma_5, \gamma_{\mu\nu}, i\gamma_\mu\gamma_3, i\gamma_\mu\gamma_5, \gamma_{35}\}\,.$$

No fermion bilinears are allowed by symmetry, only terms with $\mathcal{O} \in \{\mathbb{1}_4, \gamma_3, \gamma_5, \gamma_{35}\}$ are Lorentz-invariant, and only γ_{35} anticommutes with both γ_3 and γ_5, but it does not commute with $i\gamma_1\gamma_5$, such that $\bar{\psi}\gamma_{35}\psi$ is not invariant under time reversal.
For four-fermion terms, there are two types of terms known as singlet and nonsinglet flavor structures: $(\bar{\psi}^\alpha \mathcal{O} \psi^\alpha)(\bar{\psi}^\beta \mathcal{Q} \psi^\beta)$ and $(\bar{\psi}^\alpha \mathcal{O} \psi^\beta)(\bar{\psi}^\beta \mathcal{Q} \psi^\alpha)$. Using Fierz identities, the latter (nonsinglet) can always be rewritten as a linear combination of the former[2] [31]. Therefore, a complete Fierz basis can be constructed using only flavor singlet structure. And since no two bilinear terms share the same transformation properties under all symmetries, only the four-

[2]Similarly, terms of the form $(\psi^T O \psi)(\bar{\psi} Q \bar{\psi}^T)$ can be rewrittens in terms of the former by means of Fierz identities.

fermion terms with $\mathcal{O} = \mathcal{Q}$ can remain invariant under all symmetries. This leaves only 16 possible four-fermion terms. When further considering symmetry constraints, some of these terms can only appear in specific combinations. First, terms with $\mathcal{O} = \gamma_\mu,\ \mu = 0,1,2$ are Lorentz vectors, so they can only appear in the invariant combination $\sum_\mu(\bar{\psi}^\alpha\gamma_\mu\psi^\alpha)^2$, the same applies to $\mathcal{O} = \gamma_\mu\gamma_3$ and $\mathcal{O} = \gamma_\mu\gamma_5$. Terms with $\mathcal{O} = \gamma_{\mu\nu}$ are Lorentz tensors, and thus invariants can only be constructed in the combination $\sum_{\mu<\nu}(\bar{\psi}^\alpha\gamma_{\mu\nu}\psi^\alpha)^2$. Additionally, under the continuous chiral symmetry, $\vec{\varphi} = \mathrm{i}(\bar{\psi}^\alpha\gamma_3\psi^\alpha, \bar{\psi}^\alpha\gamma_5\psi^\alpha)^T$ transforms like a two-dimensional vector. Therefore, the terms with $\mathcal{O} = \gamma_3$ and $\mathcal{O} = \gamma_5$ can only appear in the combination $(\bar{\psi}^\alpha\gamma_3\psi^\alpha)^2 + (\bar{\psi}^\alpha\gamma_5\psi)^2$, the same applies to $\mathcal{O} = \gamma_\mu\gamma_3$ and $\mathcal{O} = \gamma_\mu\gamma_5$. In summary, the symmetry-allowed four-fermion terms in a Fierz-complete basis for the $(2+1)$-dimensional Gross-Neveu-XY model consist of the following six terms:

$$\begin{aligned}\mathcal{L}_{\text{int}} =& \frac{g_1}{2N_f}(\bar{\psi}\psi)^2 + \frac{g_2}{2N_f}(\bar{\psi}\gamma_\mu\psi)^2 + \frac{g_3}{2N_f}\left[(\bar{\psi}\gamma_3\psi)^2 + (\bar{\psi}\gamma_5\psi)^2\right] \\ &+ \frac{g_4}{2N_f}(\bar{\psi}\gamma_{\mu\nu}\psi)^2 + \frac{g_5}{2N_f}\left[(\bar{\psi}\gamma_{\mu 3}\psi)^2 + (\bar{\psi}\gamma_{\mu 5}\psi)^2\right] + \frac{g_6}{2N_f}(\bar{\psi}\gamma_{35}\psi)^2\end{aligned} \tag{2.21}$$

2.3 Gross-Neveu-Heisenberg model

2.3.1 Microscopic action

The final model we consider is the Gross-Neveu-Heisenberg model, which corresponds to a four-fermion interaction in a three-component vector mass channel. In the purely fermionic formulation, its Euclidean Lagrangian is given by

$$\mathcal{L}_{\text{H}} = \bar{\psi}^\alpha(\tau_\mu \otimes \mathbb{1}_2)\partial_\mu\psi^\alpha + \frac{g}{2N_f}\left[\bar{\psi}^\alpha(\mathbb{1}_2 \otimes \vec{\sigma})\psi^\alpha\right]^2, \tag{2.22}$$

where in $D = 2+1$ space-time dimensions the index $\mu = 0,1,2$, the vector $\vec{\sigma} = (\sigma_x, \sigma_y, \sigma_z)$ denotes the Pauli matrices acting in spin space, and the Dirac conjugate field is defined as

$$\bar{\psi}^\alpha = (\psi^\alpha)^\dagger(\tau_0 \otimes \mathbb{1}_2). \tag{2.23}$$

Throughout this subsection, we employ an irreducible two-dimensional representation of the Clifford algebra in the space-time sector, for example

$$\tau_0 = \sigma_y, \qquad \tau_1 = \sigma_x, \qquad \tau_2 = \sigma_z. \tag{2.24}$$

The GNH model is associated with a three-component order parameter transforming as an $SU(2) \simeq O(3)$ vector. The corresponding fermion bilinear

$$\vec{n} \equiv \bar{\psi}^\alpha(\mathbb{1}_2 \otimes \vec{\sigma})\psi^\alpha \tag{2.25}$$

therefore plays the role of a vector order parameter in the internal spin space. A nonvanishing expectation value $\langle \vec{n} \rangle \neq 0$ signals spontaneous breaking of the continuous spin-rotation symmetry and dynamically generates a mass gap for the Dirac fermions. From the physical point of view, the GNH universality class thus provides the natural field-theoretic description of interaction-driven transitions from a Dirac semimetal into an antiferromagnetic insulating phase.

This universality class has long been discussed in the context of correlated Dirac systems on the honeycomb lattice, where the transition between the semimetallic phase and the Néel antiferromagnet is expected to be governed by Gross-Neveu-Heisenberg criticality [4, 6, 20]. In the $(2+1)$-dimensional realization relevant to the single-layer honeycomb lattice, one has $N_f = 2$ four-component Dirac fermions. More generally, the same universality class can also arise in systems with a larger number of low-energy Dirac flavors, depending on the microscopic band structure and symmetry setting.

Beyond these more conventional lattice realizations, recent work has shown that GNH criticality also emerges in moiré Dirac materials. In particular, ABBA-stacked twisted double bilayer transition metal dichalcogenides provide a concrete example in which the noninteracting system hosts a Dirac semimetal with two gapless Dirac cones and an effective low-energy $SU(2)$ spin symmetry. By tuning the twist angle or applying pressure, the system can undergo a continuous transition into an antiferromagnetic insulator, and the corresponding quantum critical point has been identified as belonging to the $(2+1)$-dimensional relativistic Gross-Neveu-Heisenberg universality class with $N_f = 2$ four-component Dirac fermions [37]. This provides a particularly direct and experimentally relevant[39] realization of the GNH scenario in a modern moiré setting.

From the renormalization-group point of view, the GNH model is structurally richer than the GNI case. As in the Gross-Neveu-XY model, the microscopic four-fermion interaction in Eq. (2.22) is not closed under RG transformations. Already near the lower critical spacetime dimension, fermionic fluctuations generate additional local four-fermion operators compatible with the same symmetries. Consequently, a consistent RG treatment cannot be restricted to the single coupling g appearing in the microscopic Lagrangian. Instead, the Gross-Neveu-Heisenberg model must be embedded into a larger fermionic theory space containing all symmetry-allowed interaction channels. In the analysis around the lower critical dimension, this enlarged theory space is Fierz-complete and is spanned, after Fierz reduction, by six independent four-fermion couplings[23]. In the following, we carry out an analogous symmetry analysis adapted to $2+1$ dimensions.

2.3.2 Symmetries and symmetry-allowed operators

The full set of symmetries imposed in this case is as follows:

a. Relativistic symmetry. Similar to the definition in Sec. 2.2.2, but here we use $\tau_{\mu\nu} =$

$-\varepsilon_{\mu\nu\rho}\tau_\rho \otimes \mathbb{1}_2$ instead of $\gamma_{\mu\nu}$.

$$\psi(x) \mapsto \mathrm{e}^{-\frac{\mathrm{i}}{4}\omega_{\mu\nu}\tau_{\mu\nu}}\psi(x'), \quad \bar{\psi}(x) \mapsto \bar{\psi}(x')\mathrm{e}^{\frac{\mathrm{i}}{4}\omega_{\mu\nu}\tau_{\mu\nu}} \tag{2.26}$$

b. Flavor symmetry. Exactly the same as in Sec. 2.2.2.

$$\psi^\alpha \mapsto U^{\alpha\beta}\psi^\beta, \quad \bar{\psi}^\alpha \mapsto \bar{\psi}^\beta (U^\dagger)^{\beta\alpha} \tag{2.27}$$

with the unitary matrix $U \in \mathrm{SU}(N_f)$.
c. SU(2) spin symmetry.

$$\psi^\alpha \mapsto \mathrm{e}^{\mathrm{i}\phi\vec{n}\cdot(\mathbb{1}_2\otimes\vec{\sigma})}\psi^\alpha, \quad \bar{\psi}^\alpha \mapsto \bar{\psi}^\alpha \mathrm{e}^{-\mathrm{i}\phi\vec{n}\cdot(\mathbb{1}_2\otimes\vec{\sigma})} \tag{2.28}$$

Here, $\phi \in [0, 2\pi)$ denotes the rotation angle, and $\vec{n} \in \mathbb{R}^3$ is a real unit vector specifying the rotation axis in spin space. Under this symmetry operation, the order parameter $\bar{\psi}^\alpha(\mathbb{1}_2 \otimes \vec{\sigma})\psi^\alpha$ transforms as a vector.
d. Time-reversal symmetry

$$\psi^\alpha(x) \mapsto \mathcal{T}\psi^\alpha(x), \tag{2.29}$$

with the time-reversal operator $\mathcal{T} = \mathrm{i}(\tau_0 \otimes \sigma_y)\mathcal{K}$, where $\mathcal{K}$ denotes complex conjugation.
e. Parity inversion symmetry

$$\psi(x_0, x_1, x_2) \mapsto (\tau_1 \otimes \mathbb{1}_2)\psi(x_0, -x_1, x_2) \tag{2.30}$$

$$\psi(x_0, x_1, x_2) \mapsto (\tau_2 \otimes \mathbb{1}_2)\psi(x_0, x_1, -x_2) \tag{2.31}$$

Note that the mass term $\bar{\psi}(\mathbb{1}_2 \otimes \mathbb{1}_2)\psi$ is odd under both parity transformations.

There is no fermion bilinear term that remains invariant under all of the symmetry transformations specified above. Consequently, the lowest-order symmetry-allowed perturbations must start at the level of four-fermion interactions. Moreover, flavor symmetry implies that it is sufficient to restrict to flavor-singlet four-fermion operators, i.e., interaction terms built from bilinears of the form $(\bar{\psi}\mathcal{O}\psi)$, leading to operators of the form $(\bar{\psi}\mathcal{O}\psi)^2$. To enumerate these interactions systematically, we choose a 16-dimensional basis of 4×4 matrix operators given by:

$$\mathcal{O} \in \{\mathbb{1}_2, \tau_\mu\} \otimes \{\mathbb{1}_2, \vec{\sigma}\} \tag{2.32}$$

All bilinear interactions $\bar{\psi}\mathcal{O}\psi$ with $\mathcal{O} \in (X \otimes \vec{\sigma})$ transform as three-dimensional vectors under Lorentz transformations. Likewise, all bilinears with $\mathcal{O} \in (\tau_\mu \otimes Y)$ transform as three-dimensional vectors under $SU(2)$ rotations. Therefore, by contracting the corresponding Lorentz and spin $SU(2)$ indices in an invariant manner, one can pair these vector-like bilinears to construct four-fermion interactions that respect both Lorentz symmetry and the $SU(2)$

spin symmetry. Starting from the chosen Fierz-complete basis, the symmetry-compatible four-fermion interactions of the $(2+1)$-dimensional Gross-Neveu-Heisenberg model that are closed in the RG sense can be reduced to the following four independent terms:

$$\begin{aligned}\mathcal{L}_{\text{int}}^{(\text{H})} =& \frac{g_1}{2N_f}(\bar{\psi}^\alpha(\mathbb{1}_2 \otimes \mathbb{1}_2)\psi^\alpha)^2 + \frac{g_2}{2N_f}(\bar{\psi}^\alpha(\tau_\mu \otimes \mathbb{1}_2)\psi^\alpha)^2 \\ &+ \frac{g_3}{2N_f}(\bar{\psi}^\alpha(\mathbb{1}_2 \otimes \vec{\sigma})\psi^\alpha)^2 + \frac{g_4}{2N_f}(\bar{\psi}^\alpha(\tau_\mu \otimes \vec{\sigma})\psi^\alpha)^2\end{aligned} \tag{2.33}$$

3 Fermionic renormalization group

We now turn to the perturbative renormalization-group analysis of the symmetry-complete purely fermionic theory spaces constructed in Sec. 2. Our goal is to derive the one-loop flow equations for all independent local four-fermion couplings and, on this basis, to analyze the fixed-point structure associated with the Gross-Neveu-Ising, Gross-Neveu-XY, and Gross-Neveu-Heisenberg models. Since the latter two are not closed under RG transformations in the purely fermionic formulation, it is necessary to formulate the flow in the full operator space allowed by symmetry, rather than restricting the analysis to the microscopic interaction channel explicitly present in the bare action.

We consider the Euclidean action

$$S = \int \mathrm{d}^D x \Big(\mathcal{L}_0 + \mathcal{L}_{\mathrm{int}} \Big), \tag{3.1}$$

where $\mathcal{L}_0 = \bar{\psi}^\alpha \gamma_\mu \partial_\mu \psi^\alpha$ denotes the free Dirac part, while $\mathcal{L}_{\mathrm{int}}$ contains all four-fermion interaction terms spanning the corresponding symmetry-complete theory space. Throughout this section, we work directly in $D = 2 + 1$ dimensions and employ a momentum-shell Wilson RG scheme [40–42]. More specifically, we decompose the fermion fields into slow and fast modes according to their momenta, and perturbatively integrate out the fast modes within the infinitesimal shell $\Lambda e^{-\mathrm{d}t} < |q| < \Lambda$ to one-loop order. The resulting effective action is then expanded in local operators and projected back onto the chosen basis of four-fermion interactions.

At one-loop order, the renormalization of the quartic couplings is generated by one-particle-irreducible (1PI) four-fermion diagrams. These arise from contracting two interaction vertices with fast fermion propagators. By evaluating these loop contributions and matching the generated local four-fermion operators onto the basis defined in Sec. 2, we obtain the beta functions for the dimensionless couplings g_a,

$$\beta_a \equiv -\partial_t g_a. \tag{3.2}$$

The resulting RG flow encodes both the canonical scaling of the couplings and the fluctuation-induced mixing between different interaction channels under coarse graining. The latter is particularly important in the XY and Heisenberg cases, where different channels are already coupled at one-loop order and the RG flow generally leaves the microscopic subspace.

Technically, the calculation may be summarized as follows: we evaluate the one-loop four-fermion Feynman diagrams in the pointlike approximation and then reduce the generated operator products to the chosen basis. This procedure provides a direct Wilsonian derivation of the RG flow equations in the purely fermionic formulation. To ensure the reliability of the results, we independently cross-check the final expressions against the general projection formulas given in [31]. The agreement between the two methods provides a nontrivial validation of the resulting beta functions.

The flow equations derived below form the basis for the subsequent fixed-point analysis. In particular, they allow us, within the one-loop approximation, to determine the number of relevant directions associated with each fixed point, thereby identifying the quantum critical fixed points that can govern continuous phase transitions, as well as revealing more intricate scenarios such as possible fixed-point collisions. In the following subsections, we present the beta functions for the Gross-Neveu-Ising, Gross-Neveu-XY, and Gross-Neveu-Heisenberg models in turn.

3.1 Gross-Neveu-Ising model

We consider the Euclidean GNI Lagrangian:

$$\mathcal{L} = \bar{\psi}^\alpha \gamma_\mu \partial_\mu \psi^\alpha + \frac{g}{2N_f} \left(\bar{\psi}^\alpha \psi^\alpha\right)^2, \qquad \alpha = 1, \ldots, N_f, \quad \mu = 0, 1, 2. \tag{3.3}$$

We use a reducible $d_\gamma = 4$ representation of the Clifford algebra, $\{\gamma_\mu, \gamma_\nu\} = 2\delta_{\mu\nu} \mathbb{1}_4$, so that $\mathrm{Tr}\ \mathbb{1}_4 = d_\gamma = 4$.

3.1.1 RG flow

Fourier convention. With $\psi(x) = \int_p e^{\mathrm{i}p\cdot x} \psi(p)$ and $\int_p \equiv \int d^D p/(2\pi)^D$, one has $\partial_\mu \to \mathrm{i}p_\mu$ in momentum space, hence the Gaussian action is

$$S_0 = \int_p \bar{\psi}^\alpha(-p)\, (\mathrm{i}\not{p})\, \psi^\alpha(p), \qquad \not{p} \equiv \gamma_\mu p_\mu. \tag{3.4}$$

Propagator. The free fermion propagator is therefore

$$\langle \psi_a^\alpha(p)\, \bar{\psi}_b^\beta(p') \rangle_0 = (2\pi)^D \delta^{(D)}(p - p')\, \delta^{\alpha\beta}\, G_{ab}(p), \qquad G(p) = \frac{1}{\mathrm{i}\not{p}} = -\mathrm{i}\, \frac{\not{p}}{p^2}. \tag{3.5}$$

Vertex and operator projection. The interaction is

$$S_{\mathrm{int}} = \int_x \frac{g}{2N_f} (\bar{\psi}_a^\alpha \psi_a^\alpha)(\bar{\psi}_b^\beta \psi_b^\beta). \tag{3.6}$$

In the Wilsonian computation we extract the running of the same local scalar operator $(\bar{\psi}^\alpha\psi^\alpha)^2$; equivalently, in Dirac space we project onto the identity matrix $\mathbb{1}_4$.

Momentum-shell setup and the basic shell integral

We impose a hard UV cutoff Λ and split fields into slow and fast modes, $\psi = \psi_< + \psi_>$, where $\psi_>$ has support only in the thin shell

$$\Lambda/b < |q| < \Lambda, \qquad b > 1, \qquad t \equiv \ln b \ll 1. \tag{3.7}$$

Integrating out $\psi_>$ generates an effective action for $\psi_<$. The leading correction to the four-fermion interaction appears at second order in $S_{\rm int}$:

$$\delta S^{(2)} = -\frac{1}{2!}\big\langle S_{\rm int}^2 \big\rangle_{>,c}, \tag{3.8}$$

where $\langle\cdots\rangle_>$ is the Gaussian average with respect to $S_0[\psi_>]$ and the subscript c denotes connected contractions.

Diagram-by-diagram evaluation of $\delta S^{(2)}$

The cumulant (3.8) generates all one-loop, one-particle-irreducible (1PI) corrections to the four-fermion vertex. Diagrammatically, these arise from inserting two four-fermion vertices from $S_{\rm int}$ and contracting two fermion lines into fast-mode propagators, while keeping four external slow fermion legs. Since we are interested in the running of the *local* contact operator $(\bar{\psi}^\alpha\psi^\alpha)^2$, we evaluate the resulting 1PI four-point function at vanishing external momenta and project it back onto the scalar channel, i.e. onto the Dirac identity $\mathbb{1}_4$ and the flavor contraction pattern in Eq. (3.6).

Concretely, after integrating out the shell modes, the induced local four-fermion term can be written as

$$\delta S^{(2)}_{\rm local} = \int_x \frac{\delta g}{2N_f}\,(\bar{\psi}^\alpha_<\psi^\alpha_<)^2 \;+\; (\text{operators beyond the GNI truncation})^{[1]}. \tag{3.9}$$

Comparing (3.9) with the coefficient of $(\bar{\psi}^\alpha_<\psi^\alpha_<)^2$ generated by the diagrams yields the identification

$$\delta g = 2N_f \times \Big[\text{coefficient of } (\bar{\psi}^\alpha_<\psi^\alpha_<)^2 \text{ in } \delta S^{(2)}_{\rm local}\Big]. \tag{3.10}$$

[1] Here, "operators beyond the present truncation" refer to terms that are not captured by the local Gross-Neveu-Ising ansatz, such as operators with additional derivatives acting on the fermion fields, equivalently momentum-dependent four-fermion vertices, as well as higher-order contributions in a more general derivative expansion. By contrast, at the level of local quartic fermion operators, the scalar interaction channel of the GNI model is closed under the one-loop RG flow: no additional independent pointlike four-fermion structures are generated. Therefore, within the present truncation, the only effect in the local four-fermion sector is the renormalization of the coupling g associated with $(\bar{\psi}^\alpha\psi^\alpha)^2$.

At one loop there are four inequivalent 1PI contraction topologies, shown as Figs. 3.1(a)-(d). We denote their contributions by

$$\delta S^{(2)} = \delta S^{(2)}_{(a)} + \delta S^{(2)}_{(b)} + \delta S^{(2)}_{(c)} + \delta S^{(2)}_{(d)}. \tag{3.11}$$

For each diagram we (i) write down the Wick contraction from (3.8), (ii) evaluate the Dirac structure generated by the two internal propagators (3.5), (iii) perform the thin-shell momentum integral, which reduces to $J_D(\Lambda)$ in Eq. (3.15), and (iv) project onto $(\bar\psi^\alpha\psi^\alpha)^2$ to read off δg via (3.10).

Useful Dirac algebra. Using (3.5), for large loop momentum q one has

$$G(q)G(q) = \frac{1}{\mathrm{i}\not{q}}\frac{1}{\mathrm{i}\not{q}} = (-\mathrm{i})^2\frac{\not{q}\not{q}}{q^4} = -\frac{\mathbb{1}_4}{q^2}, \qquad \mathrm{Tr}[G(q)G(q)] = -\frac{d_\gamma}{q^2}. \tag{3.12}$$

Thin-shell integral.

$$\begin{aligned}\int_{\text{shell}} \frac{\mathrm{d}^D q}{(2\pi)^D} G(q)G(q) &= \int_{\Lambda/b<|q|<\Lambda} \frac{\mathrm{d}^D q}{(2\pi)^D}\left(-\frac{\mathbb{1}_4}{q^2}\right) \\ &\simeq -\mathbb{1}_4 \frac{S_D}{(2\pi)^D}\Lambda^{D-2}\ln b \qquad (\ln b \ll 1), \qquad (3.13)\\ &= -\mathbb{1}_4 \frac{S_D}{(2\pi)^D}\Lambda^{D-2} t \qquad (3.14)\end{aligned}$$

where $S_D = 2\pi^{D/2}/\Gamma(D/2)$ is the surface area of the D-dimensional unit sphere. It is convenient to introduce the standard thin-shell integral

$$J_D(\Lambda) \equiv \frac{S_D}{(2\pi)^D}\Lambda^{D-2} t, \tag{3.15}$$

Diagram (a): closed-fermion-loop (trace) contribution. Fig. 3.1(a) contains a closed fermion loop. Hence it carries the standard fermion-loop minus sign and its Dirac structure appears as a trace. The contribution to the local effective action can be written as

$$\delta S^{(2)}_{(a)} = -\frac{1}{2}\left(\frac{g}{2N_f}\right)^2 \int_{x,y} \left(\bar\psi^\alpha_< \psi^\alpha_<\right)_x \left(\bar\psi^\beta_< \psi^\beta_<\right)_y \Big[(-1)\sum_{\rho=1}^{N_f}\int_{\text{shell}} \frac{\mathrm{d}^D q}{(2\pi)^D}\,\mathrm{Tr}\left(G_\rho(q)\,G_\rho(q)\right)\Big]\,\mathcal{C}_{(a)}. \tag{3.16}$$

Here: (i) the (-1) is the fermion-loop sign, (ii) the flavor sum gives $\sum_\rho 1 = N_f$, (iii) the Dirac structure is a *trace* because the internal fermion line is closed. (iv) $\mathcal{C}_{(a)} = 2\times 2\times 2$ counts the number of distinct Wick contractions that realize topology (a) in the chosen projection. Using

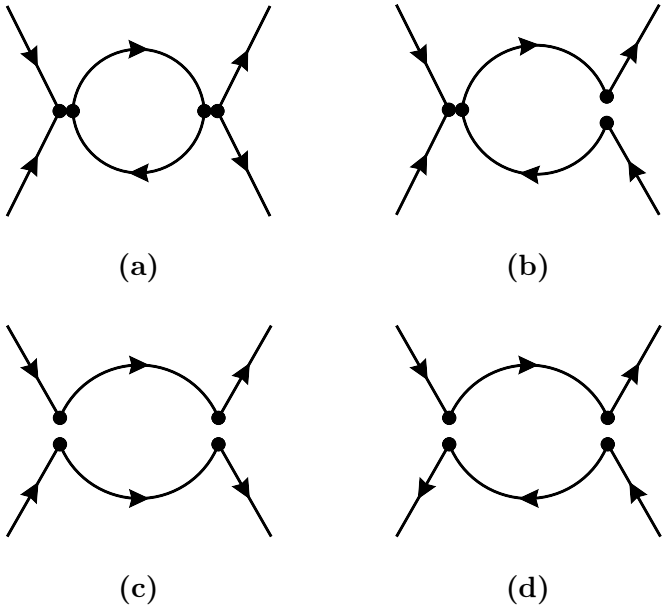

Figure 3.1: One-loop 1PI four-fermion diagrams contributing to the RG flow of the Gross-Neveu-Ising model. The internal lines are fast-mode propagators, while the external legs are slow modes. The four diagrams (a)-(d) correspond to the four inequivalent contraction topologies that contribute to $\delta S^{(2)}$ in Eq. (3.8).

(3.12) and (3.15) gives

$$\sum_{\rho=1}^{N_f} \int_{\text{shell}} \frac{\mathrm{d}^D q}{(2\pi)^D} \, \mathrm{Tr}\left(G_\rho(q) G_\rho(q)\right) = -\, N_f \, d_\gamma \, J_D(\Lambda), \tag{3.17}$$

so that

$$\delta S^{(2)}_{(a)} = -\frac{1}{2}\left(\frac{g}{2N_f}\right)^2 \Big[(+1)\, N_f d_\gamma \, J_D(\Lambda)\Big] \int_x (\bar\psi^\alpha_< \psi^\alpha_<)^2 \, \mathcal{C}_{(a)}. \tag{3.18}$$

Diagram (b): open-line (no-trace) contribution. Fig. 3.1(b) does not form a closed fermion loop. Therefore there is no fermion-loop minus sign and the Dirac structure appears as a matrix product $G(q)G(q)$ acting on external Dirac indices. Projecting onto the scalar channel simply amounts to using (3.12) at the level of matrices,

$$\Big[G(q)G(q)\Big]_{\text{scalar}} = -\frac{1}{q^2}\, \mathbb{1}_4, \qquad \int_{\text{shell}} \frac{\mathrm{d}^D q}{(2\pi)^D} \Big[G(q)G(q)\Big]_{\text{scalar}} = -J_D(\Lambda)\, \mathbb{1}_4. \tag{3.19}$$

Hence

$$\begin{aligned} \delta S^{(2)}_{(b)} =& \frac{-1}{2!}\left(\frac{g}{2N_f}\right)^2 \int_{x,y} \big(\bar\psi^\alpha_< \psi^\alpha_<\big)_x \big(\bar\psi^\beta_< \psi^\beta_<\big)_y \int_{\text{shell}} \frac{\mathrm{d}^D q}{(2\pi)^D}\, G(q)\, G(q) \times C_{(b)} \\ =& -\frac{1}{2}\left(\frac{g}{2N_f}\right)^2 \Big[-J_D(\Lambda)\Big] \int_x (\bar\psi^\alpha_< \psi^\alpha_<)^2 \, \mathcal{C}_{(b)} \end{aligned} \tag{3.20}$$

where $\mathcal{C}_{(b)}$ is the corresponding contraction-counting factor for topology (b).

Diagram (c): open-line contribution. Fig. 3.1(c) contains no closed fermion loop, hence there is no additional fermion-loop minus sign. In the local (zero-external-momentum) projection relevant for the running of $(\bar\psi\psi)^2$, the two internal fast propagators carry momenta $-q$ and q, i.e. the Dirac structure is $G(-q)G(q)$. Using $G(p) = 1/(\mathrm{i}\not{p}) = -\mathrm{i}\not{p}/p^2$, one finds

$$G(-q)G(q) = -\,G(q)G(q) = +\frac{\mathbb{1}_4}{q^2}. \tag{3.21}$$

Therefore the UV-local shell part of diagram (c) is

$$\delta S^{(2)}_{(c)} = -\frac{1}{2}\left(\frac{g}{2N_f}\right)^2 \left[\int_{\text{shell}} \frac{\mathrm{d}^D q}{(2\pi)^D}\,\frac{1}{q^2}\right] \int_x (\bar\psi^\alpha_< \psi^\alpha_<)^2 \times \mathcal{C}_{(c)} \;=\; -\frac{1}{2}\left(\frac{g}{2N_f}\right)^2 J_D(\Lambda) \int_x (\bar\psi^\alpha_< \psi^\alpha_<)^2\, \mathcal{C}_{(c)}. \tag{3.22}$$

Diagram (d): open-line contribution. Fig. 3.1(d) is again an open-line topology. In the same local projection the two internal fast propagators carry momenta q and q, giving the Dirac structure $G(q)G(q)$.

$$G(q)G(q) = -\frac{\mathbb{1}_4}{q^2}, \tag{3.23}$$

so that

$$\begin{aligned} \delta S^{(2)}_{(d)} &= -\,\frac{1}{2}\left(\frac{g}{2N_f}\right)^2 \left[\int_{\text{shell}} \frac{\mathrm{d}^D q}{(2\pi)^D}\left(-\frac{1}{q^2}\right)\right] \int_x (\bar\psi^\alpha_< \psi^\alpha_<)^2 \times \mathcal{C}_{(d)} \\ &= +\,\frac{1}{2}\left(\frac{g}{2N_f}\right)^2 J_D(\Lambda) \int_x (\bar\psi^\alpha_< \psi^\alpha_<)^2\, \mathcal{C}_{(d)}. \end{aligned} \tag{3.24}$$

In the Gross-Neveu-Ising truncation, the two open-line topologies (c) and (d) occur with identical contraction multiplicities, $\mathcal{C}_{(c)} = \mathcal{C}_{(d)}$. Consequently, their logarithmically divergent shell parts cancel,

$$\delta S^{(2)}_{(c)} + \delta S^{(2)}_{(d)} = 0, \tag{3.25}$$

so that diagrams (c) and (d) do not contribute to the one-loop beta function of g in the GNI case. (For the Gross–Neveu–XY and Gross–Neveu–Heisenberg models, the same topologies generate nonvanishing contributions in additional interaction channels.)

Reading off δg and defining the beta function

Collecting (3.18) and (3.20), and using (3.25), the local one-loop correction takes the form

$$\delta S^{(2)}_{\text{local}} = -\frac{1}{2}\left(\frac{g}{2N_f}\right)^2 \left[\mathcal{C}_{(a)}\left(+N_f d_\gamma J_D(\Lambda)\right) + \mathcal{C}_{(b)}\left(-J_D(\Lambda)\right)\right] \int_x (\bar\psi^\alpha_< \psi^\alpha_<)^2. \tag{3.26}$$

Using (3.10), we obtain

$$\delta g = (2N_f) \times \left[-\frac{1}{2} \left(\frac{g}{2N_f} \right)^2 \left(\mathcal{C}_{(a)}\, N_f d_\gamma - \mathcal{C}_{(b)} \right) J_D(\Lambda) \right]. \tag{3.27}$$

For the diagram set (a)–(d) in the $i \neq j$ scattering projection one finds

$$\mathcal{C}_{(a)} = 4, \qquad \mathcal{C}_{(b)} = 8. \tag{3.28}$$

Substituting (3.28) into (3.27) gives

$$\delta g = \left(\frac{2}{N_f} - d_\gamma \right) g^2\, J_D(\Lambda). \tag{3.29}$$

Setting $d_\gamma = 4$ and substituting the expression for J_D from Eq. (3.15) into the above result yields

$$\delta g = \left(\frac{2}{N_f} - 4 \right) g^2 \frac{S_D}{(2\pi)^D} \Lambda^{D-2} t. \tag{3.30}$$

We define the dimensionless coupling by absorbing the universal prefactor and one power of the cutoff,

$$\tilde{g} \equiv \frac{S_3}{(2\pi)^3}\, \Lambda\, g. \tag{3.31}$$

Including the canonical scaling term $(D-2)\tilde{g}$ and using (3.30) with $D = 3$, the one-loop beta function becomes

$$\beta(\tilde{g}) \equiv -\frac{\mathrm{d}\tilde{g}}{\mathrm{d}t} = \tilde{g} - \frac{1}{N_f}(2 - 4N_f)\tilde{g}^{\,2}. \tag{3.32}$$

For simplicity, in what follows we will use g to denote $\tilde{g}$,

$$\beta(g) = g - \frac{1}{N_f}(2 - 4N_f)\, g^2. \tag{3.33}$$

By our sign convention, a positive (negative) β means that the coupling decreases (increases) as the flow proceeds towards the infrared. In the above equation, we neglect contributions from other interaction channels that could in principle be generated perturbatively. This is justified because the scalar interaction channel considered here is closed under the RG flow and therefore does not generate additional channels. This, however, does not mean that other channels would not contribute if present: as we will see for the GNXY and GNH models below, additional symmetry-allowed channels indeed contribute to the coupling g.

3.1.2 Fixed points and linear stability

The fixed points are determined from $\beta(g^*) = 0$, which yields two solutions, namely the Gaussian fixed point at $g^*_{\mathrm{G}} = 0$ and the interacting Gross-Neveu-Ising fixed point at $g^*_{\mathrm{GNI}} =$

$N_f/(2-4N_f)$. The latter satisfies $g^*_{\rm GNI} > 0$ for $N_f > \frac{1}{2}$ (and changes sign for $N_f < \frac{1}{2}$).

To classify the fixed points, we linearize the flow around g^*. With our sign convention (the IR flow follows $\mathrm{d}g/\mathrm{d}t = -\beta$), the stability matrix reduces to $\mathcal{M}(g^*) \equiv \partial_g(\mathrm{d}g/\mathrm{d}t)|_{g^*} = -\beta'(g^*)$ with $\beta'(g) = 1 - 2(\frac{2}{N_f} - 4)g$. Hence one finds $\mathcal{M}(g^*_{\rm G}) = -1 < 0$ and $\mathcal{M}(g^*_{\rm GNI}) = +1 > 0$. Accordingly, the Gaussian fixed point is IR attractive, whereas the interacting GNI fixed point has one IR-repulsive (relevant) direction. In particular, for $N_f > \frac{1}{2}$ and initial conditions $0 < g < g^*_{\rm GNI}$, one has $\beta(g) > 0$ and thus g decreases towards the IR, so the flow is attracted to $g^*_{\rm G} = 0$. By contrast, for initial conditions $g > g^*_{\rm GNI}$, one has $\beta(g) < 0$, such that g increases under the IR flow and runs to strong coupling at a finite RG time. Within the present pointlike truncation, this finite-scale divergence signals the instability of the symmetric Dirac semimetal and indicates the onset of spontaneous symmetry breaking. Therefore, the interacting fixed point $g^*_{\rm GNI}$ plays the role of a quantum critical point separating the symmetric phase from the symmetry-broken phase.

3.2 Gross-Neveu-XY model

We consider the full Gross-Neveu-XY model defined by the action:

$$S = \int \mathrm{d}^D x \, \left(\bar{\psi}^\alpha \gamma_\mu \psi^\alpha + \mathcal{L}_{\rm int}\right) \tag{3.34}$$

To derive the one-loop renormalization-group flow in $D = 3$, we repeat the explicit diagrammatic calculation presented in Sec. 2.1, and verified our results against the general projection formulas of [31]. The resulting RG flow equations are given below.

$$\beta_1 = g_1 - \frac{1}{N_f}\left[(2-4N_f)g_1^2 + 6g_1g_2 + 4g_1g_3 + 6g_1g_4 + 12g_1g_5 + 2g_1g_6 + 8g_2g_4 + 8g_3g_5\right], \tag{3.35}$$

$$\beta_2 = g_2 - \frac{1}{N_f}\left[\frac{1}{3}(4N_f+2)g_2^2 - \frac{2}{3}g_1g_2 + \frac{4}{3}g_2g_3 + \frac{2}{3}g_2g_4 - \frac{4}{3}g_2g_5 + 2g_2g_6 + \frac{8}{3}g_1g_4 + \frac{16}{3}g_3g_5\right], \tag{3.36}$$

$$\beta_3 = g_3 - \frac{1}{N_f}\left[4N_fg_3^2 - 2g_1g_3 + 6g_2g_3 - 2g_3g_4 + 2g_3g_6 + 4g_1g_5 + 8g_2g_5\right], \tag{3.37}$$

$$\beta_4 = g_4 - \frac{1}{N_f}\left[\frac{1}{3}(4N_f+2)g_4^2 + \frac{4}{3}g_3^2 - \frac{4}{3}g_3g_4 + \frac{28}{3}g_5^2 + \frac{8}{3}g_1g_2 - \frac{2}{3}g_1g_4 + \frac{2}{3}g_2g_4 + \frac{4}{3}g_4g_5 + 2g_4g_6\right], \tag{3.38}$$

$$\beta_5 = g_5 - \frac{1}{N_f}\left[-\frac{4}{3}N_fg_5^2 + \frac{2}{3}g_1g_5 + \frac{2}{3}g_2g_5 + \frac{26}{3}g_4g_5 + 2g_5g_6 + \frac{4}{3}g_1g_3 + \frac{8}{3}g_2g_3\right], \tag{3.39}$$

$$\beta_6 = g_6 - \frac{1}{N_f}\left[(2-4N_f)g_6^2 + 4g_2^2 + 6g_2g_6 + 4g_4^2 + 8g_5^2 + 2g_1g_6 - 4g_3g_6 + 6g_4g_6 - 12g_5g_6\right]. \tag{3.40}$$

If we set all couplings except g_1 to zero, i.e.,

$$g_2 = g_3 = g_4 = g_5 = g_6 = 0, \tag{3.41}$$

the flow consistently closes in the g_1 direction and the above system reduces to a single beta function,

$$\beta_1 = g_1 - \frac{1}{N_f}(2-4N_f)\, g_1^2, \qquad \beta_{2,3,4,5,6} = 0, \tag{3.42}$$

which is precisely the renormalization-group flow of the Gross-Neveu-Ising (GNI) model discussed in Sec. 2.1. This implies that the GNI fixed point is also a fixed point in the Gross-Neveu-XY theory space, albeit with additional irrelevant directions. However, the GNI fixed point is not the only fixed point of the Gross-Neveu-XY model, and in particular, it does not correspond to the criticality associated with the spontaneous breaking of the $U(1)$ chiral symmetry. To identify the fixed point describing this criticality, we need to analyze the full system of flow equations.

3.2.1 Fixed-point structure

The topology of the RG flow is determined by the solutions of the fixed-point equations $\beta_i|_{g_i^*} = 0$. In the large-N_f limit, the flow equations for $g_1, \ldots, g_6$ decouple, such that our model admits up to $2^6 = 64$ possible fixed-point solutions. Here we focus on the Gross-Neveu-XY criticality, which is associated with the $U(1)$ order parameter

$$\langle\vec{\varphi}\rangle = \mathrm{i}\big(\langle\bar{\psi}^\alpha\gamma_3\psi^\alpha\rangle, \langle\bar{\psi}^\alpha\gamma_5\psi^\alpha\rangle\big)^T. \tag{3.43}$$

In the $N_f \to \infty$ limit, the corresponding fixed point is located at $(0, 0, \frac{1}{4}, 0, 0, 0)$. Here, we recall that g_3 parametrizes the four-fermion interaction already present in the microscopic Gross-Neveu-XY action, see Eq. (2.21). We therefore parametrize this subspace as

$$\mathcal{XY} = \big(0, 0, a_3, a_4, 0, a_6\big). \tag{3.44}$$

The evolution of the three nonvanishing couplings at this fixed point as a function of N_f is shown in Fig. 3.2(a). To determine its critical properties, we evaluate the eigenvalues Θ_i of the stability matrix $(-\partial\beta_i/\partial g_j)$ at $\mathcal{XY}$. As shown in Fig. 3.2(b), the second-largest eigenvalue changes sign at the critical flavor number $N_f^c = N_f^{(1)} \approx 2.07$. Accordingly, the fixed point $\mathcal{XY}$ possesses a single relevant direction ($\Theta > 0$) for $N_f > N_f^c$, and thus describes the Gross-Neveu-XY universality class in this regime.

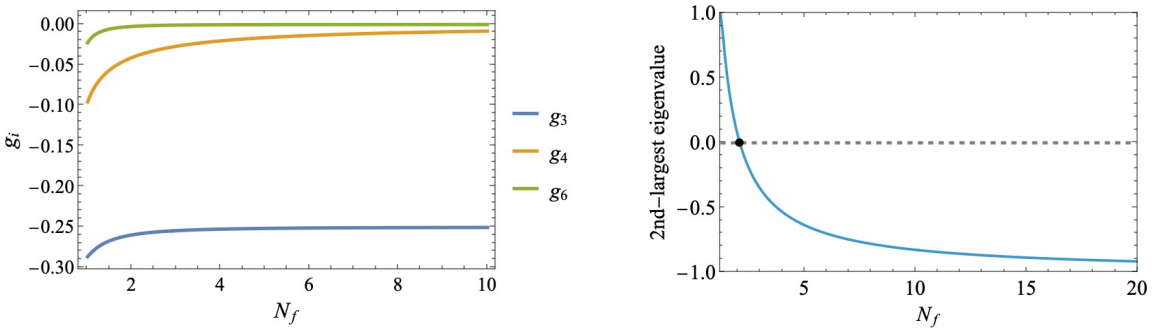

(a) (b)

Figure 3.2: Properties of the Gross-Neveu-XY fixed point as a function of the flavor number N_f. (a) The three nonvanishing couplings g_3, g_4, and g_6 at the Gross-Neveu-XY fixed point. (b) The second-largest eigenvalue of the stability matrix evaluated at the Gross-Neveu-XY fixed point. It changes sign at the critical flavor number $N_f^c \simeq 2.07$.

As N_f approaches N_f^c, $\mathcal{XY}$ collides with another fixed point $\mathcal{B} = (b_1, b_2, b_3, b_4, b_5, b_6)$ and the two fixed points exchange their roles with respect to RG stability, as illustrated in Fig. 3.4. In particular, for $N_f < N_f^c$, $\mathcal{XY}$ has two relevant directions and thus does not represent the critical point, while $\mathcal{B}$ has only one relevant direction and therefore describes the Gross-Neveu-XY universality class in this regime. The fixed point $\mathcal{C}$, which is also shown in Fig. 3.4, has only one relevant direction within the projected subspace spanned by the two leading eigendirections of the stability matrix at each given N_f, but possesses additional relevant direction(s) in the full coupling space and therefore does not represent a critical point.

Likewise, $\mathcal{B}$ collides with a further fixed point as N_f approaches a second critical value $N_f^{(2)} \approx 2.08$, and the pair annihilates into the complex coupling plane for $N_f > N_f^{(2)}$. Two more successive collisions then occur, so that in the large-N_f limit the fixed points $\mathcal{B}$ lie at one of the three locations $\left(-\frac{1}{4}, 0, 0, \frac{3}{4}, -\frac{3}{4}, 0\right)$, $\left(-\frac{1}{4}, 0, 0, 0, -\frac{3}{4}, 0\right)$, $\left(0, 0, \frac{1}{4}, 0, -\frac{3}{4}, 0\right)$, as shown in Fig. 3.3.

3.2.2 Critical Exponents

a. Correlation-length exponent ν

By ordering the eigenvalues of the stability matrix from largest to smallest, the correlation-length exponent ν is determined by $\Theta_1 = 1/\nu$. In $(2+1)$ dimensions, at the Gross-Neveu-XY fixed point we find:

$$\frac{1}{\nu} = 1 \tag{3.45}$$

b. Order-parameter anomalous dimension η_ϕ

Adding an infinitesimal symmetry-breaking term to the effective Lagrangian [23, 43]:

$$\mathcal{L} \mapsto \mathcal{L} + \Delta \bar{\psi}^\alpha \mathcal{M} \psi^\alpha, \tag{3.46}$$

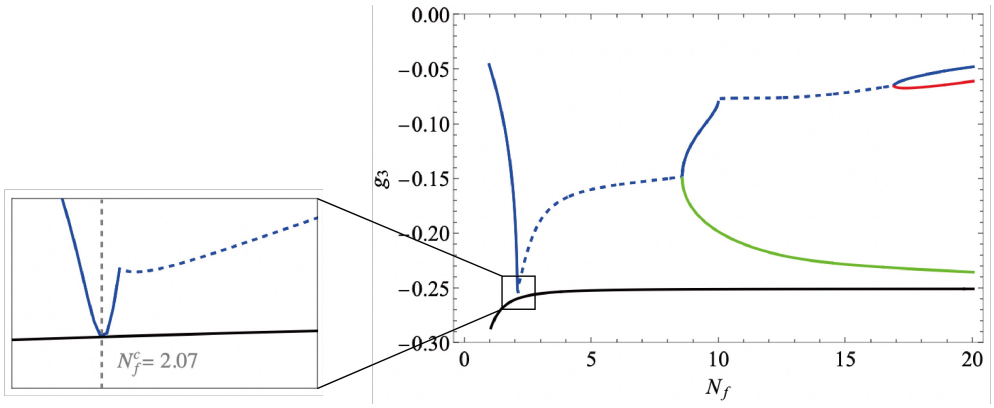

Figure 3.3: Real part of the coupling g_3 along the fixed-point branch $\mathcal{B}$ as a function of N_f. For comparison, the Gross-Neveu-XY fixed point is shown in black. The blue branch collides with the Gross-Neveu-XY fixed point at the critical flavor number N_f^c, where the two fixed points exchange their criticality. Dashed segments mark regions where the branch $\mathcal{B}$ becomes complex, such that only $\mathrm{Re}(g_3)$ is displayed. With increasing N_f, this branch undergoes a sequence of further fixed-point collisions and eventually approaches, in the large-N_f limit, one of the three asymptotic fixed points $(-1/4, 0, 0, 3/4, -3/4, 0)$, $(-1/4, 0, 0, 0, -3/4, 0)$, and $(0, 0, 1/4, 0, -3/4, 0)$.

where $\Delta \in \mathbb{R}$, $\mathcal{M} = \mathbb{1}_4$ for Gross-Neveu-Ising criticality and $\mathcal{M} = \{\gamma_3, \gamma_5\}$ for Gross-Neveu-XY criticality. To derive the RG flow of the mass parameter Δ, we evaluate the contributions of the two Feynman diagrams shown in Fig. 3.5.

As a consistency check, the result can also be recovered from the general one-loop formula given in [23]. The RG flow of Δ then reads

$$\beta_\Delta = -x\Delta + \mathcal{O}(\Delta^2), \quad x = 1 + \sum_i c_i g_i \,, \tag{3.47}$$

where $c_i = -\frac{1}{4DN_f} \sum_\mu \left[N_f \,\mathrm{Tr}(\mathcal{M}\gamma_\mu \mathcal{O}_i \gamma_\mu)\,\mathrm{Tr}(\mathcal{M}\mathcal{O}_i) - \mathrm{Tr}(\mathcal{O}_i \gamma_\mu \mathcal{M} \gamma_\mu \mathcal{O}_i \mathcal{M})\right]$ and $\mathcal{O}_i$ denotes the 4×4 matrix associated with coupling g_i. The susceptibility exponent γ relates to x via

$$\gamma = (2x - D)\nu \,, \tag{3.48}$$

and, combining this with the hyperscaling relation $\eta_\phi = 2 - \gamma/\nu$, we obtain

$$\eta_\phi = D - 2\sum_i c_i g_i^* \,, \tag{3.49}$$

where g_i^* denotes the fixed-point couplings.

Evaluating the matrix algebra for the Gross-Neveu-Ising (GNI) criticality with $\mathcal{M} = \mathbb{1}_4$ and the GNI fixed-point value $g^*_{\mathrm{GNI}} = (N_f/(4N_f - 2), 0, 0, 0, 0, 0)$, yields

$$\eta_\phi^{\mathrm{GNI}} = 1 + \frac{1}{1 - 2N_f} \tag{3.50}$$

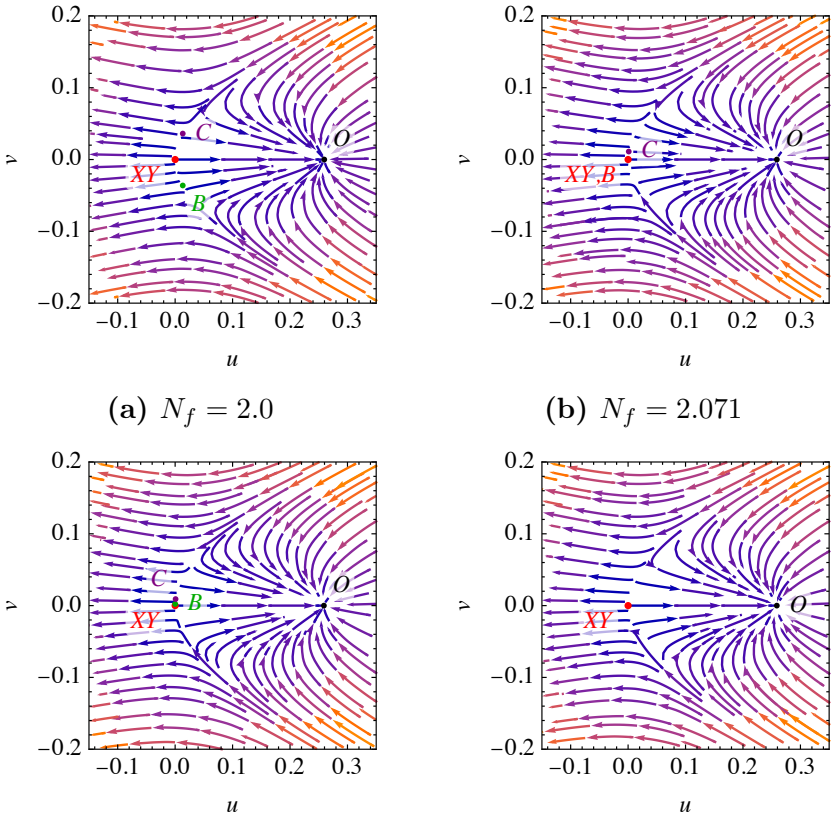

(a) $N_f = 2.0$ **(b)** $N_f = 2.071$

(c) $N_f = 2.073$ **(d)** $N_f = 2.08$

Figure 3.4: Projected RG flow in the (u, ν) plane for several values of N_f in the vicinity of the Gross-Neveu-XY fixed point. Here, u and ν denote the two leading eigendirections of the stability matrix at each given N_f, and the origin is chosen as the projection of the Gross-Neveu-XY fixed point. The point O denotes the projection of the Gaussian fixed point. In panel (a), the Gross-Neveu-XY fixed point has two relevant directions, while fixed point $\mathcal{B}$ has one relevant direction and therefore represents the quantum critical point. Fixed point $\mathcal{C}$ has only one relevant direction within this projected subspace, but possesses additional relevant direction(s) in the full coupling space. As N_f increases from (a) to (b), the Gross-Neveu-XY and $\mathcal{B}$ fixed points approach each other and collide at the critical flavor number N_f^c, shown in panel (b). Upon further increasing N_f to panel (c), the two fixed points exchange their criticality, such that the Gross-Neveu-XY fixed point then has a single relevant direction and becomes the quantum critical point. Finally, in panel (d), fixed points $\mathcal{B}$ and $\mathcal{C}$ collide and move into the complex plane.

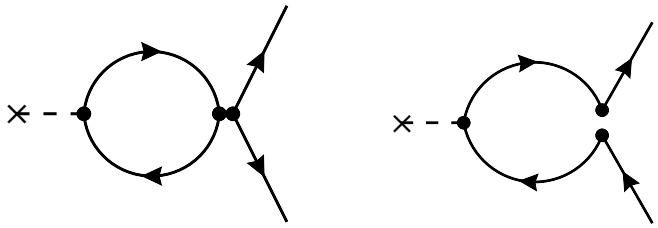

(a) (b)

Figure 3.5: One-loop Feynman diagrams contributing to the RG flow of the symmetry-breaking mass parameter Δ

which agrees with [23, 24] upon setting $\epsilon = 1$ there and truncating the result at leading order. Performing the same calculation for the Gross-Neveu-XY fixed point, one finds that for $N_f > N_f^c$ the bosonic anomalous dimension is given by

$$\eta_\phi^{\mathrm{GNXY}}(N_f > N_f^c) = 1 + \frac{1}{6N_f^2} - \frac{1}{27N_f^3} + \mathcal{O}\left(\frac{1}{N_f^4}\right). \tag{3.51}$$

For $N_f < N_f^c$, the fixed-point collision leads to an exchange of criticality between the colliding fixed points. Consequently, the universal behavior associated with the Gross-Neveu-XY transition is governed by the fixed point that becomes critical below N_f^c.
For the physically relevant cases, namely $N_f = 2, 4$, and 8 [7, 9, 18], the resulting bosonic anomalous dimension reads

$$\eta_\phi = \begin{cases} 1.548, & \text{for the } \mathcal{B} \text{ fixed point at } N_f = 2, \\ 1.043, & \text{for the GNXY fixed point at } N_f = 2, \\ 1.010, & \text{for } N_f = 4, \\ 1.002, & \text{for } N_f = 8. \end{cases} \tag{3.52}$$

Figure 3.6 shows the different susceptibility exponents $x_i = -\partial\beta_{\Delta_i}/\partial\Delta_i$ for the various interaction channels $\mathcal{M}_i = \mathbb{1}_4, \gamma_0, \gamma_3, \gamma_{01}, \gamma_{35}$ at the Gross-Neveu-XY fixed point. Importantly, for all $N_f > N_f^c$, the Gross-Neveu-XY interaction channel associated with the mass term $\Delta_3\bar{\psi}\mathcal{M}_3\psi$ exhibits the largest susceptibility. This confirms that the Gross-Neveu-XY fixed point governs the quantum critical point associated with the spontaneous breaking of the $U(1)$ symmetry, as expected.

c. Fermion anomalous dimension η_ψ

In the purely fermionic formulation with pointlike four-fermion interactions, the one-loop tadpole diagram does not contribute to the fermion anomalous dimension. The reason is that the tadpole self-energy is momentum independent and therefore only generates a term proportional to the identity in spinor space; after projecting onto the $\not{p}$ structure of the fermion

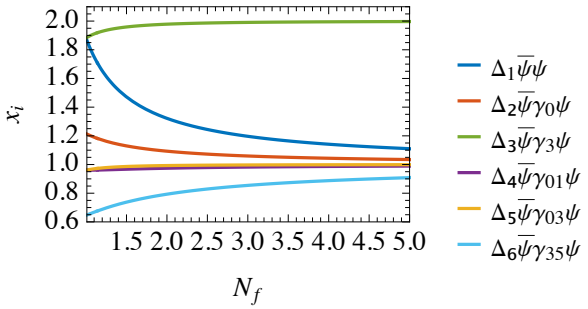

Figure 3.6: Susceptibility exponents $x_i = -\partial\beta_{\Delta_i}/\partial\Delta_i$ as functions of N_f for interaction channels $\mathcal{M}_i = \mathbb{1}_4, \gamma_0, \gamma_3, \gamma_{01}, \gamma_{35}$ at the Gross-Neveu-XY fixed point. For all $N_f > N_f^c$, the Gross-Neveu-XY interaction channel with mass parameter $\Delta_3\bar{\psi}g_3\psi$ has the largest susceptibility, confirming that the Gross-Neveu-XY fixed point describes a quantum critical point across which the U(1) symmetry breaks spontaneously.

two-point function, its contribution vanishes identically. As a consequence, the leading non-trivial contribution to η_ψ can only arise from the two-loop sunset-type self-energy diagrams shown in Fig. 3.7.

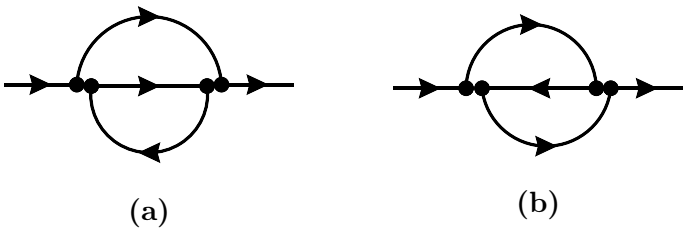

Figure 3.7: Two-loop Feynman diagrams contributing to the fermionic self-energy and thus the fermion anomalous dimension η_ψ in the purely fermionic formulation. The internal vertices are pointlike four-fermion interactions.

Projecting the sunset diagrams in Fig. 3.7 onto the $\not{p}$ part of the fermion self-energy, one may formally write

$$\eta_\psi = g_i^*\, H_{ij}^{(3)}\, g_j^*, \tag{3.53}$$

where g_i^* denote the fixed-point values of the four-fermion couplings. Following the same matrix-algebra decomposition as in the lower-critical-dimension analysis, the coefficient matrix $H_{ij}^{(3)}$ can be written as [23, 44]

$$\begin{aligned} H_{ij}^{(3)} = \frac{1}{40N_f^2} \sum_{\mu,\nu,\lambda} &\big(\delta_{\mu 0}\delta_{\nu\lambda} + \delta_{\nu 0}\delta_{\mu\lambda} + \delta_{\lambda 0}\delta_{\mu\nu}\big) \\ &\times \Big\{ N_f\ \mathrm{Tr}(\gamma_0\mathcal{O}_i\gamma_\mu\mathcal{O}_j)\,\mathrm{Tr}(\gamma_\nu\mathcal{O}_j\gamma_\lambda\mathcal{O}_i) - \mathrm{Tr}(\gamma_0\mathcal{O}_i\gamma_\mu\mathcal{O}_j\gamma_\nu\mathcal{O}_i\gamma_\lambda\mathcal{O}_j)\Big\}, \end{aligned} \tag{3.54}$$

where $\mathcal{O}_i$ denotes the Dirac matrix structure associated with the corresponding four-fermion interaction channel. Accordingly, $H_{ij}^{(3)}$ encodes the complete matrix-algebra part of the sunset contribution, while the dependence on the interacting fixed point enters only through the

fixed-point couplings g_i^*.

Applying the above projection to the Gross-Neveu-Ising fixed point, one obtains

$$\eta_\psi^{\mathrm{GNI}} = \frac{4N_f - 1}{8(2N_f - 1)^2}, \tag{3.55}$$

which is consistent with the result reported in [23, 24] after truncating the ϵ expansion at order ϵ^2 and setting $\epsilon = 1$.

Performing the same calculation for the Gross-Neveu-XY fixed point, one finds that for $N_f > N_f^c$ the fermion anomalous dimension is given by

$$\eta_\psi^{\mathrm{GNXY}}(N_f > N_f^c) = \frac{1}{4N_f} + \mathcal{O}(1/N_f^4), \tag{3.56}$$

We note that the values for $\eta_\phi^{\mathrm{GNXY}}$ and $\eta_\psi^{\mathrm{GNXY}}$ at finite N_f do not agree with those of the $(2+\epsilon)$-expansion results [5, 27], because of the different competing interaction channels present in $D = 2 + \epsilon$ versus $D = 3$ space-time dimensions.

For $N_f < N_f^c$, the fixed-point collision leads to an exchange of criticality between the colliding fixed points. Consequently, the universal behavior associated with the Gross-Neveu-XY transition is governed by the fixed point that becomes critical below N_f^c.

For the physically relevant cases, namely $N_f = 2, 4$, and 8 [7, 9, 18], the resulting fermion anomalous dimension reads

$$\eta_\psi^{\mathrm{GNXY}} = \begin{cases} 0.121, & \text{for the } \mathcal{B} \text{ fixed point at } N_f = 2, \\ 0.125, & \text{for the GNXY fixed point at } N_f = 2, \\ 0.062, & \text{for } N_f = 4, \\ 0.031, & \text{for } N_f = 8. \end{cases} \tag{3.57}$$

As a consequence, within this approximation the critical behavior is governed solely by the flow of the local four-fermion couplings, and the resulting set of critical exponents is correspondingly restricted. In particular, effects associated with dynamical bosonic fluctuations and momentum-dependent interaction channels—which can generate a nontrivial correlation-length exponent and a nontrivial fermion anomalous dimension already at one-loop order in Yukawa-type formulations—are not captured.

To overcome these limitations and obtain a more complete description of the universal properties, we therefore complement the purely fermionic analysis by a *partially bosonized* formulation, which will be presented in Sec. 4. Introducing Hubbard-Stratonovich (auxiliary) bosonic fields for the relevant interaction channels promotes the four-fermion couplings to Yukawa interactions and bosonic self-interactions. This enlarged field provides access to improved estimates for critical exponents beyond the pointlike fermionic truncation.

After introducing the partially bosonized framework and, subsequently, the dynamical bosonization procedure, we will present in Sec. 5 a systematic comparison of universal quantities across all three models. Specifically, we will compile the three critical exponents obtained for the Gross–Neveu–Ising, Gross–Neveu–XY, and Gross–Neveu–Heisenberg universality classes using (i) the purely fermionic pointlike approach, (ii) partial bosonization, and (iii) dynamical bosonization, and plot their N_f dependence in a set of unified figures. This side-by-side visualization will make transparent both the quantitative differences between the schemes and the regime of validity of the pointlike fermionic truncation, in particular in the vicinity of the respective critical flavor numbers where fixed-point collisions occur.

3.2.3 Emergent symmetry

a. Broken U(1) chiral symmetry

The Gross-Neveu-XY model describes the quantum phase transition from a two-dimensional Dirac semimetal to a Kekulé-ordered phase. Its low-energy degrees of freedom are given by massless Dirac fermions, while the order parameter is represented by a two-dimensional internal space spanned by the two independent fermion bilinears $(\bar{\psi}^\alpha\gamma_3\psi^\alpha, \bar{\psi}^\alpha\gamma_5\psi^\alpha)$. From the viewpoint of the low-energy theory, the model therefore naturally contains a two-component order-parameter structure. If one considers only continuous rotations within this two-dimensional space, the interaction channel exhibits an angular structure of $U(1)$ type. For the Kekulé problem, however, the microscopic symmetry does not allow this continuous structure to remain fully intact, but instead reduces it to a discrete $\mathbb{Z}_3$ symmetry. As a consequence, cubic anisotropy terms are allowed in the effective theory describing this transition, in contrast to the usual case of a continuous $O(2)$-type order-parameter theory.

This symmetry structure makes the nature of the phase transition nontrivial from the outset. According to the usual Landau criterion, the cubic terms allowed by the discrete $\mathbb{Z}_3$ symmetry tend to drive the transition first order. For the quantum critical behavior of Dirac semimetals, however, what must be determined is whether these cubic terms remain relevant in the infrared limit. Previous studies based on the $4-\epsilon$ expansion [7, 45] and the functional renormalization group (FRG) [38] have shown that the fixed point corresponding to the potentially continuous Kekulé transition may exhibit an enhanced $U(1)$ symmetry. Consequently, all couplings that reduce the $U(1)$ symmetry to $\mathbb{Z}_3$ vanish at the fixed point. In the following, we directly examine within perturbative RG at $D = 3$ whether these couplings are relevant at the fixed point.

We first determine which additional couplings are allowed in the Lagrangian by the $\mathbb{Z}_3$ symmetry. Because among the terms involving $\mathcal{O} \in \{\gamma_\mu, \gamma_{\mu\nu}, \gamma_{\mu 3}, \gamma_{\mu 5}\}$, only even powers remain invariant under Lorentz transformations, the only possible cubic terms within the purely fermionic formulation of the theory are the real and imaginary parts of $(\bar{\psi}^\alpha\gamma_3\psi^\alpha + i\bar{\psi}^\alpha\gamma_5\psi^\alpha)^3$. In order for either one to be symmetry-allowed, one of the two $\mathbb{Z}_2$ symmetries must also be broken simultaneously. Moreover, for operators with $\mathcal{O} \in \{\gamma_{\mu 3}, \gamma_{\mu 5}\}$, Since the $\mathbb{Z}_3$ symmetry permits

quadratic terms in the form $(\bar{\psi}^\alpha\gamma_{\mu 3}\psi^\alpha)^3 + (\bar{\psi}^\alpha\gamma_{\mu 5}\psi^\alpha)^3$, $\mu = 0, 1, 2$, while Lorentz symmetry only allows even-order terms of $(\bar{\psi}^\alpha\gamma_{\mu 3}\psi^\alpha)^{2n}$ and $(\bar{\psi}^\alpha\gamma_{\mu 5}\psi^\alpha)^{2n}$, breaking the $\mathbb{Z}_2$ symmetry does not enable any additional terms to appear. Here we assume that only the $\mathbb{Z}_2^3$ symmetry is broken. Consequently, the only symmetry-allowed cubic term is:

$$\lambda\left[(\bar{\psi}^\alpha\gamma_3\psi^\alpha)^3 - 3(\bar{\psi}^\alpha\gamma_3\psi^\alpha)(\bar{\psi}^\alpha\gamma_5\psi^\alpha)^2\right]. \tag{3.58}$$

Upon computing the RG flow of λ at one-loop order,

$$\beta_\lambda = \left\{3 - \frac{1}{N_f}[(12N_f - 12)g_3 - 3g_1 + 9g_2 - 21g_4 + 3g_6]\right\}\lambda \tag{3.59}$$

we find that the β function of λ is proportional to λ itself, so the RG scaling due to the cubic term at $\lambda^* = 0$ is given by $\theta = -\partial\beta_\lambda/\partial\lambda$. At the GNXY fixed point and at fixed point $\mathcal{B}$, we find that θ is negative for all values of N_f and approaches zero as $N_f \to \infty$, indicating an emergent $U(1)$ symmetry at the GNXY fixed point. Our results qualitatively agree with [38, 45] in the large-N_f region, but for small N_f, our calculation suggests that the cubic term remains irrelevant for all values of N_f, whereas [38, 45] finds a critical N_f below which the cubic term becomes relevant.

b. Broken Lorentz symmetry

The Gross-Neveu-XY model can be used as an effective low-energy field-theoretical description of ordering transitions in twisted bilayer graphene. In the present formulation, the theory is written in a relativistic Dirac form, which provides a convenient framework for analyzing the interacting fixed-point structure and the infrared fate of symmetry-breaking perturbations. It should be emphasized, however, that the microscopic twisted bilayer graphene system is a condensed-matter lattice system defined on a moiré superlattice and does not possess exact Lorentz invariance. Similarly, the Kekulé problem mentioned above is defined on the honeycomb lattice without explicit Lorentz invariance. In particular, the underlying band structure, and residual interactions such as the long-range Coulomb interaction generally distinguish temporal and spatial directions and thus lie outside the strictly Lorentz-invariant continuum limit. Therefore, if the critical behavior is to be governed by a relativistic Gross-Neveu-XY fixed point, it is necessary to examine whether perturbations that explicitly break Lorentz symmetry are relevant in its vicinity. Only when such perturbations are RG irrelevant can the Lorentz-symmetric continuum theory be regarded as a self-consistent infrared description of the transition.

The $O(3)$ Lorentz symmetry in Euclidean spacetime can be broken to $O(2)$ rotational symmetry, by adding the following three infinitesimal symmetry-breaking terms,

$$\delta_1(\bar{\psi}^\alpha\gamma_0\psi^\alpha)^2,\ \delta_2(\bar{\psi}^\alpha\gamma_{01}\psi^\alpha)^2,\ \delta_3[(\bar{\psi}^\alpha\gamma_{03}\psi^\alpha)^2 + (\bar{\psi}^\alpha\gamma_{05}\psi^\alpha)^2] \tag{3.60}$$

Calculating the β function for each coupling,

$$\beta_{\delta_1} = \left\{1 - \frac{1}{3N_f}[8N_f g_2 - 2g_1 + 4g_3 + 2g_4 - 4g_5 - 2g_6]\right\}\delta_1 \tag{3.61}$$

$$\beta_{\delta_2} = \left\{1 - \frac{1}{3N_f}[8N_f g_4 - 2g_1 + 2g_2 - 4g_3 + 4g_5 - 2g_6]\right\}\delta_2 \tag{3.62}$$

$$\beta_{\delta_3} = \left\{1 - \frac{1}{3N_f}[(2 - 8N_f)g_5 + 2g_1 + 2g_2 - 2g_4 - 2g_6]\right\}\delta_3 \tag{3.63}$$

we find that at the GNXY fixed point, all $\theta_i = (-\partial\beta_{\delta_i}/\partial\delta_i),\ i = 1, 2, 3$ are negative, and thus Lorentz symmetry emerges near a Gross-Neveu-XY quantum critical point at low energy.

3.3 Gross-Neveu-Heisenberg model

For the Gross-Neveu-Heisenberg model, the interaction Lagrangian is specified in Sec.2.3. Building on the Fierz-complete operator basis established there, we employ the general one-loop projection scheme of [31] to derive the RG flow within the symmetry-allowed Gross-Neveu-Heisenberg theory space. This yields a coupled set of beta functions for the associated four-fermion couplings:

$$\begin{aligned}
\beta_1 =& g_1 - \frac{1}{N_f}\left[(2 - 4N_f)g_1^2 + 6g_1\,(g_2 + g_3 + 3g_4) + 4(g_2^2 + 3g_4^2)\right] \\
\beta_2 =& g_2 - \frac{1}{N_f}\left[\tfrac{2}{3}g_2\big(3g_1 + (1 + 2N_f)g_2 - 3g_3\big) + 2(g_2 + 4g_3)g_4\right] \\
\beta_3 =& g_3 - \frac{1}{N_f}\left[2g_3\big(g_1 + 3g_2 - (1 + 2N_f)g_3\big) + 2(4g_2 + g_3)g_4\right] \\
\beta_4 =& g_4 - \frac{1}{3N_f}\left[4g_3(2g_2 + g_3) + 2(3g_1 + g_2 + g_3)g_4 + 2(13 + 2N_f)g_4^2\right]
\end{aligned} \tag{3.64}$$

Focusing on the GNH criticality associated with an $SU(2)$ vector order parameter,

$$\langle\vec{n}\rangle \equiv \big(\langle\bar{\psi}\sigma^x\psi\rangle, \langle\bar{\psi}\sigma^y\psi\rangle, \langle\bar{\psi}\sigma^z\psi\rangle\big)^T, \tag{3.65}$$

the corresponding fixed point in the large-N_f limit is located at $(0, 0, \frac{1}{4}, 0)$, with g_3 parametrizing the Gross-Neveu-Heisenberg interaction. We parametrize the corresponding RG fixed point at finite N_f by

$$\mathcal{H} \equiv (h_1, h_2, h_3, h_4). \tag{3.66}$$

The evolution of the four nonvanishing couplings at $\mathcal{H}$ as a function of N_f is shown in Fig. 3.8(a).

Upon decreasing N_f, the fixed point $\mathcal{H}$ approaches a second fixed point $\mathcal{H}' = (h_1', h_2', h_3', h_4')$ and the two collide at the critical flavor number $N_f^{(\mathrm{H})} \approx 1.95$, as shown in Fig. 3.8(b). For smaller

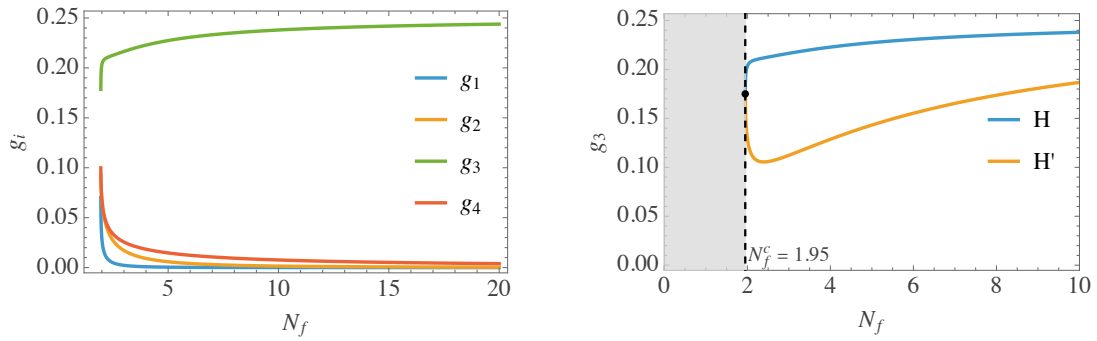

Figure 3.8: Fixed-point structure of the Gross-Neveu-Heisenberg model as a function of the flavor number N_f. (a) The four nonvanishing couplings g_1, g_2, g_3, and g_4 at the GNH fixed point $\mathcal{H}$. (b) The coupling g_3 for the two fixed points $\mathcal{H}$ and $\mathcal{H}'$. The two fixed points collide at the critical flavor number $N_f^c = 1.95$ and subsequently move into the complex plane. The shaded region indicates the parameter regime in which no corresponding real fixed points exist.

N_f, the pair $(\mathcal{H}, \mathcal{H}')$ moves off the real coupling space and becomes a complex-conjugate pair in the complexified coupling plane, so that they no longer represent real RG fixed points. In the large-N_f limit, $\mathcal{H}'$ tends to the asymptotic location $\left(0, 0, \frac{1}{4}, -\frac{3}{4}\right)$. This behavior also highlights a difference from the $2 + \epsilon$ expansion analysis of Ref. [23], in which no collision between the GNH fixed point and a non-Gaussian fixed point was observed.

This fixed-point collision can be visualized more directly in the projected RG flow shown in Fig. 3.9. In panel (a), $\mathcal{H}$ has a single relevant direction and therefore corresponds to the quantum critical point. As N_f is lowered toward N_f^c, $\mathcal{H}$ approaches the second fixed point and the collision occurs at $N_f \simeq 1.95$ [panel (b)]. For $N_f < N_f^c$, shown in panel (c), the two fixed points have moved into the complex plane, leaving only two real fixed points in this projected subspace, neither of which is quantum critical.

This type of fixed-point collision represents an instance of fixed-point annihilation and complexification, or equivalently, as a mechanism for the loss of conformality [46, 47]. In this interpretation, the collision at N_f^c indicates that the real GNH critical fixed point terminates within the present truncation. For $N_f < N_f^c$, the absence of a real critical fixed point suggests that the corresponding continuous transition is lost. Nevertheless, the nearby complex-conjugate fixed points may still induce slow RG flow and approximate scaling over a broad intermediate regime, leading to walking or pseudocritical behavior rather than true asymptotic criticality [47, 48].

Next, we discuss the fermion anomalous dimension associated with the GNH fixed point $\mathcal{H}$. Repeating the calculation described in Eqs. (3.53)–(3.54), with the matrix structures $\mathcal{O}_i$ specialized to the Gross-Neveu-Heisenberg case, i.e. $\gamma_i = (\tau_i \otimes \mathbb{1}_2)$, one obtains for $N_f > N_f^c$

$$\eta_\psi^{\mathrm{GNH}} = \frac{3}{8N_f} - \frac{9}{32N_f^2} + \mathcal{O}(1/N_f^4), \tag{3.67}$$

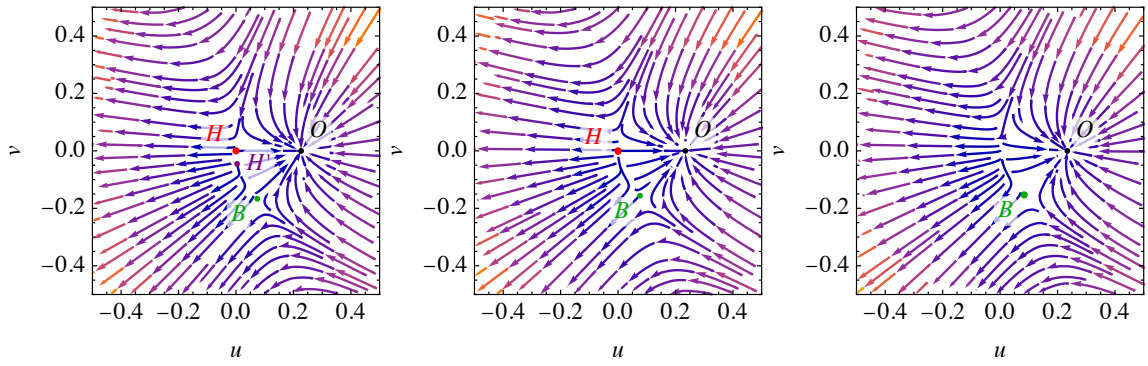

(a) $N_f = 2.0$ **(b)** $N_f = 1.95$ **(c)** $N_f = 1.9$

Figure 3.9: Projected RG flow in the (u, ν) plane for the Gross-Neveu-Heisenberg model at different values of N_f. The coordinates u and ν are chosen along the two leading eigendirections of the stability matrix at each given N_f, and the origin is set by the projection of the Gross-Neveu-Heisenberg fixed point $\mathcal{H}$. In panel (a), $\mathcal{H}$ has a single relevant direction and therefore corresponds to the quantum critical point, while O denotes the projection of the Gaussian fixed point. As N_f decreases from (a) to (b), $\mathcal{H}$ approaches fixed point $\mathcal{A}$ and collides with it in panel (b), after which the two fixed points move into the complex plane. Consequently, for still smaller N_f, as shown in panel (c), only two real fixed points remain in this projected subspace, and neither of them is quantum critical.

This agrees with Ref. [23] up to order $1/N_f^2$ after truncating the ϵ expansion at order ϵ^2 and setting $\epsilon = 1$. At order $1/N_f^3$, however, the two results differ: our expression has a vanishing coefficient, whereas Ref. [23] yields $-3/4$. For the physically relevant cases, namely $N_f = 2, 4$, and 8 [4, 20, 37, 49], we obtain

$$\eta_\psi^{\mathrm{GNH}} = \begin{cases} 0.121, & \text{for } N_f = 2, \\ 0.077, & \text{for } N_f = 4, \\ 0.043, & \text{for } N_f = 8. \end{cases} \tag{3.68}$$

The correlation-length exponent ν is obtained from the stability matrix

$$B_{ij} \equiv \left.\frac{\partial \beta_i}{\partial g_j}\right|_{\mathcal{H}}, \qquad i, j = 1, \ldots, 4, \tag{3.69}$$

whose eigenvalues $\{\theta_k\}$ define the RG scaling exponents. The relevant direction is given by the largest positive eigenvalue $\theta_{\max}$, and we extract

$$\nu^{-1} = \theta_{\max} = 1. \tag{3.70}$$

Finally, the anomalous dimension of the $SU(2)$ vector order parameter is computed in complete analogy to the procedure employed for the GN-XY universality class, i.e., by evaluating the corresponding one-loop renormalization of the composite operator in the fermionic formulation

and projecting onto the $SU(2)$ vector channel. For $N_f > N_f^c$, one finds

$$\eta_\phi^{\mathrm{GNH}}(N_f > N_f^c) = 1 + \frac{1}{2N_f} + \frac{7}{12N_f^2} - \frac{397}{216N_f^3} + \mathcal{O}\big(1/N_f^4\big)\,. \tag{3.71}$$

We note that this expression agrees with Ref. [23] at leading order in $1/N_f$ after truncating the ϵ expansion at order ϵ and setting $\epsilon = 1$, but starts to differ from it at order $1/N_f^2$. For the physically relevant cases, the corresponding values read

$$\eta_\phi = \begin{cases} 1.548, & \text{for } N_f = 2, \\ 1.147, & \text{for } N_f = 4, \\ 1.069, & \text{for } N_f = 8. \end{cases} \tag{3.72}$$

3.4 Gross-Neveu-Spin-XY model

Besides the chiral realization of the Gross-Neveu-XY model discussed above, one may also formulate an alternative *spin-XY* version in which the continuous symmetry acts in spin space rather than in the chiral sector [5]. This model can be understood as an easy-plane deformation of the SU(2)-symmetric Gross-Neveu-Heisenberg theory: the full spin-vector interaction is restricted to the xy plane, such that the SU(2) spin symmetry is reduced to a residual $U(1)$ rotation around the z axis. In this sense, the spin-XY model provides an anisotropic descendant of the Heisenberg theory, with the easy-plane spin rotation symmetry replacing the continuous chiral symmetry of the original Gross-Neveu-XY formulation.

Concretely, starting from the Heisenberg interaction, the easy-plane deformation amounts to the replacement

$$\big[\bar\psi(\mathbb{1}_2 \otimes \vec\sigma)\psi\big]^2 \;\longrightarrow\; \big[\bar\psi(\mathbb{1}_2 \otimes \sigma_x)\psi\big]^2 + \big[\bar\psi(\mathbb{1}_2 \otimes \sigma_y)\psi\big]^2, \tag{3.73}$$

so that only the planar spin components remain dynamically equivalent, while the z direction is distinguished. The residual continuous symmetry is therefore generated by $\mathbb{1}_2 \otimes \sigma_z$, together with the flavor symmetry, leading to a global $U(N_f) \times U(N_f)$ structure.

The construction of the complete quartic interaction basis follows directly from this symmetry reduction. Every four-fermion operator transforming as a spin vector under SU(2) is decomposed into an easy-plane part and a longitudinal part, i.e.

$$\frac{g}{2N_f}\big[\bar\psi(N \otimes \vec\sigma)\psi\big]^2 \;\longrightarrow\; \frac{g_{xy}}{2N_f}\big[\bar\psi(N \otimes \vec\sigma_{xy})\psi\big]^2 + \frac{g_z}{2N_f}\big[\bar\psi(N \otimes \sigma_z)\psi\big]^2, \tag{3.74}$$

where $\vec\sigma_{xy} = (\sigma_x, \sigma_y)$ and N denotes the matrix structure in the Dirac sector. Applying this decomposition to all symmetry-allowed interaction channels yields, in the present $D = 3$

formulation, the quartic interaction

$$\begin{aligned}\mathcal{L}_{\text{int}}^{\text{spin-XY}} =&\frac{1}{2N_f}\Big[g_1\big(\bar\psi^\alpha(\mathbb{1}_2\otimes\mathbb{1}_2)\psi^\alpha\big)^2+g_2\big(\bar\psi^\alpha(\tau_\mu\otimes\mathbb{1}_2)\psi^\alpha\big)^2+g_3\big(\bar\psi^\alpha(\mathbb{1}_2\otimes\sigma_{xy})\psi^\alpha\big)^2\\&+g_4\big(\bar\psi^\alpha(\tau_\mu\otimes\sigma_z)\psi^\alpha\big)^2+g_5\big(\bar\psi^\alpha(\tau_\mu\otimes\sigma_{xy})\psi^\alpha\big)^2+g_6\big(\bar\psi^\alpha(\mathbb{1}_2\otimes\sigma_z)\psi^\alpha\big)^2\Big].\end{aligned} \tag{3.75}$$

This representation makes transparent that the spin-XY theory is built from the same general class of quartic fermion operators as the chiral Gross-Neveu-XY model, but organized according to a different symmetry realization. More precisely, the easy-plane spin channels and the chiral channels can be mapped into each other by an appropriate relabeling of interaction structures. The two formulations therefore describe the same type of symmetry-allowed quartic theory space, although the couplings are parameterized differently and the associated RG trajectories need not be identical a priori.

Repeating the one-loop momentum-shell calculation in $D = 3$ for the interaction (3.75), one obtains the flow equations

$$\beta_1 = g_1 - \frac{1}{N_f}\Big[2(1-2N_f)g_1^2+2(g_2^2+g_4^2+2g_5^2)+g_1(3g_2+2g_3+3g_4+6g_5+g_6)\Big], \tag{3.76}$$

$$\beta_2 = g_2 - \frac{2}{3N_f}\Big[3g_1g_2+(1+2N_f)g_2^2+8g_3g_5+g_2(-2g_3+g_4+2g_5-g_6)+4g_4g_6\Big], \tag{3.77}$$

$$\beta_3 = g_3 - \frac{1}{N_f}\Big[2g_1g_3-4N_fg_3^2+g_2(6g_3+8g_5)+4g_5g_6-2g_3(g_4+g_6)\Big], \tag{3.78}$$

$$\beta_4 = g_4 - \frac{2}{3N_f}\Big[2g_3^2+3g_1g_4+2g_3g_4+(1+2N_f)g_4^2+14g_5^2-g_4(2g_5+g_6)+g_2(g_4+4g_6)\Big], \tag{3.79}$$

$$\beta_5 = g_5 - \frac{2}{3N_f}\Big[g_2(4g_3+g_5)+2g_3g_6+g_5(3g_1+13g_4+2N_fg_5+g_6)\Big], \tag{3.80}$$

$$\beta_6 = g_6 - \frac{2}{N_f}\Big[g_3(4g_5-2g_6)+g_2(4g_4+3g_6)+g_6(g_1+3g_4-6g_5+g_6-2N_fg_6)\Big]. \tag{3.81}$$

The relation to the $D = 3$ Gross-Neveu-XY flow becomes explicit after the transformation

$$g_1 \leftrightarrow g_6, \qquad g_3 \mapsto -g_3, \qquad g_5 \mapsto -g_5. \tag{3.82}$$

Under this relabeling, the spin-XY beta functions are mapped onto those of the chiral Gross-Neveu-XY model. This shows that the two formulations are not independent at the level of the quartic interaction algebra; rather, they provide two equivalent parameterizations of the same interaction space, adapted respectively to spin and chiral symmetry realizations.

The connection to the Gross-Neveu-Heisenberg model is equally direct. In the isotropic limit, the distinction between the easy-plane and longitudinal spin channels disappears, which is

implemented by the identifications

$$g_6 \to g_3, \qquad g_5 \to g_4. \tag{3.83}$$

Substituting these relations into Eq. (3.81) reproduces exactly the beta functions of the Gross-Neveu-Heisenberg model. The spin-XY theory may therefore be viewed as the easy-plane anisotropic deformation of the Heisenberg theory, while the latter is recovered as the isotropic limit of the former.

4 Partially bosonized formulation

To complement the RG analysis in the purely fermionic formulation, we now adopt a partially bosonized description [50]. Concretely, we perform a Hubbard-Stratonovich (HS) transformation [30] to decouple the four-fermion interaction into a Yukawa-type coupling [10] and introduce an explicit bosonic field associated with the relevant order-parameter channel, as illustrated in Fig. 4.1. In this representation, the order-parameter fluctuations appear as independent dynamical degrees of freedom. At the same time, the tuning parameter controlling the approach to criticality, namely the bosonic mass r, as well as the interaction strengths encoded in the Yukawa coupling h and the bosonic self-interaction λ, can be treated within a common and more transparent framework.

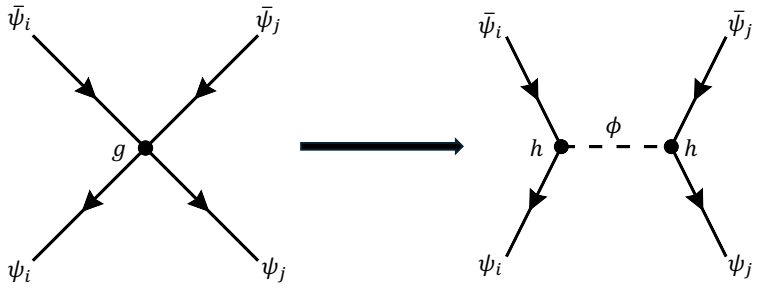

Figure 4.1: Schematic illustration of the Hubbard–Stratonovich transformation. The local four-fermion interaction is rewritten in terms of an auxiliary bosonic order-parameter field, resulting in a Yukawa-type fermion-boson coupling and a bosonic mass term.

A further motivation for this reformulation is provided by the structure of the theory near its critical dimensions. As discussed in Sec. 2, in a purely fermionic description the fermion anomalous dimension η_ψ arises only beyond leading order in the loop expansion; in particular, it is generated at two-loop order by the sunset self-energy diagram.

By contrast, after partial bosonization the relevant interaction channel is represented by a Yukawa coupling to an auxiliary bosonic field. This reformulation is not merely technically convenient, but is especially natural near the upper critical dimension, where the Gross–Neveu–Yukawa description becomes perturbatively controlled. It therefore provides a framework in which fermionic and bosonic anomalous dimensions, as well as the associated critical exponents, can be treated on equal footing.

4.1 Gross-Neveu-Ising model

Starting from the purely fermionic action Eq. (2.1), we illustrate the HS decoupling using the four-fermion interaction of the Gross-Neveu-Ising model as an example. Consider

$$\mathcal{L}_{\text{int}} = \frac{g}{2N_f}(\bar{\psi}^\alpha \psi^\alpha)^2 \tag{4.1}$$

The HS transformation is equivalent to inserting into the partition function a Gaussian functional integral over an auxiliary bosonic field ϕ,

$$1 = \mathcal{N} \int \mathcal{D}\phi \, \exp\left[- \int \mathrm{d}^3x \, \frac{r}{2} \phi^2 \right] \tag{4.2}$$

and then performing an appropriate shift of ϕ such that the cross term generates a Yukawa coupling while the original four-fermion term is canceled. The shift is most conveniently written by completing the square:

$$\frac{r}{2}\left(\phi + \frac{h}{r}\,\bar{\psi}\psi\right)^2 = \frac{r}{2}\phi^2 + h\,\phi\,(\bar{\psi}\psi) + \frac{h^2}{2r}(\bar{\psi}\psi)^2. \tag{4.3}$$

Requiring the newly generated four-fermion term to cancel the original $\mathcal{L}_{\text{int}}$ fixes the relation between couplings,

$$\frac{h^2}{2r} = -\frac{g}{2N_f} \qquad \Longleftrightarrow \qquad g = -\frac{N_f h^2}{r}. \tag{4.4}$$

This yields the partially bosonized decomposition of the Lagrangian,

$$\mathcal{L} = \mathcal{L}_\psi + \mathcal{L}_{\psi\phi} + \mathcal{L}_\phi, \tag{4.5}$$

with

$$\mathcal{L}_\psi = \sum_{i=1}^{N_f} \bar{\psi}_i \, \gamma_\mu \partial_\mu \, \psi_i, \qquad \mathcal{L}_{\psi\phi} = h\,\phi\,(\bar{\psi}\psi), \tag{4.6}$$

and a purely bosonic sector (which is naturally allowed in the critical theory and is generically generated under RG),

$$\mathcal{L}_\phi = \frac{1}{2}(\partial_\mu \phi)^2 + \frac{r}{2}\phi^2 + \lambda\phi^4. \tag{4.7}$$

Mode splitting and shell integration. We introduce a sharp UV cutoff Λ and split all fields into slow and fast modes,

$$\phi = \phi_< + \phi_>, \qquad \psi = \psi_< + \psi_>, \qquad \bar{\psi} = \bar{\psi}_< + \bar{\psi}_>, \tag{4.8}$$

where the fast modes carry momenta in the thin shell $\Lambda/b < |q| < \Lambda$, with $b > 1$. We denote $t \equiv \ln b$ and assume $t \ll 1$.

The Gaussian part yields the free propagators

$$G_\phi(q) = \frac{1}{q^2 + r}, \qquad G_\psi(q) = \frac{1}{\mathrm{i}\not{q}} = -\mathrm{i}\,\frac{\not{q}}{q^2}, \qquad \not{q} \equiv \gamma_\mu q_\mu. \tag{4.9}$$

The shell integral is written as

$$\int_{\text{shell}} \frac{\mathrm{d}^D q}{(2\pi)^D}(\cdots) = \int_{\Lambda/b}^{\Lambda} \mathrm{d}q\, \frac{S_D\, q^{D-1}}{(2\pi)^D}(\cdots), \qquad S_D = \frac{2\pi^{D/2}}{\Gamma(D/2)}. \tag{4.10}$$

For a thin shell one uses

$$\int_{\Lambda/b}^{\Lambda} \mathrm{d}q\, q^{D-1} f(q) \simeq \Lambda^D f(\Lambda)\, t, \tag{4.11}$$

which amounts to evaluating the integrand at $q = \Lambda$ to linear order in t.

It is convenient to abbreviate the angular prefactor as

$$K_D \equiv \frac{S_D}{(2\pi)^D}. \tag{4.12}$$

Two shell integrals occur repeatedly:

$$\begin{aligned} I_1(r) &\equiv \int_{\text{shell}} \frac{\mathrm{d}^D q}{(2\pi)^D} \frac{1}{q^2 + r} = \int_{\Lambda/b}^{\Lambda} \mathrm{d}q\; K_D\, q^{D-1} \frac{1}{q^2 + r} \simeq K_D\, \Lambda^D \frac{1}{\Lambda^2 + r}\, t \\ &= K_D\, \Lambda^{D-2}\, \frac{1}{1 + \tilde{r}}\, t, \end{aligned} \tag{4.13}$$

$$\begin{aligned} I_2(r) &\equiv \int_{\text{shell}} \frac{\mathrm{d}^D q}{(2\pi)^D} \frac{1}{(q^2 + r)^2} = \int_{\Lambda/b}^{\Lambda} \mathrm{d}q\; K_D\, q^{D-1} \frac{1}{(q^2 + r)^2} \simeq K_D\, \Lambda^D \frac{1}{(\Lambda^2 + r)^2}\, t \\ &= K_D\, \Lambda^{D-4}\, \frac{1}{(1 + \tilde{r})^2}\, t. \end{aligned} \tag{4.14}$$

In the last step of (4.13)–(4.14) we have introduced the dimensionless mass parameter $\tilde{r} \equiv r/\Lambda^2$.

Dimensionless couplings and rescaling. To obtain the flow equations, we define dimensionless couplings by absorbing the geometric factor K_D and explicit cutoff powers:

$$\tilde{h}^2 \equiv K_D\, \Lambda^{D-4}\, h^2, \qquad \tilde{\lambda} \equiv K_D\, \Lambda^{D-4}\, \lambda, \qquad \tilde{r} \equiv \frac{r}{\Lambda^2}. \tag{4.15}$$

After integrating out the fast modes, we rescale momenta and fields to restore the cutoff to Λ. Canonical dimensions yield $(D-4)$ for h^2 and λ, and -2 for r. Wave-function renormalizations are encoded by the anomalous dimensions η_ψ and η:

$$\psi \to b^{(D+1-\eta_\psi)/2}\psi, \qquad \phi \to b^{(D+2-\eta)/2}\phi, \tag{4.16}$$

so that

$$\beta_{h^2}|_{\text{scaling}} = (D{-}4{+}\eta{+}2\eta_\psi)h^2, \qquad \beta_\lambda|_{\text{scaling}} = (D{-}4{+}2\eta)\lambda, \qquad \beta_r|_{\text{scaling}} = (-2{+}\eta)r, \tag{4.17}$$

where $\beta_\cdot \equiv -\mathrm{d}(\cdot)/\mathrm{d}t$.

In the following we derive the one-loop corrections from integrating out the shell modes. All loop corrections are computed at zero external momenta and kept to linear order in t.

4.1.1 Flow of the boson mass parameter r

At one loop, r receives a bosonic tadpole correction of order $\mathcal{O}(\lambda)$ and a fermionic bubble correction of order $\mathcal{O}(h^2)$.

(i) Bosonic tadpole $\mathcal{O}(\lambda)$. The quartic interaction reads

$$S_\lambda = \int \mathrm{d}^D x \; \lambda\phi^4. \tag{4.18}$$

Expanding $\phi = \phi_< + \phi_>$ and selecting the term with two slow and two fast fields yields

$$\phi^4 \supset \binom{4}{2}\phi_<^2\phi_>^2 = 6\,\phi_<^2\phi_>^2. \tag{4.19}$$

Hence the one-loop correction to the effective action is

$$\delta S_{\text{eff}}\big|_\lambda = \int \mathrm{d}^D x \; 6\,\lambda\,\phi_<^2(x)\,\langle\phi_>^2(x)\rangle, \tag{4.20}$$

with

$$\langle\phi_>^2(x)\rangle = \int_{\text{shell}} \frac{\mathrm{d}^D q}{(2\pi)^D}\, G_\phi(q) = I_1(r). \tag{4.21}$$

Therefore

$$\delta S_{\text{eff}}\big|_\lambda = 12 \int \mathrm{d}^D x \; \frac{1}{2}\phi_<^2(x)\lambda\, I_1(r). \tag{4.22}$$

Comparing with the mass term $\int \mathrm{d}^D x \, \frac{r}{2}\phi^2$ gives

$$\delta r\big|_\lambda = 12\lambda\, I_1(r). \tag{4.23}$$

Using (4.13) and dividing by Λ^2 to obtain the dimensionless $\delta\tilde{r}$,

$$\delta\tilde{r}\big|_\lambda = \frac{\delta r}{\Lambda^2} = 12\lambda\, K_D\, \Lambda^{D-4}\, \frac{1}{1+\tilde{r}}\, t. \tag{4.24}$$

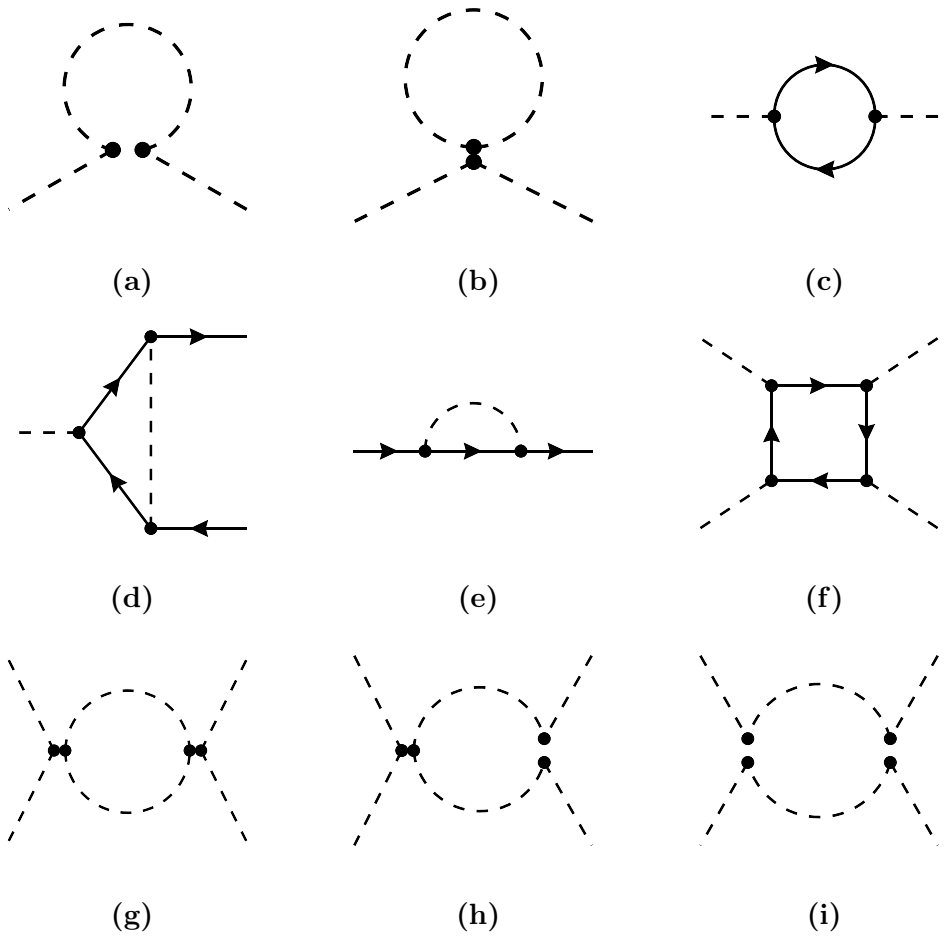

Figure 4.2: One-loop Feynman diagrams contributing to the partially bosonized truncation.

In terms of the dimensionless coupling (4.15), this becomes

$$\delta\tilde{r}\big|_{\lambda} = 12\,\frac{\tilde{\lambda}}{1+\tilde{r}}\,t. \tag{4.25}$$

(ii) Fermionic bubble $\mathcal{O}(h^2)$. To extract not only the static mass correction but also the order-parameter anomalous dimension, we keep a nonzero external bosonic momentum p and compute the induced bosonic two-point function. Starting from

$$S_h = \int \mathrm{d}^D x\; h\,\phi\,(\bar{\psi}\psi), \tag{4.26}$$

the connected second-order cumulant reads

$$\delta S_{\mathrm{eff}}\big|_{h^2} = -\frac{1}{2}\big\langle S_h^2\big\rangle_{>,c}. \tag{4.27}$$

In momentum space, selecting two external slow boson legs with momenta $\pm p$ and contracting two fast fermion lines into a loop gives

$$\delta S_{\text{eff}}\big|_{h^2} = -\frac{1}{2}\int_{|p|<\Lambda/b} (\mathrm{d}p)\ \phi(-p)\,\Pi(p)\,\phi(p), \tag{4.28}$$

with the one-loop polarization

$$\Pi(p) = -\,N_f\,h^2 \int_{\text{shell}} \frac{\mathrm{d}^D q}{(2\pi)^D}\ \mathrm{Tr}[G_\psi(q)\,G_\psi(p+q)]\,. \tag{4.29}$$

Using $G_\psi(k) = -\mathrm{i}\not{k}/k^2$, we obtain

$$\begin{aligned}\mathrm{Tr}[G_\psi(q)\,G_\psi(p+q)] &= (-\mathrm{i})^2\ \mathrm{Tr}\left[\frac{\not{q}\,(\not{p}+\not{q})}{q^2(p+q)^2}\right] = -\,\frac{1}{q^2(p+q)^2}\ \mathrm{Tr}\left[\not{q}\not{p}+\not{q}\not{q}\right] \\ &= -\,\frac{1}{q^2(p+q)^2}\ \left(d_\gamma\,p_\mu q^\mu + d_\gamma\,q^2\right) = -\,d_\gamma\,\frac{p\cdot q+q^2}{q^2(p+q)^2}.\end{aligned} \tag{4.30}$$

Inserting (4.30) into (4.29) yields

$$\Pi(p) = +\,d_\gamma N_f\,h^2 \int_{\text{shell}} \frac{\mathrm{d}^D q}{(2\pi)^D}\ \frac{p\cdot q+q^2}{q^2(p+q)^2}. \tag{4.31}$$

Expansion to $\mathcal{O}(p^2)$. Near the Gaussian fixed point the relevant contribution is obtained by expanding the integrand to second order in the external momentum p. We use

$$\frac{1}{(p+q)^2} = \frac{1}{q^2}\left(1 - \frac{2p\cdot q}{q^2} - \frac{p^2}{q^2} + \frac{4(p\cdot q)^2}{q^4} + \mathcal{O}(p^3)\right), \tag{4.32}$$

so that

$$\frac{p\cdot q+q^2}{q^2(p+q)^2} = \left(\frac{p\cdot q}{q^2}+1\right)\frac{1}{(p+q)^2} = \frac{1}{q^2} - \frac{p\cdot q}{q^4} - \frac{p^2}{q^4} + \frac{2(p\cdot q)^2}{q^6} + \mathcal{O}(p^3). \tag{4.33}$$

The second term is odd in q and vanishes upon shell integration. For the last term we use rotational invariance,

$$\int_{\text{shell}} \frac{\mathrm{d}^D q}{(2\pi)^D}\ q_\mu q_\nu\,F(q^2) = \frac{\delta_{\mu\nu}}{D}\int_{\text{shell}} \frac{\mathrm{d}^D q}{(2\pi)^D}\ q^2\,F(q^2), \tag{4.34}$$

which implies

$$\int_{\text{shell}} \frac{\mathrm{d}^D q}{(2\pi)^D}\ \frac{2(p\cdot q)^2}{q^6} = \frac{2p^2}{D}\int_{\text{shell}} \frac{\mathrm{d}^D q}{(2\pi)^D}\ \frac{1}{q^4}. \tag{4.35}$$

Collecting the surviving contributions in (4.33) gives

$$\Pi(p) = d_\gamma N_f\, h^2 \left[\int_{\text{shell}} \frac{\mathrm{d}^D q}{(2\pi)^D} \frac{1}{q^2} + p^2 \left(\frac{2}{D} - 1 \right) \int_{\text{shell}} \frac{\mathrm{d}^D q}{(2\pi)^D} \frac{1}{q^4} \right] + \mathcal{O}(p^3). \tag{4.36}$$

Explicit shell integrals. With $K_D \equiv S_D/(2\pi)^D$ we evaluate

$$\int_{\text{shell}} \frac{\mathrm{d}^D q}{(2\pi)^D} \frac{1}{q^2} = \int_{\Lambda/b}^{\Lambda} \mathrm{d}q\; K_D\, q^{D-1} \frac{1}{q^2} = \int_{\Lambda/b}^{\Lambda} \mathrm{d}q\; K_D\, q^{D-3} \simeq K_D\, \Lambda^{D-2}\, t, \tag{4.37}$$

$$\int_{\text{shell}} \frac{\mathrm{d}^D q}{(2\pi)^D} \frac{1}{q^4} = \int_{\Lambda/b}^{\Lambda} \mathrm{d}q\; K_D\, q^{D-1} \frac{1}{q^4} = \int_{\Lambda/b}^{\Lambda} \mathrm{d}q\; K_D\, q^{D-5} \simeq K_D\, \Lambda^{D-4}\, t. \tag{4.38}$$

Therefore

$$\Pi(p) = d_\gamma N_f\, h^2\, K_D \left[\Lambda^{D-2} + p^2 \left(\frac{2}{D} - 1 \right) \Lambda^{D-4} \right] t + \mathcal{O}(p^3). \tag{4.39}$$

Mass renormalization and Z_ϕ. Inserting (4.39) into (4.28) and comparing with the Gaussian bosonic part,

$$S_{\phi,0} = \frac{1}{2} \int_{|p|<\Lambda/b} \mathrm{d}p\; \phi(-p)\, (p^2 + r)\, \phi(p), \tag{4.40}$$

we identify the static contribution $\Pi(0)$ as a correction to the mass parameter and the p^2 term as the wave-function renormalization:

$$\delta r\big|_{h^2} = -\Pi(0) = -d_\gamma N_f\, h^2\, K_D\, \Lambda^{D-2}\, t, \tag{4.41}$$

$$\delta Z_\phi\big|_{h^2} = -d_\gamma N_f\, h^2\, K_D \left(\frac{2}{D} - 1 \right) \Lambda^{D-4}\, t. \tag{4.42}$$

After rescaling $\tilde{r} \equiv r/\Lambda^2$ and absorbing the common prefactor into the definition of the dimensionless Yukawa coupling h^2, the mass correction takes the form used in the main text,

$$\delta\tilde{r}\big|_{h^2} = -\, d_\gamma N_f\, \tilde{h}^2\, t, \tag{4.43}$$

Result for $\dot{r}$. Including scaling, (4.25) and (4.43) gives

$$\beta_{\tilde{r}} = (-2 + \eta)\, \tilde{r} - 12\, \frac{\tilde{\lambda}}{1 + \tilde{r}} + d_\gamma N_f\, \tilde{h}^2. \tag{4.44}$$

while the wave-function renormalization (4.42) provides the one-loop contribution to the bosonic anomalous dimension via $\eta \equiv \partial_t \ln Z_\phi$:

$$\eta\big|_{h^2} = d_\gamma N_f\, \tilde{h}^2 \left(1 - \frac{2}{D} \right). \tag{4.45}$$

4.1.2 Flow of the Yukawa coupling h^2

The one-loop correction to the Yukawa vertex comes from the triangle diagram with three Yukawa insertions. At zero external momenta its loop integral has the structure

$$\delta h = \frac{1}{3!} A_h \, h^3 \int_{\text{shell}} \frac{\mathrm{d}^D q}{(2\pi)^D} \, G_\phi(q) \, G_\psi(q) \, G_\psi(q), \tag{4.46}$$

where A_h is a purely combinatorial factor (in the present normalization $A_h = 3 \times 2 = 6$). Using $G_\psi(q) G_\psi(q) = -\mathbb{1}/q^2$ as above, we find

$$G_\phi(q) \, G_\psi(q) \, G_\psi(q) = -\frac{1}{q^2(q^2+r)} \, \mathbb{1}. \tag{4.47}$$

We evaluate the shell integral explicitly:

$$\begin{aligned} \int_{\text{shell}} \frac{\mathrm{d}^D q}{(2\pi)^D} \frac{1}{q^2(q^2+r)} &= \int_{\Lambda/b}^{\Lambda} \mathrm{d}q \; K_D \, q^{D-1} \frac{1}{q^2(q^2+r)} = \int_{\Lambda/b}^{\Lambda} \mathrm{d}q \; K_D \, q^{D-3} \frac{1}{q^2+r} \\ &\simeq K_D \, \Lambda^{D-2} \frac{1}{\Lambda^2+r} \, t = K_D \, \Lambda^{D-4} \frac{1}{1+\tilde{r}} \, t. \end{aligned} \tag{4.48}$$

Substituting (4.48) into (4.46) and setting $A_h = 6$,

$$\delta h = -\, h^3 \, K_D \, \Lambda^{D-4} \frac{1}{1+\tilde{r}} \, t. \tag{4.49}$$

Converting to the flow of h^2 (using $\delta(h^2) = 2h\delta h$) and expressing the result in terms of the dimensionless h^2 defined in (4.15) leads to the one-loop vertex contribution

$$\beta_{\tilde{h}^2}\big|_{\text{vertex}} = \frac{2\tilde{h}^4}{1+\tilde{r}}. \tag{4.50}$$

Including scaling and anomalous dimensions then gives

$$\beta_{\tilde{h}^2} = (D - 4 + \eta + 2\eta_\psi) \, \tilde{h}^2 + \frac{2\tilde{h}^4}{1+\tilde{r}}. \tag{4.51}$$

4.1.3 Fermion self-energy and anomalous dimension η_ψ

To determine the fermionic anomalous dimension, we evaluate the one-loop correction to the fermion two-point function (Fig. 4.2(e)). Keeping an external slow fermion momentum p and integrating out shell modes yields a self-energy contribution of the form

$$\delta S_{\text{eff}}\big|_\Sigma = -\frac{1}{2} \int_{|p|<\Lambda/b} \mathrm{d}p \; \bar{\psi}(p) \, \Sigma(p) \, \psi(p). \tag{4.52}$$

At order $\mathcal{O}(h^2)$, contracting the fast boson and fast fermion lines gives

$$\Sigma(p) = 2\,h^2 \int_{\text{shell}} \frac{\mathrm{d}^D q}{(2\pi)^D}\, \frac{-\mathrm{i}\gamma_\mu q^\mu}{q^2}\, \frac{1}{(p-q)^2 + r}. \tag{4.53}$$

Here the factor 2 accounts for the two inequivalent contractions of the fermionic fields at the two Yukawa vertices.

Since the fermion kinetic term is linear in p, it suffices to expand the integrand to first order in p. Using

$$\frac{1}{(p-q)^2 + r} = \frac{1}{q^2 + r}\left(1 + \frac{2p\cdot q}{q^2 + r} + \mathcal{O}(p^2)\right), \tag{4.54}$$

we obtain

$$\frac{q^\mu}{q^2[(p-q)^2 + r]} = \frac{q^\mu}{q^2(q^2 + r)} + \frac{2q^\mu q_\nu}{q^2(q^2 + r)^2}\, p^\nu + \mathcal{O}(p^2). \tag{4.55}$$

The first term in (4.55) is odd in q and vanishes upon shell integration. The second term contributes to the renormalization of the kinetic term. By rotational invariance,

$$\int_{\text{shell}} \frac{\mathrm{d}^D q}{(2\pi)^D}\, \frac{q^\mu q^\nu}{q^2}\, F(q^2) = \frac{\delta^{\mu\nu}}{D} \int_{\text{shell}} \frac{\mathrm{d}^D q}{(2\pi)^D}\, F(q^2), \tag{4.56}$$

so that

$$\int_{\text{shell}} \frac{\mathrm{d}^D q}{(2\pi)^D}\, \frac{2q^\mu q_\nu}{q^2(q^2 + r)^2}\, p^\nu = \frac{2}{D}\, p^\mu \int_{\text{shell}} \frac{\mathrm{d}^D q}{(2\pi)^D}\, \frac{1}{(q^2 + r)^2}. \tag{4.57}$$

Inserting this into (4.53) gives, to linear order in p,

$$\Sigma(p) = -2\,h^2\, \mathrm{i}\gamma_\mu p^\mu\, \frac{2}{D} \int_{\text{shell}} \frac{\mathrm{d}^D q}{(2\pi)^D}\, \frac{1}{(q^2 + r)^2} + \mathcal{O}(p^2). \tag{4.58}$$

Evaluating the remaining shell integral explicitly,

$$\int_{\text{shell}} \frac{\mathrm{d}^D q}{(2\pi)^D} \frac{1}{(q^2 + r)^2} = \int_{\Lambda/b}^{\Lambda} \mathrm{d}q\; K_D\, q^{D-1} \frac{1}{(q^2 + r)^2} \simeq K_D\, \Lambda^{D-4}\, \frac{1}{(1 + \tilde{r})^2}\, t, \tag{4.59}$$

we can rewrite (4.58) as

$$\Sigma(p) = -\mathrm{i}\not{p}\left[\frac{2}{D}\, \frac{2\,h^2\, K_D\, \Lambda^{D-4}}{(1 + \tilde{r})^2}\right] t. \tag{4.60}$$

Hence the fermion kinetic term is renormalized according to

$$\int (\mathrm{d}p)\, \bar{\psi}\, \mathrm{i}\not{p}\, \psi \;\longrightarrow\; \int (\mathrm{d}p)\, \bar{\psi}\, \mathrm{i}\not{p}\, \psi \left[1 + \delta Z_\psi\right], \qquad \delta Z_\psi = \frac{2}{D}\, \frac{h^2\, K_D\, \Lambda^{D-4}}{(1 + \tilde{r})^2}\, t. \tag{4.61}$$

Using the dimensionless Yukawa coupling defined in (4.15), this becomes

$$Z_\psi = 1 + \frac{2}{D}\, \frac{\tilde{h}^2}{(1 + \tilde{r})^2}\, t, \qquad \eta_\psi \equiv \partial_t \ln Z_\psi = \frac{2}{D}\, \frac{\tilde{h}^2}{(1 + \tilde{r})^2}, \tag{4.62}$$

which is the one-loop fermionic anomalous dimension used in (4.51).

4.1.4 Flow of the quartic boson coupling λ

At one loop, λ receives a purely bosonic contribution of order $\mathcal{O}(\lambda^2)$ and a fermionic box contribution of order $\mathcal{O}(h^4)$.

(i) Bosonic one-loop correction $\mathcal{O}(\lambda^2)$. The relevant term arises from the connected second-order cumulant

$$\delta S_{\text{eff}}\big|_{\lambda^2} = -\frac{1}{2}\langle S_\lambda^2\rangle_{>,c}. \tag{4.63}$$

Selecting four external slow fields and contracting the remaining fast fields into a loop yields three topologically equivalent one-loop diagrams, as shown in Fig. (g)–(i). In the Ising case, these three contributions carry identical loop integrals and their symmetry/combinatorial weights add up to $8 + 32 + 32 = 72$. Consequently, the correction to the physical quartic coupling reads

$$\delta\lambda\big|_{\lambda^2} = -36\,\lambda^2 \int_{\text{shell}} \frac{\mathrm{d}^D q}{(2\pi)^D}\,\frac{1}{(q^2+r)^2} = -36\,\lambda^2\, I_2(r). \tag{4.64}$$

Using (4.14) and expressing the result in terms of the dimensionless λ from (4.15) yields

$$\dot{\tilde{\lambda}}\Big|_{\lambda^2} = -36\,\frac{\tilde{\lambda}^2}{(1+\tilde{r})^2}. \tag{4.65}$$

(ii) Fermionic box correction $\mathcal{O}(h^4)$. Four Yukawa vertices generate an effective ϕ^4 interaction via a closed fast-fermion loop. At vanishing external momenta, the corresponding contribution is proportional to

$$-\frac{1}{4!}\times 3\times 2\times(-1)\times N_f\,h^4 \int_{\text{shell}} \frac{\mathrm{d}^D q}{(2\pi)^D}\,\mathrm{Tr}\big[G(q)^4\big]\,, \tag{4.66}$$

where the factor 3×2 counts the distinct contractions of four Yukawa vertices into a closed fermion box, the factor (-1) is the standard sign of a closed fermion loop, and N_f arises from the internal flavor summation.

Using the free propagator

$$G(q) = \frac{1}{\mathrm{i}\not{q}} = -\,\mathrm{i}\,\frac{\not{q}}{q^2}, \tag{4.67}$$

one finds

$$\mathrm{Tr}\big[G(q)^4\big] = \frac{1}{q^8}\,\mathrm{Tr}\big[(\not{q})^4\big] = \frac{1}{q^8}\,q_\mu q_\nu q_\rho q_\sigma\,\mathrm{Tr}(\gamma_\mu\gamma_\nu\gamma_\rho\gamma_\sigma)\,. \tag{4.68}$$

To evaluate the angular average, it is convenient to use rotational invariance. For the shell

integrals one has

$$\int_{\text{shell}} \frac{\mathrm{d}^D q}{(2\pi)^D} \frac{q_i^4}{q^8} = \frac{3}{D(D+2)} \int_{\text{shell}} \frac{\mathrm{d}^D q}{(2\pi)^D} q^{-4} \simeq \frac{3}{D(D+2)} \frac{S_D}{(2\pi)^D} \Lambda^{D-4}\, t, \tag{4.69}$$

$$\int_{\text{shell}} \frac{\mathrm{d}^D q}{(2\pi)^D} \frac{q_i^2 q_j^2}{q^8} = \frac{1}{D(D+2)} \int_{\text{shell}} \frac{\mathrm{d}^D q}{(2\pi)^D} q^{-4} \simeq \frac{1}{D(D+2)} \frac{S_D}{(2\pi)^D} \Lambda^{D-4}\, t \qquad (i \neq j). \tag{4.70}$$

Combining these angular averages with

$$\mathrm{Tr}(\gamma_\mu \gamma_\nu \gamma_\rho \gamma_\sigma) = d_\gamma \big(\delta_{\mu\nu}\delta_{\rho\sigma} - \delta_{\mu\rho}\delta_{\nu\sigma} + \delta_{\mu\sigma}\delta_{\nu\rho}\big), \tag{4.71}$$

the diagonal terms $\propto q_i^4$ and off-diagonal terms $\propto q_i^2 q_j^2$ recombine into

$$\int_{\text{shell}} \frac{\mathrm{d}^D q}{(2\pi)^D}\, \mathrm{Tr}\big[G(q)^4\big] = d_\gamma \frac{S_D}{(2\pi)^D} \Lambda^{D-4}\, t. \tag{4.72}$$

In the shell normalization adopted in (4.15), one therefore obtains

$$\beta_{\tilde\lambda}|_{\tilde h^4} = -\left.\frac{\mathrm{d}\tilde\lambda}{\mathrm{d}t}\right|_{\tilde h^4} = \frac{1}{4!} \times 3 \times 2 \times (-1) \times d_\gamma N_f\, \tilde h^4 = N_f \tilde h^4. \tag{4.73}$$

Result for $\dot\lambda$. Including scaling and the boson anomalous dimension gives

$$\beta_{\tilde\lambda} = (D - 4 + 2\eta)\, \tilde\lambda + 36\, \frac{\tilde\lambda^2}{(1+\tilde r)^2} - N_f\, \tilde h^4. \tag{4.74}$$

4.1.5 Summary of the one-loop RG flow

Collecting Eqs. (4.51), (4.74), and (4.44), and suppressing the tildes on $\tilde h^2$, $\tilde\lambda$, and $\tilde r$ for simplicity, the one-loop RG flow equations for the partially bosonized Gross-Neveu-Ising truncation read

$$\dot h^2 = (D - 4 + \eta + 2\eta_\psi)\, h^2 + \frac{2h^4}{1+r}, \tag{4.75}$$

$$\dot\lambda = (D - 4 + 2\eta)\, \lambda + 36\, \frac{\lambda^2}{(1+r)^2} - N_f\, h^4, \tag{4.76}$$

$$\dot r = (-2 + \eta)\, r - 12\, \frac{\lambda}{1+r} + d_\gamma N_f\, h^2. \tag{4.77}$$

$$\eta_\psi = \frac{2}{D} \frac{h^2}{(1+r)^2}, \qquad \eta = \left(1 - \frac{2}{D}\right) d_\gamma N_f h^2. \tag{4.78}$$

To make contact with the purely fermionic description, we eliminate the Yukawa coupling in

favor of the four-fermion coupling by using the Hubbard–Stratonovich relation

$$g \;=\; -\frac{N_f h^2}{r} \qquad \Longleftrightarrow \qquad h^2 \;=\; -\frac{r}{N_f}\, g. \tag{4.79}$$

Substituting (4.79) into Eqs. (4.75)–(4.77) and taking the limit $r \to \infty$ (such that the bosonic field becomes infinitely massive and can be integrated out again), one recovers the RG flow obtained in the purely fermionic formulation.

Critical exponents at the GNI fixed point. At the Gross-Neveu-Ising fixed point, for different fermion flavor numbers N_f we obtain the following results for three critical exponents:

N_f	$1/\nu$	η	η_ψ
2	0.946	0.677	0.039
4	0.929	0.865	0.012
8	0.958	0.939	0.005

These values should be regarded as representative results within our present approximation. More accurate estimates from fixed-dimension RG approaches of the GNI critical exponents have been reported in functional renormalization-group studies [51], where they were shown to be in close agreement with MC simulations [52, 53].

4.2 Gross-Neveu-XY model

In the purely fermionic formulation, the RG-closed Gross-Neveu-XY theory space contains six independent four-fermion couplings, which we denote by $g_1, \ldots, g_6$. As shown in Sec. 2, the Gross-Neveu-XY fixed point is confined to the invariant subspace spanned by the three couplings (g_3, g_4, g_6). To simplify the partially bosonized treatment while retaining the correct critical fixed point, we therefore bosonize only these three channels and set the remaining couplings to zero within this subsection.

We introduce auxiliary bosonic fields via a Hubbard-Stratonovich transformation in the g_3-, g_4-, and g_6-channels. The resulting partially bosonized Lagrangian is written as

$$\mathcal{L} = \mathcal{L}_F + \mathcal{L}_{FB} + \mathcal{L}_B \tag{4.80}$$

with fermionic kinetic term

$$\mathcal{L}_F = \bar{\psi}^\alpha \gamma_\mu \partial_\mu \psi^\alpha \tag{4.81}$$

The Yukawa sector contains three couplings, ordered to correspond to g_3, g_4, g_6,

$$\mathcal{L}_{FB} = \bar{\psi}^\alpha \big[h_1 \Phi + h_2 \Omega + h_3 X \big] \psi^\alpha \tag{4.82}$$

where the bosonic fields are embedded into the Dirac space as

$$\Phi = i\gamma_3\phi_1 + i\gamma_5\phi_2, \quad \Omega = \gamma_{01}\omega_2 + \gamma_{02}\omega_1 + \gamma_{12}\omega_3, \quad X = \gamma_{35}\chi \tag{4.83}$$

Here (ϕ_1, ϕ_2) is the two-component order parameter associated with the chiral $U(1)$ channel, $(\omega_2, \omega_1, \omega_3)$ parametrizes the antisymmetric tensor channel $(\bar{\psi}\gamma_{\mu\nu}\psi)^2$, and χ bosonizes the $(\bar{\psi}\gamma_{35}\psi)^2$ channel. As in the Ising case, completing the square fixes the relation between the original four-fermion couplings and the Yukawa/mass parameters in each channel (up to the overall sign convention)at the microscopic scale, but we will treat (h_i, r_i) as independent running couplings in the RG analysis.

The purely bosonic part is taken in the symmetry-allowed local truncation with three mass parameters and six quartic couplings,

$$\begin{aligned}\mathcal{L}_B =& \frac{1}{2}\phi_a\big(-\partial_\mu^2 + r_1\big)\phi_a + \frac{1}{2}\omega_b\big(-\partial_\mu^2 + r_2\big)\omega_b + \frac{1}{2}\chi\big(-\partial_\mu^2 + r_3\big)\chi + \lambda_1(\phi_a^2)^2 + \lambda_2(\omega_b^2)^2 \\ &+ \lambda_3\chi^4 + 2\lambda_4\phi_a^2\omega_b^2 + 2\lambda_5\phi_a^2\chi^2 + 2\lambda_6\omega_b^2\chi^2,\end{aligned} \tag{4.84}$$

where $a = 1, 2$ and $b = 1, 2, 3$, and we use the shorthand $\phi_a^2 \equiv \sum_{a=1}^{2}\phi_a^2$ and $\omega_b^2 \equiv \sum_{b=1}^{3}\omega_b^2$. In total, this truncation contains three Yukawa couplings (h_1, h_2, h_3), three bosonic masses (r_1, r_2, r_3), and six quartic bosonic couplings $(\lambda_1, \ldots, \lambda_6)$.

Repeating the calculation outlined in Sec. 3.1, we obtain the RG flow equations for this partially bosonized Gross-Neveu-XY truncation as follows:

$$\dot{h}_1^2 = \big(D - 4 + \eta_1 + 2\eta_\psi\big)h_1^2 + 2\Big(-N_2h_2^2\frac{1}{1+r_2} + N_3h_3^2\frac{1}{1+r_3}\Big)h_1^2 \tag{4.85}$$

$$\dot{h}_2^2 = \big(D - 4 + \eta_2 + 2\eta_\psi\big)h_2^2 + \frac{2}{3}h_2^4\frac{1}{1+r_2} + \frac{2}{3}\Big(-N_1h_1^2\frac{1}{1+r_1} - N_3h_3^2\frac{1}{1+r_3}\Big)h_2^2 \tag{4.86}$$

$$\dot{h}_3^2 = \big(D - 4 + \eta_3 + 2\eta_\psi\big)h_3^2 + 2N_3h_3^4\frac{1}{1+r_3} + 2\Big(-N_1h_1^2\frac{1}{1+r_1} + N_2h_2^2\frac{1}{1+r_2}\Big)h_3^2 \tag{4.87}$$

$$\dot{\lambda}_1 = \big(D - 4 + 2\eta_1\big)\lambda_1 + 4(N_1+8)\lambda_1^2\frac{1}{(1+r_1)^2} + 4N_2\lambda_4^2\frac{1}{(1+r_2)^2} + 4N_3\lambda_6^2\frac{1}{(1+r_3)^2} - N_fh_1^4 \tag{4.88}$$

$$\dot{\lambda}_2 = \big(D - 4 + 2\eta_2\big)\lambda_2 + 4(N_2+8)\lambda_2^2\frac{1}{(1+r_2)^2} + 4N_1\lambda_4^2\frac{1}{(1+r_1)^2} + 4N_3\lambda_5^2\frac{1}{(1+r_3)^2} + \frac{1}{15}N_fh_2^4 \tag{4.89}$$

$$\dot{\lambda}_3 = \big(D - 4 + 2\eta_3\big)\lambda_3 + 4(N_3+8)\lambda_3^2\frac{1}{(1+r_3)^2} + 4N_2\lambda_5^2\frac{1}{(1+r_2)^2} + 4N_1\lambda_6^2\frac{1}{(1+r_1)^2} - N_fh_3^4 \tag{4.90}$$

$$\begin{aligned}\dot{\lambda}_4 =& \big(D - 4 + \eta_1 + \eta_2\big)\lambda_4 + 16\lambda_4^2\frac{1}{(1+r_1)(1+r_2)} + 4(N_1+2)\lambda_1\lambda_4\frac{1}{(1+r_1)^2} \\ &+ 4(N_2+2)\lambda_2\lambda_4\frac{1}{(1+r_2)^2} - \frac{5}{3}N_fh_1^2h_2^2\end{aligned} \tag{4.91}$$

$$\dot{\lambda}_5 = \big(D-4+\eta_2+\eta_3\big)\lambda_5 + 16\lambda_5^2\frac{1}{(1+r_2)(1+r_3)} + 4(N_2+2)\lambda_2\lambda_5\frac{1}{(1+r_2)^2} + 4(N_3+2)\lambda_3\lambda_5\frac{1}{(1+r_3)^2} - \frac{1}{3}N_f h_2^2 h_3^2 \tag{4.92}$$

$$\dot{\lambda}_6 = \big(D-4+\eta_1+\eta_3\big)\lambda_6 + 16\lambda_6^2\frac{1}{(1+r_1)(1+r_3)} + 4(N_1+2)\lambda_1\lambda_6\frac{1}{(1+r_1)^2} + 4(N_3+2)\lambda_3\lambda_6\frac{1}{(1+r_3)^2} + 3N_f h_1^2 h_3^2 \tag{4.93}$$

$$\dot{r}_1 = \big(\eta_1-2\big)r_1 - \big(8+4N_1\big)\lambda_1\frac{1}{1+r_1} - 4\Big(N_2\lambda_4\frac{1}{1+r_2} + N_3\lambda_6\frac{1}{1+r_3}\Big) - d_\gamma N_f h_1^2 \tag{4.94}$$

$$\dot{r}_2 = \big(\eta_2-2\big)r_2 - \big(8+4N_2\big)\lambda_2\frac{1}{1+r_2} - 4\Big(N_1\lambda_4\frac{1}{1+r_1} + N_3\lambda_5\frac{1}{1+r_3}\Big) - \frac{1}{3}d_\gamma N_f h_2^2, \tag{4.95}$$

$$\dot{r}_3 = \big(\eta_3-2\big)r_3 - \big(8+4N_3\big)\lambda_3\frac{1}{1+r_3} - 4\Big(N_2\lambda_5\frac{1}{1+r_2} + N_1\lambda_6\frac{1}{1+r_1}\Big) + d_\gamma N_f h_3^2. \tag{4.96}$$

where $N_1 = 2, N_2 = 3$, and $N_3 = 1$ are the numbers of components of the three bosonic multiplets in the g_3-, g_4-, and g_6-channels, respectively.
The anomalous dimensions are given by

$$\begin{aligned} \eta_\psi &= \frac{2}{D}\left(-\frac{2h_1^2}{(1+r_1)^2} - \frac{h_2^2}{(1+r_2)^2} + \frac{h_3^2}{(1+r_3)^2}\right), \\ \eta_1 = \left(\frac{2}{D}-1\right)d_\gamma N_f h_1^2, \quad \eta_2 &= \left(\frac{2}{D}-1\right)\frac{1}{3}d_\gamma N_f h_2^2, \quad \eta_3 = \left(1-\frac{2}{D}\right)d_\gamma N_f h_3^2. \end{aligned} \tag{4.97}$$

Having derived the RG flow for the GNXY model, we now proceed to the fixed-point analysis. Our calculation shows that the GNXY fixed point is confined to the subspace spanned by (h_1, λ_1, r_1). This is directly analogous to the purely fermionic analysis in which one neglects the contributions from the Feynman diagrams in Fig. 1(c,d): in that approximation, the GNXY fixed point moves only along the g_3 axis (which corresponds to h_1 in the partially bosonized formulation). In both situations, the GNXY fixed point does not collide with any other fixed point. The reason is that, within the partially bosonized description, box diagrams involving four Yukawa vertices regenerate four-fermion interactions, but this box-generated contribution has been completely neglected in the above truncation. In Sec. 5 we will therefore include these effects by means of dynamical bosonization.
For the GNXY fixed point, the resulting critical exponents for different fermion flavor numbers N_f are summarized in Table 4.1.

N_f	$1/\nu$	η_ϕ	η_ψ
2	0.764	0.867	0.067
4	0.868	0.956	0.022
8	0.929	0.981	0.009

Table 4.1: Critical exponents at the GNXY fixed point obtained from the linearized stability matrix for representative values of N_f.

4.3 Gross-Neveu-Heisenberg model

We now partially bosonize the Gross-Neveu-Heisenberg (GNH) model. The symmetry-complete purely fermionic interaction has been given in Eq. (2.33). Following the same decomposition of the partially bosonized Lagrangian as in Eq. (4.80), we specify here the explicit forms of $\mathcal{L}_F$, $\mathcal{L}_{FB}$, and $\mathcal{L}_B$ for the GNH truncation.

The fermionic kinetic term reads

$$\mathcal{L}_F = \bar{\psi}^\alpha(\tau_\mu \otimes \mathbb{1}_2)\partial_\mu \psi^\alpha. \tag{4.98}$$

We introduce four Hubbard-Stratonovich fields, in one-to-one correspondence with the four channels in Eq. (2.33), leading to the Yukawa sector

$$\mathcal{L}_{FB} = \bar{\psi}^\alpha\Big[h_1\phi(\mathbb{1}_2 \otimes \mathbb{1}_2) + h_2 A_\mu(\tau_\mu \otimes \mathbb{1}_2) + h_3\vec{\varphi}\cdot(\mathbb{1}_2 \otimes \vec{\sigma}) + h_4\vec{B}_\mu\cdot(\tau_\mu \otimes \vec{\sigma})\Big]\psi^\alpha \tag{4.99}$$

Here ϕ is a real scalar, A_μ is a real Lorentz vector, $\vec{\varphi}$ is a real $SU(2)$ vector, and $\vec{B}_\mu$ transforms as a vector under both Lorentz rotations (index μ) and $SU(2)$ spin rotations (arrow).

The purely bosonic sector is taken in the symmetry-allowed local truncation with four mass parameters and ten quartic couplings,

$$\begin{aligned}\mathcal{L}_B =& \frac{1}{2}\,\phi\big(-\partial_\mu^2 + r_1\big)\phi + \frac{1}{2}\,A_\mu\big(-\partial_\nu^2 + r_2\big)A_\mu + \frac{1}{2}\,\vec{\varphi}\big(-\partial_\mu^2 + r_3\big)\vec{\varphi} + \frac{1}{2}\,\vec{B}_\mu\big(-\partial_\nu^2 + r_4\big)\vec{B}_\mu \\ &+ \lambda_1\,\phi^4 + \lambda_2\,(A_\mu A_\mu)^2 + \lambda_3\,(\vec{\varphi}\cdot\vec{\varphi})^2 + \lambda_4\,(\vec{B}_\mu\cdot\vec{B}_\mu)^2 + 2\lambda_5\,\phi^2(A_\mu A_\mu) + 2\lambda_6\,\phi^2(\vec{\varphi}\cdot\vec{\varphi}) \\ &+ 2\lambda_7\,\phi^2(\vec{B}_\mu\cdot\vec{B}_\mu) + 2\lambda_8\,(A_\mu A_\mu)(\vec{\varphi}\cdot\vec{\varphi}) + 2\lambda_9\,(A_\mu A_\mu)(\vec{B}_\nu\cdot\vec{B}_\nu) + 2\lambda_{10}\,(\vec{\varphi}\cdot\vec{\varphi})(\vec{B}_\mu\cdot\vec{B}_\mu)\end{aligned} \tag{4.100}$$

Altogether, this truncation involves four Yukawa couplings (h_1, h_2, h_3, h_4), four bosonic masses (r_1, r_2, r_3, r_4), and ten quartic bosonic couplings $(\lambda_1, \ldots, \lambda_{10})$.

The corresponding RG flow equations (including anomalous dimensions) for the partially bosonized Gross-Neveu-Heisenberg model read as follows:

$$\begin{aligned}\dot{h}_1^2 =& \big(D - 4 + \eta_1 + 2\eta_\psi\big)h_1^2 - 2(N_1 - 2)h_1^4\frac{1}{1+r_1} \\ &- 2\Big(-N_2 h_2^2\frac{1}{1+r_2} - N_3 h_3^2\frac{1}{1+r_3} - N_4 h_4^2\frac{1}{1+r_4}\Big)h_1^2\end{aligned} \tag{4.101}$$

$$\begin{aligned}\dot{h}_2^2 =& \big(D - 4 + \eta_2 + 2\eta_\psi\big)h_2^2 + \frac{2}{3}(N_2 - 2)h_2^4\frac{1}{1+r_2} \\ &- 2\Big(\frac{1}{3}N_1 h_1^2\frac{1}{1+r_1} + \frac{1}{3}N_3 h_3^2\frac{1}{1+r_3} - h_4^2\frac{1}{1+r_4}\Big)h_2^2\end{aligned} \tag{4.102}$$

$$\begin{aligned}\dot{h}_3^2 =&\big(D-4+\eta_3+2\eta_\psi\big)h_3^2-2(N_3-2)h_3^4\frac{1}{1+r_3}\\&-2\Big(-N_1h_1^2\frac{1}{1+r_1}-N_2h_2^2\frac{1}{1+r_2}+3h_4^2\frac{1}{1+r_4}\Big)h_3^2\end{aligned}\tag{4.103}$$

$$\begin{aligned}\dot{h}_4^2 =&\big(D-4+\eta_4+2\eta_\psi\big)h_4^2-\frac{2}{3}h_4^4\frac{1}{1+r_4}\\&-2\Big(\frac{1}{3}N_1h_1^2\frac{1}{1+r_1}-\frac{1}{3}(N_2-2)h_2^2\frac{1}{1+r_2}-\frac{1}{3}(N_3-2)h_3^2\frac{1}{1+r_3}\Big)h_4^2\end{aligned}\tag{4.104}$$

$$\begin{aligned}\dot{\lambda}_1 =&\big(D-4+2\eta_1\big)\lambda_1+4(N_1+8)\lambda_1^2\frac{1}{(1+r_1)^2}\\&+4\Big(N_2\lambda_5^2\frac{1}{(1+r_2)^2}+N_3\lambda_6^2\frac{1}{(1+r_3)^2}+N_4\lambda_7^2\frac{1}{(1+r_4)^2}\Big)-N_fh_1^4,\end{aligned}\tag{4.105}$$

$$\begin{aligned}\dot{\lambda}_2 =&\big(D-4+2\eta_2\big)\lambda_2+4(N_2+8)\lambda_2^2\frac{1}{(1+r_2)^2}\\&+4\Big(N_1\lambda_5^2\frac{1}{(1+r_1)^2}+N_3\lambda_8^2\frac{1}{(1+r_3)^2}+N_4\lambda_9^2\frac{1}{(1+r_4)^2}\Big)+\frac{1}{15}N_fh_2^4\end{aligned}\tag{4.106}$$

$$\begin{aligned}\dot{\lambda}_3 =&\big(D-4+2\eta_3\big)\lambda_3+4(N_3+8)\lambda_3^2\frac{1}{(1+r_3)^2}\\&+4\Big(N_1\lambda_6^2\frac{1}{(1+r_1)^2}+N_2\lambda_8^2\frac{1}{(1+r_2)^2}+N_4\lambda_{10}^2\frac{1}{(1+r_4)^2}\Big)-N_fh_3^4\end{aligned}\tag{4.107}$$

$$\begin{aligned}\dot{\lambda}_4 =&\big(D-4+2\eta_4\big)\lambda_4+4(N_4+8)\lambda_4^2\frac{1}{(1+r_4)^2}\\&+4\Big(N_1\lambda_7^2\frac{1}{(1+r_1)^2}+N_2\lambda_9^2\frac{1}{(1+r_2)^2}+N_3\lambda_{10}^2\frac{1}{(1+r_3)^2}\Big)+\frac{1}{15}N_fh_4^4\end{aligned}\tag{4.108}$$

$$\begin{aligned}\dot{\lambda}_5 =&\big(D-4+\eta_1+\eta_2\big)\lambda_5+16\lambda_5^2\frac{1}{(1+r_1)(1+r_2)}+4(N_1+2)\lambda_1\lambda_5\frac{1}{(1+r_1)^2}\\&+4(N_2+2)\lambda_2\lambda_5\frac{1}{(1+r_2)^2}-\frac{1}{3}N_fh_1^2h_2^2\end{aligned}\tag{4.109}$$

$$\begin{aligned}\dot{\lambda}_6 =&\big(D-4+\eta_1+\eta_3\big)\lambda_6+16\lambda_6^2\frac{1}{(1+r_1)(1+r_3)}+4(N_1+2)\lambda_1\lambda_6\frac{1}{(1+r_1)^2}\\&+4(N_3+2)\lambda_3\lambda_6\frac{1}{(1+r_3)^2}-3N_fh_1^2h_3^2\end{aligned}\tag{4.110}$$

$$\begin{aligned}\dot{\lambda}_7 =&\big(D-4+\eta_1+\eta_4\big)\lambda_7+16\lambda_7^2\frac{1}{(1+r_1)(1+r_4)}+4(N_1+2)\lambda_1\lambda_7\frac{1}{(1+r_1)^2}\\&+4(N_4+2)\lambda_4\lambda_7\frac{1}{(1+r_4)^2}-\frac{1}{3}N_fh_1^2h_4^2\end{aligned}\tag{4.111}$$

$$\begin{aligned}\dot{\lambda}_8 =&\big(D-4+\eta_2+\eta_3\big)\lambda_8+16\lambda_8^2\frac{1}{(1+r_2)(1+r_3)}+4(N_2+2)\lambda_2\lambda_8\frac{1}{(1+r_2)^2}\\&+4(N_3+2)\lambda_3\lambda_8\frac{1}{(1+r_3)^2}-\frac{1}{3}N_fh_2^2h_3^2\end{aligned}\tag{4.112}$$

$$\begin{aligned}\dot{\lambda}_9 =&\big(D-4+\eta_2+\eta_4\big)\lambda_9+16\lambda_9^2\frac{1}{(1+r_2)(1+r_4)}+4(N_2+2)\lambda_2\lambda_9\frac{1}{(1+r_2)^2}\\&+4(N_4+2)\lambda_4\lambda_9\frac{1}{(1+r_4)^2}+\frac{1}{5}N_fh_2^2h_4^2\end{aligned}\tag{4.113}$$

$$\begin{aligned}\dot{\lambda}_{10} =&\big(D-4+\eta_3+\eta_4\big)\lambda_{10}+16\lambda_{10}^2\frac{1}{(1+r_3)(1+r_4)}+4(N_3+2)\lambda_3\lambda_{10}\frac{1}{(1+r_3)^2}\\&+4(N_4+2)\lambda_4\lambda_{10}\frac{1}{(1+r_4)^2}-\frac{1}{3}N_fh_3^2h_4^2\end{aligned}\tag{4.114}$$

$$\dot{r}_1 = (\eta_1 - 2) r_1 - (8 + 4N_1)\lambda_1 \frac{1}{1+r_1} - 4\Big(N_2\lambda_5 \frac{1}{1+r_2} + N_3\lambda_6 \frac{1}{1+r_3} + N_4\lambda_7 \frac{1}{1+r_4}\Big) + d_\gamma N_f h_1^2 \tag{4.115}$$

$$\dot{r}_2 = (\eta_2 - 2) r_2 - (8 + 4N_2)\lambda_2 \frac{1}{1+r_2} - 4\Big(N_1\lambda_5 \frac{1}{1+r_1} + N_3\lambda_8 \frac{1}{1+r_3} + N_4\lambda_9 \frac{1}{1+r_4}\Big) - \frac{1}{3} d_\gamma N_f h_2^2 \tag{4.116}$$

$$\dot{r}_3 = (\eta_3 - 2) r_3 - (8 + 4N_3)\lambda_3 \frac{1}{1+r_3} - 4\Big(N_1\lambda_6 \frac{1}{1+r_1} + N_2\lambda_8 \frac{1}{1+r_2} + N_4\lambda_{10} \frac{1}{1+r_4}\Big) + d_\gamma N_f h_3^2 \tag{4.117}$$

$$\dot{r}_4 = (\eta_4 - 2) r_4 - (8 + 4N_4)\lambda_4 \frac{1}{1+r_4} - 4\Big(N_1\lambda_7 \frac{1}{1+r_1} + N_2\lambda_9 \frac{1}{1+r_2} + N_3\lambda_{10} \frac{1}{1+r_3}\Big) - \frac{1}{3} d_\gamma N_f h_4^2 \tag{4.118}$$

where $N_1 = 1, N_2 = 3, N_3 = 3, N_4 = 9$ are numbers of components of the three bosonic multiplets in the g_1-, g_2-, g_3, and g_4-channels, respectively.
The anomalous dimensions are given by

$$\begin{aligned} \eta_\psi &= \frac{2}{D}\left(\frac{h_1^2}{(1+r_1)^2} - \frac{h_2^2}{(1+r_2)^2} + \frac{3h_3^2}{(1+r_3)^2} - \frac{3h_4^2}{(1+r_4)^2}\right), \\ \eta_1 &= \left(1 - \frac{2}{D}\right) d_\gamma N_f h_1^2, \quad \eta_2 = \left(\frac{2}{D} - 1\right)\frac{1}{3} d_\gamma N_f h_2^2, \\ \eta_3 &= \left(1 - \frac{2}{D}\right) d_\gamma N_f h_3^2, \quad \eta_4 = \left(\frac{2}{D} - 1\right)\frac{1}{3} d_\gamma N_f h_4^2, \end{aligned} \tag{4.119}$$

Analogous to the GNXY case discussed above, the GNH fixed point in the partially bosonized flow does not undergo any collision with other fixed points. As in the GNXY model, this absence of fixed-point collisions is a consequence of neglecting the box-generated regeneration of four-fermion interactions from four Yukawa vertices within the present truncation. The corresponding critical exponents at the GNH fixed point for different fermion flavor numbers N_f are summarized in Table 4.2.

N_f	$1/\nu$	η_ϕ	η_ψ
2	0.692	1.101	0.067
4	0.828	1.049	0.029
8	0.905	1.024	0.013

Table 4.2: Critical exponents at the GNH fixed point obtained from the linearized stability matrix for representative values of N_f in the partially bosonized truncation.

5 Dynamically bosonized RG flow

In the partially bosonized framework introduced above, we performed a single HS transformation to replace the targeted four-fermion interaction by a Yukawa coupling, leading to an effective description in terms of the couplings (h, r, λ). However, this replacement is generally not closed under RG transformations: even if the four-fermion coupling is set to zero at the initial scale, one-loop box diagrams (Fig. 5.1) regenerate four-fermion terms along the flow. Neglecting these regenerated contributions amounts to projecting the theory back onto the single-interaction-channel subspace at every scale. While such a projection can be safely justified near $D = 4$, where the corresponding four-fermion operators are typically irrelevant by power counting, in $D = 3$ they can become relevant or at least quantitatively important and may therefore affect the flow and fixed-point structure. Including the full set of interaction channels becomes particularly important in situations where different interactions compete, potentially giving rise to phenomena such as fixed-point collisions and annihilations, as observed in the purely fermionic formulation. To consistently incorporate such effects, we employ the method of dynamical bosonization [54–57].

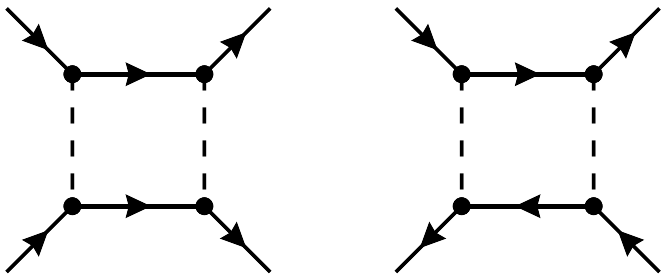

Figure 5.1: One-loop box diagrams generating the effective four-fermion box term from four Yukawa vertices.

The central idea of dynamical bosonization is to allow, after each infinitesimal RG step, a field redefinition of the bosonic order-parameter field by a fermion bilinear, which is equivalent to performing a HS decoupling repeatedly along the flow. In practice, this is implemented by an infinitesimal shift of the bosonic field such that the newly generated four-fermion term is

continuously absorbed into the Yukawa sector. The partition function is written as

$$\mathcal{Z} = \int \mathcal{D}\bar{\psi}\mathcal{D}\psi\mathcal{D}\phi \; e^{-S[\bar{\psi},\psi,\phi]} \tag{5.1}$$

For any fixed configuration of ψ and $\bar{\psi}$, we perform an infinitesimal shift of the order-parameter field inside the bosonic functional integral,

$$\phi \longrightarrow \phi + \delta\omega(\bar{\psi}\mathcal{M}\psi) \tag{5.2}$$

where $\delta\omega = \mathcal{O}(\delta t)$ is of the same order as the infinitesimal logarithmic RG step δt, and $\mathcal{M}$ is the matrix associated with the particular channel. Expanding the action to linear order in $\delta\omega$ shows that the bosonic mass term $\frac{1}{2}r\phi^2$ together with the Yukawa term $h\phi(\bar{\psi}\mathcal{M}\psi)$ generates an additional four-fermion contribution. At the same time, integrating out fast modes produces a box-diagram contribution that induces an increment δg_{box} in the four-fermion coupling. At this order, the net coefficient of the four-fermion term takes the form

$$\delta g_{\text{box}} + h\delta\omega \tag{5.3}$$

Therefore, choosing

$$\delta\omega \equiv -\frac{\delta g_{\text{box}}}{h} \tag{5.4}$$

cancels the newly generated four-fermion term exactly at each RG step. In this way, the theory is kept on the partially bosonized subspace with vanishing explicit four-fermion couplings, while the physical effect of the regenerated interaction is retained through the induced running of the Yukawa sector. Consequently, the flow of the Yukawa coupling is no longer given solely by the standard one-loop contributions; it receives additional terms originating from the field redefinition in Eqs. (5.2)-(5.4). Equivalently, the box-diagram contribution δg_{box} is mapped into the running of h, yielding RG equations that remain closed in terms of (h, r, λ) while consistently incorporating the potentially relevant four-fermion effects in $D = 3$.
In the following, we implement this dynamical bosonization prescription explicitly: we first compute the box-induced four-fermion contribution δg_{box} within the chosen truncation, and then use the condition in Eq. (5.4) to transfer this contribution into the Yukawa sector, obtaining the dynamical-bosonization-improved RG flow and fixed-point structure.

5.1 Bosonization of the Gross-Neveu-Ising model

In the partially bosonized formulation of the Gross-Neveu-Ising model, the Yukawa interaction involves only a single scalar channel,

$$\mathcal{L}_{\psi\phi} = h\phi(\bar{\psi}\psi) \tag{5.5}$$

At one-loop order, box diagrams built from four Yukawa vertices can in principle regenerate a four-fermion operator. For the scalar channel considered here, there are two topologically distinct box contributions: a direct contraction and a crossed contraction. Both contributions project onto the same operator $(\bar{\psi}\psi)^2$, but they enter with opposite relative sign due to the exchange of fermionic lines. As a result, the two box diagrams cancel exactly in the projection onto $(\bar{\psi}\psi)^2$, and no net four-fermion interaction is generated,

$$\delta g^{(\mathrm{I})}_{\mathrm{box}} = 0 \tag{5.6}$$

Consequently, for the Gross–Neveu–Ising truncation the dynamical-bosonization step does not produce any additional correction: the dynamical-bosonization contribution to the Yukawa flow vanishes,

$$\Delta\beta^{(\mathrm{I})}_{h^2} = 0 \tag{5.7}$$

and the RG flow equations coincide with those obtained without dynamical bosonization.

5.2 Bosonization of the Gross-Neveu-XY model

We now include the dynamical-bosonization correction for the Gross-Neveu-XY model. Here we restrict the analysis to the invariant Gross-Neveu-XY subspace spanned by (g_3, g_4, g_6), and compute the corresponding box-induced four-fermion beta functions, denoted by $\beta_{g_{\mathrm{box}}}$.

$$\begin{aligned}
\beta_{g_1} =& 2h_1^2 h_2^2 \frac{1}{1+r_1}\frac{1}{1+r_2} \\
\beta_{g_2} =& \frac{4}{3}h_1^4 \frac{1}{(1+r_1)^2} + \frac{4}{3}h_2^2 h_3^2 \frac{1}{(1+r_2)(1+r_3)} \\
\beta_{g_3} =& 4h_2^4 \frac{1}{(1+r_2)^2}
\end{aligned} \tag{5.8}$$

Imposing the dynamical-bosonization condition that the regenerated four-fermion term is absorbed back into the Yukawa sector, the Yukawa-coupling flow is modified accordingly. In terms of the dimensionless quantity h^2, the corrected flow takes the form

$$\begin{aligned}
\beta_{h^2} =& -\frac{\mathrm{d}h^2}{\mathrm{d}t} = \big(D - 4 + \eta_\phi + 2\eta_\psi\big)h^2 - 2h\,\frac{\partial\,\delta h}{\partial t} + 2r\,\frac{\partial\,\delta g}{\partial t} \\
=& \big(D - 4 + \eta_\phi + 2\eta_\psi\big)h^2 + 2h\,\beta_h - 2r\beta_g
\end{aligned} \tag{5.9}$$

The first two contributions on the right-hand side are contained in the partially bosonized flow listed in Sec. 4.2, while the last term encodes the dynamical-bosonization correction generated by the box-induced four-fermion interaction δg.

By locating the Gross-Neveu-XY fixed point of the RG flow (4.85)–(4.96), we find that it collides with another fixed point A at $N_f \simeq 1.71$ and exchanges its criticality. (For comparison,

in the purely fermionic RG flow this collision occurs at $N_f \simeq 2.07$.) Upon further decreasing N_f, the GNXY fixed point and A pass through each other; in this regime the stability matrix of the GNXY fixed point exhibits two relevant directions, such that it no longer corresponds to a quantum critical point. Therefore, to obtain critical exponents for $N_f < 1.71$, one should instead evaluate the exponents at fixed point A. However, determining A requires implementing dynamical bosonization for the full model with all six interaction channels, which leads to substantially more involved RG flow equations and makes the numerical search for the corresponding solutions considerably more demanding. For this reason, we do not pursue this analysis further here.

For the GNXY fixed point, the resulting three critical exponents for different fermion flavor numbers N_f are summarized in Table 5.1.

N_f	$1/\nu$	η_ϕ	η_ψ
2	0.851	0.756	0.087
4	0.903	0.941	0.023
8	0.948	0.979	0.009

Table 5.1: Three critical exponents at the GNXY fixed point for representative values of N_f, from dynamical bosonization.

To compare the different approximation schemes more systematically, we plot the three critical exponents $1/\nu$, η_ϕ, and η_ψ as functions of the fermion flavor number N_f, contrasting the results obtained from the purely fermionic RG, the partially bosonized flow, and the dynamically bosonized flow. The corresponding results are shown in Fig. 5.2.

As seen from Fig. 5.2(a), the inverse correlation-length exponent $1/\nu$ exhibits a noticeable scheme dependence at small N_f, while the three approaches gradually approach each other for larger N_f. In particular, the dynamically bosonized result shifts the collision point of the critical fixed point to a lower value of N_f compared with the purely fermionic treatment.

The comparison of the anomalous dimensions in Figs. 5.2(b) and 5.2(c) reveals a similar trend. For η_ψ, all three schemes yield relatively small values and approach each other rather quickly as N_f increases. By contrast, the bosonic anomalous dimension η_ϕ is much more sensitive to the approximation scheme at small N_f. In the purely fermionic RG, the red curve in the regime $N_f < N_f^c \simeq 2.07$ is evaluated not at the original GNXY fixed point, but at the new fixed point $\mathcal{B}$ that becomes quantum critical after the fixed-point collision, see Sec. 3.2. As a consequence, the fermionic estimates in this regime are significantly enhanced compared with a naive continuation of the original GNXY branch. This behavior is in agreement with the analytical results obtained from the $(2+\epsilon)$ expansion, where the universal critical behavior for $N_f < N_f^c$ is governed by the new quantum critical fixed point and, in particular for $N_f = 2$, one obtains $\eta_\phi(N_f = 2) = 2 - \frac{1}{6}\epsilon + \mathcal{O}(\epsilon^2)$ and $\eta_\psi(N_f = 2) = \frac{7}{72}\epsilon^2 + \mathcal{O}(\epsilon^3)$ [23]. In contrast, the partially bosonized and dynamically bosonized flows display a smooth evolution of both anomalous dimensions.

Most importantly, the dynamically bosonized flow consistently pushes the fixed-point collision from the purely fermionic value $N_f \simeq 2.07$ down to $N_f \simeq 1.71$. This indicates that the explicit inclusion of scale-dependent rebosonization effects improves the stability of the Gross-Neveu-XY critical fixed point and enlarges the range of fermion flavor numbers for which it remains a viable candidate for a quantum critical point.

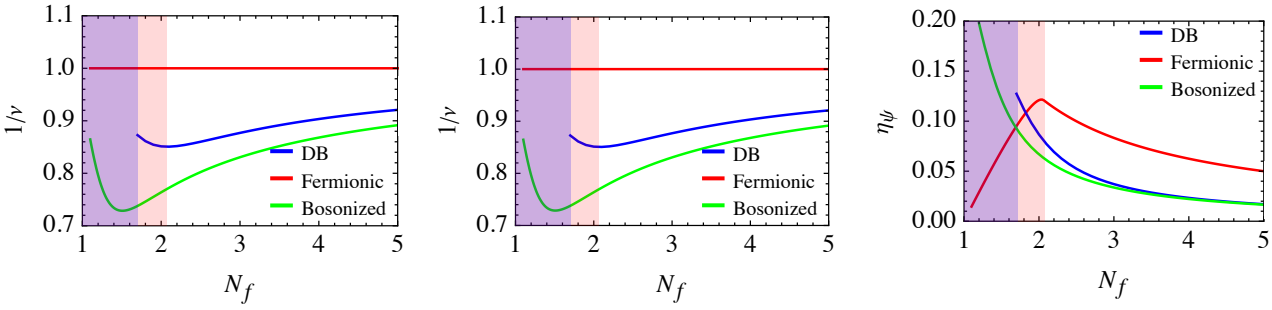

(a) $1/\nu$ **(b)** η_ϕ **(c)** η_ψ

Figure 5.2: Comparison of the three critical exponents obtained from the purely fermionic RG (red), the partially bosonized flow (green), and the dynamically bosonized flow (DB, blue) for the Gross-Neveu-XY universality class as functions of N_f. Panel (a) shows the inverse correlation-length exponent $1/\nu$, while panels (b) and (c) display the bosonic and fermionic anomalous dimensions, respectively. The shaded regions mark the parameter intervals beyond the fixed-point collision, where the original GNXY fixed point has exchanged criticality with its collision partner. In these regions, the universal critical behavior is governed by the new quantum critical fixed point.

5.3 Bosonization of the Gross-Neveu-Heisenberg model

We next incorporate the dynamical-bosonization contribution for the Gross-Neveu-Heisenberg model. Working within the symmetry-closed Gross-Neveu-Heisenberg truncation introduced above, we extract the corresponding box-generated contribution to the four-fermion beta functions, which we denote by $\beta_{g,\mathrm{box}}$.

$$
\begin{aligned}
\delta\dot{g}_1 =& 4h_2^4\frac{1}{(1+r_2)^2} + 12h_4^4\frac{1}{(1+r_4)^2}\\
\delta\dot{g}_2 =& \frac{8}{3}h_1^2h_2^2\frac{1}{(1+r_1)(1+r_2)} + 8h_3^2h_4^2\frac{1}{(1+r_3)(1+r_4)}\\
\delta\dot{g}_3 =& 8h_4^2\frac{1}{1+r_4}\left(h_2^2\frac{1}{1+r_2} + h_3^2\frac{1}{1+r_3}\right)\\
\delta\dot{g}_4 =& \frac{8}{3}h_2^2h_3^2\frac{1}{(1+r_2)(1+r_3)} + \frac{4}{3}h_3^2\frac{1}{(1+r_3)^2} + \frac{8}{3}h_1^2h_4^2\frac{1}{(1+r_1)(1+r_4)}\\
&+ \frac{28}{3}h_4^2\frac{1}{(1+r_4)^2}
\end{aligned}
\tag{5.10}
$$

The regenerated four-fermion interaction is reabsorbed into the Yukawa sector by the dynamical-

bosonization prescription, leading to the analogous modified Yukawa flow as in Eq. (5.9). The first two contributions are provided by the partially bosonized flow collected in Sec. 4.3, while the dynamical-bosonization correction is encoded in the box-induced term δg.

Importantly, the above flow equations in the dynamical bosonization scheme reduce to the ones obtained in the purely fermionic scheme in the limit $r_i \to \infty$. This allows us to identify the GNH fixed point in the coupled set of nonlinear fixed-point equations. For sufficiently large N_f, the GNH fixed point possesses a single relevant direction and therefore represents a quantum critical point. Upon decreasing N_f, the second-largest eigenvalue increases monotonically until, at $N_f^c \simeq 2.08$ (to be compared with $N_f^c \simeq 1.95$ in the purely fermionic calculation), the GNH fixed point collides with another fixed point, denoted $\mathcal{H}'$, and the pair disappears into the complex plane. A posteriori, one can verify that in the large-N_f limit the fixed point $\mathcal{H}'$ agrees with the counterpart found in the purely fermionic analysis. Beyond the collision, the two fixed points form a complex-conjugate pair, and their stability eigenvalues likewise occur as complex-conjugate pairs. In this regime, both fixed points exhibit two eigenvalues with positive real part, indicating the presence of two relevant directions and hence the absence of quantum criticality associated with either of them.

For the GNH fixed point, the resulting three critical exponents for different fermion flavor numbers N_f are summarized in Table 5.2.

N_f	$1/\nu$	η_ϕ	η_ψ
2	(0.743)	(0.758)	(0.122)
4	0.802	1.038	0.029
8	0.895	1.022	0.013

Table 5.2: Critical exponents at the GNH fixed point for representative values of N_f. For $N_f = 2 < N_f^c$, where the GNH and H' fixed points have collided and become complex, the listed values denote their real parts.

To compare the different truncation schemes more systematically, we now plot the three critical exponents $1/\nu$, η_ϕ, and η_ψ as functions of the fermion flavor number N_f, contrasting the results obtained from the purely fermionic RG, the partially bosonized flow, and the dynamically bosonized flow. The corresponding comparison is shown in Fig. 5.3.

As seen from Fig. 5.3(a), the inverse correlation-length exponent $1/\nu$ exhibits a noticeable scheme dependence at small N_f, while the three approaches gradually approach each other as N_f increases. In particular, the dynamically bosonized result remains close to the partially bosonized one for intermediate and large N_f, but leads to a visible shift of the fixed-point collision compared with the purely fermionic treatment.

A similar trend is observed for the anomalous dimensions in Figs. 5.3(b) and 5.3(c). For η_ψ, all three schemes yield relatively small values and become increasingly close to one another toward larger N_f. By contrast, the bosonic anomalous dimension η_ϕ is much more sensitive to the truncation at small N_f. In the purely fermionic description, once the GNH fixed point collides

with $\mathcal{H}'$ and moves into the complex plane, the corresponding continuation is represented by taking the real parts of the critical exponents, which leads to a pronounced deviation from the bosonized results. In the partially bosonized and dynamically bosonized treatments, on the other hand, the evolution of both anomalous dimensions remains considerably smoother.

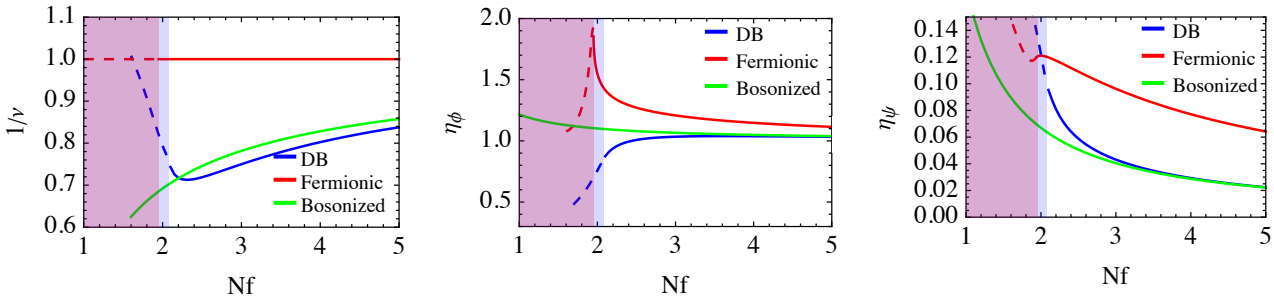

(a) $1/\nu$ **(b)** η_ϕ **(c)** η_ψ

Figure 5.3: Comparison of the three critical exponents obtained from the purely fermionic RG (red), the partially bosonized flow (green), and the dynamically bosonized flow (DB, blue) for the Gross-Neveu-Heisenberg universality class as functions of N_f. Panel (a) shows the inverse correlation-length exponent $1/\nu$, while panels (b) and (c) display the bosonic and fermionic anomalous dimensions, respectively. The shaded regions mark the regime beyond the fixed-point collision, where the fixed points form a complex-conjugate pair. Accordingly, the curves in these regions are drawn dashed and denote the real parts of the corresponding critical exponents.

5.4 Comparison with analytical and numerical estimates

The critical exponents obtained in the partially bosonized and dynamically bosonized descriptions can be further compared with existing estimates in the literature. To this end, we summarize in the following the available analytical and numerical results for the GNXY and GNH universality classes in a common format. At this stage, our goal is only to provide a structured overview of the corresponding values from different methods, including perturbative expansions, large-N_f approaches, functional renormalization-group calculations, and QMC simulations. A detailed discussion of the level of agreement and of the systematic differences between these approaches will be deferred to the subsequent text.

For the analytical side, we include representative estimates from ϵ-type expansions around the lower and upper critical dimensions, large-N_f calculations, and functional renormalization-group approaches. For the numerical side, we include available QMC results obtained from lattice realizations believed to fall into the corresponding GNXY and GNH universality classes. Since different works sometimes quote different sets of exponents, we focus on the three quantities most relevant for the present analysis, namely the inverse correlation-length exponent $1/\nu$, the bosonic anomalous dimension η_ϕ, and the fermionic anomalous dimension η_ψ.

The comparison in Table 5.3 suggests a clear overall trend. Although the present calculations are based only on comparatively simple one-loop analysis, the inclusion of dynamical bosonization systematically improves the agreement with available QMC estimates for both the GNXY and GNH universality classes. In particular, for both models, the three critical exponents obtained in the dynamically bosonized scheme move closer to the numerical values than their counterparts from the naively partially bosonized flow. This tendency is especially visible for the bosonic and fermionic anomalous dimensions, where the partially bosonized results show larger deviations, while the dynamically bosonized treatment yields a more balanced description of the coupled fermion-boson criticality.

This trend is physically plausible, because the partially bosonized formulation treats the Yukawa sector and bosonic self-interactions explicitly, but does not fully incorporate the feedback of four-fermion interactions regenerated along the RG flow. Dynamical bosonization restores this missing feedback by reabsorbing the regenerated fermionic interactions into the bosonic sector, and the resulting improvement of agreement with QMC indicates that such symmetry-allowed regenerated channels are quantitatively important for the multi-component GNXY and GNH universality classes. The contrast with the Gross-Neveu-Ising case is instructive: there the interaction sector is closed at the present truncation level, so that dynamical bosonization produces no additional contribution, and the agreement between analytical and QMC results is already comparatively good. This suggests that the larger discrepancies in GNXY and GNH from large-N_f and ϵ-expansion results compared with the QMC results are not merely due to limited loop order, but reflect a more structural issue associated with the incomplete treatment of symmetry-allowed interaction channels and their feedback on the critical flow on the analytical side.

Of course, this conclusion should be interpreted with some caution. Even after dynamical bosonization, noticeable quantitative differences with QMC remain, which indicates that the present truncation is likely still not fully sufficient for a quantitatively precise description. Higher-order derivative terms, improved momentum dependence, and a more complete treatment of the coupled fermionic and bosonic sectors may all lead to further corrections. Nevertheless, the comparison strongly supports the view that the proper treatment of regenerated interactions is an essential ingredient for understanding GNXY and GNH criticality in $(2+1)$ dimensions, and that it likely plays a central role in explaining why these two universality classes have so far shown a more persistent tension between analytical estimates and unbiased numerical results than the simpler GNI case.

Gross-Neveu-Ising	$1/\nu$	η_ϕ	η_ψ
this work, PB and DB	0.946	0.677	0.039
FRG(NLO) [51]	0.994(2)	0.7765	0.0276
ϵ-exp w / DREG3 [25]	0.993(27)	0.704(15)	0.043(12)
Large-N_f expansion [21]	0.962	0.776	0.044
conformal bootstrap [14]	0.998(12)	0.7329(27)	0.04238(11)
MC [52]	1.00(4)	0.754(8)	
QMC [53]	1.07(12)	0.72(6)	0.04(2)
Gross-Neveu-XY	$1/\nu$	η_ϕ	η_ψ
this work, PB	0.764	0.867	0.067
this work, DB	0.851	0.756	0.087
FRG (LPA′4) [58]	0.86	0.87	0.063
ϵ-exp (interpolation) [5]	0.904(9)	0.85(3)	0.095(19)
Large-N_f expansion [27]	0.84(8)	0.90(2)	0.082(6)
QMC, triangular [9]	0.94(1)	0.64(2)	0.15(1)
QMC, honeycomb [8]	0.95(5)	0.75(13)	0.25(5)
Gross-Neveu-Heisenberg	$1/\nu$	η_ϕ	η_ψ
this work, PB	0.692	1.101	0.067
this work, DB	0.743	0.758	0.122
FRG (LPA′4) [58]	0.795	1.032	0.071
ϵ-exp (interpolation) [23]	0.83(12)	1.01(6)	0.13(3)
Large-N_f expansion [26]	0.85	1.18	0.11
HMC [59]	0.84(4)	0.52(1)	
DQMC [60]	1.11(4)	0.80(9)	0.29(2)
DQMC [61]	0.90(7)	0.79(2)	0.189(4)
QMC (SLAC) [62]	0.98(3)	0.73(1)	0.09(1)

Table 5.3: Comparison of critical exponents for the Gross-Neveu-Ising, -XY and -Heisenberg universality classes in $2+1$ dimensions at $N_f = 2$. Shown are the inverse correlation-length exponent $1/\nu$ and the anomalous dimensions η_ϕ and η_ψ. The table includes the results of the present work obtained from the partially bosonized (PB) and dynamically bosonized (DB) flows, together with representative analytical (FRG in local potential approximation (LPA) and/or next-to-next-to-leading order truncation (NNLO), large-N_f expansion and ϵ-expansion (ϵ-exp) around upper and lower critical dimension) and numerical (hybrid Monte Carlo (HMC) simulations and determinantal quantum Monte Carlo (DQMC) simulations in different lattice formulations) estimates from the literature. For consistency, literature values quoted in terms of ν have been converted to $1/\nu$ whenever needed.

6 Summary and Outlook

In this thesis, the Gross-Neveu-Ising, Gross-Neveu-XY, and Gross-Neveu-Heisenberg universality classes in $(2+1)$ dimensions were studied within three complementary renormalization-group descriptions: the purely fermionic formulation, the partially bosonized formulation, and the dynamically bosonized formulation. The purpose was to compare how these descriptions capture the RG flow, the fixed-point structure, and the resulting critical behavior of interacting Dirac fermions, and to determine in which cases a restricted truncation is sufficient and in which cases additional interaction channels have to be retained.

The analysis in Sec. 2 was based on the purely fermionic formulation. There, the symmetry-allowed four-fermion interaction channels were identified for the three universality classes, and the corresponding one-loop RG flow equations were derived directly in $D = 3$. Already at this stage, a clear distinction emerges between the Ising case and the multi-component XY and Heisenberg cases. For the Gross-Neveu-Ising model, the scalar interaction sector is closed at the present level of truncation, so that the flow can be described consistently within a one-coupling setting. In the Gross-Neveu-XY and Gross-Neveu-Heisenberg models, by contrast, additional four-fermion channels are symmetry-allowed and are generated under the RG flow. A consistent treatment therefore requires an enlarged theory space.

The fixed-point analysis in the purely fermionic description shows that the three models differ not only quantitatively but also qualitatively. In the Gross-Neveu-Ising model, the critical fixed point remains comparatively stable in the physically relevant range of flavor number N_f, and the only collision occurs at $N_f = \frac{1}{2}$, outside the regime relevant for the applications discussed here. In the Gross-Neveu-XY model, two real fixed points collide and exchange their critical character, so that after the collision the criticality is described by a different branch. In the Gross-Neveu-Heisenberg model, the collision is stronger and drives the fixed points into the complex plane. These results show that the global RG structure depends sensitively on the symmetry of the order parameter.

The discussion of the Gross-Neveu-XY model also included the question of emergent symmetry. In the Sec. 3, particular attention was paid to the emergence of the continuous $U(1)$ symmetry associated with the chiral Gross-Neveu-XY description, as well as to the emergence of Lorentz symmetry at criticality. This is relevant because microscopic systems that motivate such effective field theories, including moiré Dirac materials such as twisted bilayer graphene, are not Lorentz invariant at the lattice scale and may contain anisotropies or other Lorentz-

breaking perturbations. From this perspective, the RG analysis is not restricted to locating a critical fixed point, but also addresses whether the low-energy critical theory acquires a larger effective symmetry than the microscopic model. The results support the view that the infrared critical behavior is governed by an effectively $U(1)$-symmetric and Lorentz-invariant field theory.

In Sec. 4, the same universality classes were reformulated in a partially bosonized language through a Hubbard-Stratonovich transformation. This representation introduces bosonic order-parameter fields explicitly and rewrites the theory in terms of bosonic masses, Yukawa couplings, and bosonic self-interactions. Such a formulation is well suited for describing fermion-boson criticality and makes the role of order-parameter fluctuations more transparent. At the same time, the analysis also shows the limitation of the naively partially bosonized truncation: once four-fermion interactions are regenerated along the flow, their feedback is no longer fully incorporated if one works only with the bosonized variables in a fixed truncation.

This issue was addressed in Sec. 5 by means of dynamical bosonization, where regenerated four-fermion interactions are continuously reabsorbed into the bosonic sector during the RG flow. The effect of this procedure depends strongly on the universality class. For the Gross-Neveu-Ising model, the box-generated contribution vanishes, so that dynamical bosonization does not alter the flow at the present level of truncation. For the Gross-Neveu-XY and Gross-Neveu-Heisenberg models, nonvanishing box contributions appear and modify the beta functions. Once these terms are included, the dynamically bosonized description reproduces the same fixed-point collision pattern that was found in the purely fermionic formulation. This agreement indicates that the collision scenario is not an artifact of a particular parametrization, but a robust feature of the RG flow. It also shows explicitly that the naive partially bosonized truncation is incomplete in the multi-component cases if regenerated fermionic channels are omitted.

The comparison of critical exponents from the different RG schemes, discussed in the later part of the thesis, leads to a similarly differentiated picture. For the Gross-Neveu-Ising universality class, the results from the different formulations are relatively consistent with each other and remain in comparatively good agreement with available quantum Monte Carlo data. For the Gross-Neveu-XY and Gross-Neveu-Heisenberg universality classes, larger deviations between analytical approaches and QMC remain. Even so, including dynamical bosonization systematically shifts the results toward the numerical estimates, in particular for the anomalous dimensions. This suggests that the feedback of symmetry-allowed regenerated interaction channels is already quantitatively relevant at the present level of approximation.

Overall, the comparison between the Gross-Neveu-Ising, -XY, and -Heisenberg cases shows that their differences are not exhausted by different numerical values of critical exponents. The symmetry of the order parameter determines which interaction channels are allowed, whether the single interaction channel is RG closed, how the fixed points evolve with N_f, and

whether a restricted bosonized truncation can be trusted. In this sense, the Gross-Neveu-Ising model remains structurally simpler, whereas the Gross-Neveu-XY and Gross-Neveu-Heisenberg models require a more careful treatment of the enlarged RG flow.

Several extensions suggest themselves naturally. On the methodological side, it would be useful to enlarge the truncation by including higher-order bosonic operators, more complete momentum dependencies, and improved treatments of anomalous dimensions. This would help assess how stable the fixed-point collision scenarios remain beyond the present approximation and may further reduce the remaining discrepancy with QMC. On the physical side, a more direct connection to concrete microscopic systems remains of interest, especially for moiré Dirac materials, where the interplay between microscopic symmetry breaking, emergent symmetry, and interaction-driven criticality is expected to be particularly important.

7 Bibliography

[1] A. H. Castro Neto et al. “The Electronic Properties of Graphene”. In: *Reviews of Modern Physics* 81.1 (2009), pp. 109–162.

[2] V. N. Kotov et al. “Electron-Electron Interactions in Graphene: Current Status and Perspectives”. In: *Reviews of Modern Physics* 84.3 (2012), pp. 1067–1125.

[3] T. Wehling et al. “Dirac Materials”. In: *Advances in Physics* 63.1 (2014), pp. 1–76.

[4] I. F. Herbut. “Interactions and Phase Transitions on Graphene’s Honeycomb Lattice”. In: *Physical Review Letters* 97.14 (2006), p. 146401.

[5] B. Hawashin et al. “Gross-Neveu-XY Quantum Criticality in Moiré Dirac Materials”. In: *Physical Review B* 111.20 (2025), p. 205129.

[6] F. F. Assaad and I. F. Herbut. “Pinning the Order: The Nature of Quantum Criticality in the Hubbard Model on Honeycomb Lattice”. In: *Physical Review X* 3.3 (2013), p. 031010.

[7] Z.-X. Li et al. “Fermion-Induced Quantum Critical Points”. In: *Nature Communications* 8.1 (2017), p. 314.

[8] X. Y. Xu et al. “Kekulé Valence Bond Order in an Extended Hubbard Model on the Honeycomb Lattice with Possible Applications to Twisted Bilayer Graphene”. In: *Physical Review B* 98.12 (2018), p. 121406.

[9] Y. Otsuka et al. “Quantum Criticality in the Metal-Superconductor Transition of Interacting Dirac Fermions on a Triangular Lattice”. In: *Physical Review B* 98.3 (2018), p. 035126.

[10] D. J. Gross and A. Neveu. “Dynamical Symmetry Breaking in Asymptotically Free Field Theories”. In: *Physical Review D* 10.10 (1974), pp. 3235–3253.

[11] B. Rosenstein et al. “Critical Exponents of New Universality Classes”. In: *Physics Letters B* 314.3 (1993), pp. 381–386.

[12] R. Boyack et al. “Quantum Phase Transitions in Dirac Fermion Systems”. In: *The European Physical Journal Special Topics* 230.4 (2021), pp. 979–992.

[13] N. Zerf et al. “Four-Loop Critical Exponents for the Gross-Neveu-Yukawa Models”. In: *Physical Review D* 96.9 (2017), p. 096010.

[14] R. S. Erramilli et al. "The Gross-Neveu-Yukawa Archipelago". In: *Journal of High Energy Physics* 2023.2 (2023), p. 36.

[15] L. Wang et al. "Fermionic Quantum Critical Point of Spinless Fermions on a Honeycomb Lattice". In: *New Journal of Physics* 16.10 (2014), p. 103008.

[16] C. Chen et al. "Charge-Density-Wave Transitions of Dirac Fermions Coupled to Phonons". In: *Physical Review Letters* 122.7 (2019), p. 077601.

[17] L. Janssen et al. "Confinement transition in the QED_3-Gross-Neveu-XY universality class". In: *Physical Review B* 101.23 (2020), p. 235118.

[18] J. Biedermann and L. Janssen. "Twist-Tuned Quantum Criticality in Moiré Bilayer Graphene". In: *Physical Review B* 112.4 (2025), p. L041109.

[19] C. Huang et al. "Angle-Tuned Gross-Neveu Quantum Criticality in Twisted Bilayer Graphene". In: *Nature Communications* 16.1 (2025), p. 7176.

[20] Y. Otsuka et al. "Universal Quantum Criticality in the Metal-Insulator Transition of Two-Dimensional Interacting Dirac Electrons". In: *Physical Review X* 6.1 (2016), p. 011029.

[21] L. Janssen and I. F. Herbut. "Antiferromagnetic Critical Point on Graphene's Honeycomb Lattice: A Functional Renormalization Group Approach". In: *Physical Review B* 89.20 (2014), p. 205403.

[22] T. C. Lang and A. M. Läuchli. "Quantum Monte Carlo Simulation of the Chiral Heisenberg Gross-Neveu-Yukawa Phase Transition with a Single Dirac Cone". In: *Physical Review Letters* 123.13 (2019), p. 137602.

[23] K. Ladovrechis et al. "Gross-Neveu-Heisenberg criticality from $2 + \epsilon$ expansion". In: *Physical Review B* 107.3 (2023), p. 035151.

[24] J. A. Gracey et al. "Four Loop Renormalization of the Gross-Neveu Model". In: *Physical Review D* 94.12 (2016), p. 125028.

[25] B. Ihrig et al. "Critical Behavior of Dirac Fermions from Perturbative Renormalization". In: *Physical Review B* 98.12 (2018), p. 125109.

[26] J. A. Gracey. "Large N critical exponents for the chiral Heisenberg Gross-Neveu universality class". In: *Physical Review D* 97.10 (2018), p. 105009.

[27] J. A. Gracey. "Critical exponent η at $O(1/N^3)$ in the chiral XY model using the large N conformal bootstrap". In: *Physical Review D* 103.6 (2021), p. 065018.

[28] L. Rosa et al. "Critical Exponents of the Gross-Neveu Model from the Effective Average Action". In: *Physical Review Letters* 86.6 (2001), pp. 958–961.

[29] B. Knorr. "Ising and Gross-Neveu Model in next-to-Leading Order". In: *Physical Review B* 94.24 (2016), p. 245102.

[30] I. Herbut. *A Modern Approach to Critical Phenomena*. 2007.

[31] F. Gehring et al. "Fixed-Point Structure of Low-Dimensional Relativistic Fermion Field Theories: Universality Classes and Emergent Symmetry". In: *Physical Review D* 92.8 (2015), p. 085046.

[32] B. Roy et al. "Quantum Superconducting Criticality in Graphene and Topological Insulators". In: *Physical Review B* 87.4 (2013), p. 041401.

[33] C.-Y. Hou et al. "Electron Fractionalization in Two-Dimensional Graphenelike Structures". In: *Physical Review Letters* 98.18 (2007), p. 186809.

[34] S. Ryu et al. "Masses in Graphenelike Two-Dimensional Electronic Systems: Topological Defects in Order Parameters and Their Fractional Exchange Statistics". In: *Physical Review B* 80.20 (2009), p. 205319.

[35] B. Roy and I. F. Herbut. "Unconventional Superconductivity on Honeycomb Lattice: Theory of Kekule Order Parameter". In: *Physical Review B* 82.3 (2010), p. 035429.

[36] S. Ray and L. Janssen. "Gross-Neveu-Heisenberg Criticality from Competing Nematic and Antiferromagnetic Orders in Bilayer Graphene". In: *Physical Review B* 104.4 (2021), p. 045101.

[37] J. Biedermann and L. Janssen. *Dirac Quantum Criticality in Twisted Double Bilayer Transition Metal Dichalcogenides*. 2026. arXiv: 2509.04561.

[38] L. Classen et al. "Fluctuation-Induced Continuous Transition and Quantum Criticality in Dirac Semimetals". In: *Physical Review B* 96.11 (2017), p. 115132.

[39] L. Ma et al. "Relativistic Mott Transition in Twisted WSe2 Tetralayers". In: *Nature Materials* (2025), pp. 1–7.

[40] K. G. Wilson. "Renormalization Group and Critical Phenomena. II. Phase-Space Cell Analysis of Critical Behavior". In: *Physical Review B* 4.9 (1971), pp. 3184–3205.

[41] J. Polchinski. "Renormalization and Effective Lagrangians". In: *Nuclear Physics B* 231.2 (1984), pp. 269–295.

[42] R. Shankar. "Renormalization-Group Approach to Interacting Fermions". In: *Reviews of Modern Physics* 66.1 (1994), pp. 129–192.

[43] L. Janssen. "Spontaneous breaking of Lorentz symmetry in $(2 + \epsilon)$-dimensional QED". In: *Physical Review D* 94.9 (2016), p. 094013.

[44] A. Bondi et al. "Metric and Central Charge in the Perturbative Approach to Two Dimensional Fermionic Models". In: *Annals of Physics* 199.2 (1990), pp. 268–339.

[45] M. M. Scherer and I. F. Herbut. "Gauge-Field-Assisted Kekulé Quantum Criticality". In: *Physical Review B* 94.20 (2016), p. 205136.

[46] D. B. Kaplan et al. “Conformality Lost”. In: *Physical Review D* 80.12 (2009), p. 125005.

[47] V. Gorbenko et al. “Walking, Weak First-Order Transitions, and Complex CFTs”. In: *Journal of High Energy Physics* 2018.10 (2018), p. 108.

[48] B. Ihrig et al. “Abelian Higgs Model at Four Loops, Fixed-Point Collision, and Deconfined Criticality”. In: *Physical Review B* 100.13 (2019), p. 134507.

[49] S. Pujari et al. “Interaction-Induced Dirac Fermions from Quadratic Band Touching in Bilayer Graphene”. In: *Physical Review Letters* 117.8 (2016), p. 086404.

[50] J. Braun et al. “Asymptotic Safety: A Simple Example”. In: *Physical Review D* 83.8 (2011), p. 085012.

[51] J. Braun. “Fermion Interactions and Universal Behavior in Strongly Interacting Theories”. In: *Journal of Physics G: Nuclear and Particle Physics* 39 (2012).

[52] L. Kärkkäinen et al. “Critical Behaviour of the Three-Dimensional Gross-Neveu and Higgs-Yukawa Models”. In: *Nuclear Physics B* 415.3 (1994), pp. 781–796.

[53] T.-T. Wang and Z. Y. Meng. “Quantum Monte Carlo Calculation of Critical Exponents of the Gross-Neveu-Yukawa on a Two-Dimensional Fermion Lattice Model”. In: *Phys. Rev. B* 108.12 (2023), p. L121112.

[54] H. Gies and C. Wetterich. “Renormalization Flow of Bound States”. In: *Physical Review D* 65.6 (2002), p. 065001.

[55] J. M. Pawlowski. “Aspects of the Functional Renormalisation Group”. In: *Annals of Physics* 322.12 (2007), pp. 2831–2915.

[56] S. Floerchinger and C. Wetterich. “Exact Flow Equation for Composite Operators”. In: *Physics Letters B* 680.4 (2009), pp. 371–376.

[57] D. J. Moser and L. Janssen. “Continuous Order-to-Order Quantum Phase Transitions from Fixed-Point Annihilation”. In: *Reports on Progress in Physics* 88.9 (2025), p. 098001.

[58] M. Tolosa-Simeón et al. “Relativistic Mott Transitions and Finite-Temperature Effects of Quantum Criticality in Dirac Semimetals”. In: *Physical Review B* 112.11 (2025), p. 115133.

[59] J. Ostmeyer et al. “Antiferromagnetic Character of the Quantum Phase Transition in the Hubbard Model on the Honeycomb Lattice”. In: *Physical Review B* 104.15 (2021), p. 155142.

[60] Y. Liu et al. “Gross-Neveu Heisenberg Criticality: Dynamical Generation of Quantum Spin Hall Masses”. In: *Physical Review B* 104.3 (2021), p. 035107.

[61] F.-H. Wang et al. *Resolving Quantum Criticality in the Honeycomb Hubbard Model*. 2026. arXiv: 2602.03656.

[62] T. C. Lang and A. M. Läuchli. “Chiral Heisenberg Gross-Neveu-Yukawa Criticality: Honeycomb versus SLAC Fermions”. In: *Physical Review B* 112.24 (2025), p. 245121.

Acknowledgements

I would like to express my sincere gratitude to my supervisor, Lukas Janssen, for his guidance throughout this project. I am especially thankful for the step-by-step supervision, the patience, the many valuable discussions that greatly contributed to the development of this work, as well as the careful proofreading and numerous helpful suggestions.
I am deeply grateful to my parents, Qiaozhen Yuan and Xinhui Yuan, for their constant support, encouragement, and understanding throughout my studies.

Erklärung

Hiermit erkläre ich, dass ich diese Arbeit im Rahmen der Betreuung am Institut für Theoretische Physik ohne unzulässige Hilfe Dritter verfasst und alle Quellen als solche gekennzeichnet habe.

Hao Yuan
Dresden, April 2026